The Exploration of Less Expensive Materials for the Direct Synthesis of Hydrogen Peroxide

Thesis submitted in accordance with the requirements of the University of Cardiff for the degree of doctor of philosophy by

Yingyu Wang

School Of Chemistry

Cardiff University

2014

Summary

This work aims to explore less expensive catalysts for the direct synthesis of hydrogen peroxide. Two chosen strategies for achieving this goal are (i) finding a cheap and effective secondary metal added to Pd as an alternative to Au and (ii) using a simple and effective preparation method for supported Au-Pd alloys with a low metal loading. The results of hydrogen peroxide direct synthesis proved the positive effect of Ni as an additive to Pd. A variety of techniques including X-ray photoelectron spectroscopy (XPS), X-ray diffraction (XRD), temperature programmed reduction (TPR), CO-chemisorption and scanning transmission electron microscopy (STEM) were used for an understanding of the relation between catalytic performance and catalyst morphology. A modified impregnation (M_{Im}) method for Au-Pd nanoparticles is then discussed. Prepared M_{Im} catalysts were tested for hydrogen peroxide direct formation and also characterized by XRD, XPS and other techniques, according to which the superiority of the new method compared to the conventional impregnation and an understanding of selective sites for H_2O_2 synthesis are addressed.

Abstract

The research presented in this thesis describes the direct synthesis of hydrogen peroxide from H_2 and O_2 using supported palladium based catalysts. The direct synthesis of hydrogen peroxide offers a more straightforward and sustainable alternative to the current industrial anthraquinone autoxidation (AO) process. Au-Pd bimetallic catalysts have been proved to be highly active for the direct synthesis process. The work presented in this thesis attempted to produce less expensive catalysts through adding cheap secondary metal to Pd as an effective substitute to Au or using an effective preparation for a low metal loading of Au-Pd nanoparticles. In addition, a comprehension of the actual active sites over bimetallic and Pd monometallic particles for H_2O_2 direct synthesis was also attempted.

The first part of this work aims to explain an interesting phenomenon – an increase of activity for H_2O_2 direct synthesis and a decrease of hydrogenation of H_2O_2 over carbon supported Ni-Pd bimetallic and Pd only catalysts after both hydrogen peroxide synthesis and storage under ambient conditions. Based on the results of XPS, XRD and CO-chemisorption integrated with previous publications, it was concluded that (i) both the reaction of hydrogen peroxide direct synthesis and catalyst storage led to an decrease of particle dispersion; (ii) relative to the active sites on high energy surfaces/small particles of Pd (0), those on low energy surfaces/large particles are more selective for H_2O_2 synthesis, as the latter demonstrates lower activity of dissociative adsorption of O_2 and H_2O_2.

The role of secondary metal-Ni added to Pd was also investigated for H_2O_2 direct synthesis in the thesis. For carbon supported Ni/Pd catalysts (including Ni monometallic, Pd monometallic and Ni-Pd bimetallic catalysts), the addition of Ni to Pd enhanced catalytic activity and selectivity for H_2O_2 synthesis. The results of MP-AES, XPS, XRD and TPR implied that metallic Pd may sit on the top of Ni oxides with a dissolution of metallic Ni in Pd to some degree. Electron transfer from Ni to Pd probably also occurred which was inferred by XPS analysis. The role of Ni in Pd for H_2O_2 direct synthesis was

also investigated over TiO_2 supported catalysts which led to an enhancement of H_2O_2 productivity, H_2 conversion rate and H_2O_2 selectivity relative to Pd only catalyst. Based on the results of XPS, TPR and STEM, it was concluded that inactive Ni species diluted Pd sites as individual Pd atoms which are the selective active sites for H_2O_2 direct formation.

The next part of the study addressed a modified impregnation method (M_{Im}) for the preparation of Au-Pd nanoparticles. These nanoparticles have been proved previously by STEM which are well dispersed homogeneous particles because of excess amount of Cl^- ions in the preparation. As a consequence, the resulted catalyst demonstrated a superior activity than conventional impregnation method (C_{Im}) analogues even the latter loaded with a quintuple metal loading. Through tuning Pd metal loading in 1 wt% Au-Pd and Pd only catalysts for H_2O_2 direct synthesis, two typical phenomena were observed in general: (i) an enhanced synergistic effect of Au and Pd by M_{Im} than C_{Im} and (ii) a rise of H_2O_2 productivity based on the mass of Pd loading with the addition of Au in 1 wt% Au-Pd M_{Im} catalysts. As the possible formation of homogeneous Au-Pd alloy, an increase of H_2O_2 productivity based on Pd with the increase of Au content is probably out of the ensemble effect from the secondary metal.

Acknowledgement

First of all, I would like to thank my supervisor Professor Graham Hutchings for his patient advice, guidance and support during the 3 years of my Ph. D. Study.

I would also like to thank Dr Jennifer Edwards for helping me to get started in Cardiff and her supervision and advices for my study. I would like to thank Dr Dave Morgan, Dr Simon Kondrat, Dr Thomas Davies and Dr Marco Conte for patient teaching and explanation of different techniques along with Professor Chris Kiely and his staff, for the helpful STEM analysis.

I would like to thank all of Ph. D.s, post docs and technicians who have worked alongside and supported me during the three years. All of you have helped me in some way and pulled me out of troubles and difficulties. I would especially like to thank the hydrogen peroxide team, especially Marco Piccinini and James Pritchard who helped me and gave me advices at the beginning of my study, and Adeeba Akram who has been a good company of my three-year research.

I gratefully acknowledge Simon Freakley and Greg Shaw whose careful and detailed corrections of my thesis. Your questions inspired me a lot of good ideas and deliberation of my writing.

Many thanks to Ragini Ramdas who warmly greeted with me on my first day joined the group and has patiently supported me for my study as a very good friend.

Many thanks to all the other friends both inside and outside of Cardiff who have helped me through different ways. This could not happen without you, and each of you means a lot to me.

Most importantly I would like to thank my parents who are also very good friends for me. Thank you for being always supportive and understanding.

Table of Contents

Chapter 1

Introduction

1.1 Catalysis

Catalysis, as a tool for increasing the rate of chemical reactions, has been applied for thousands of years in processes such as fermentation. The term of catalysis was first put forward by Jons Jakob Berzelius in 1836, namely a new operative force besides "Affinity" - "Catalysis Force".[1] Throughout the course of history, catalysis has been widely developed and applied in various fields and have profoundly changed human life and industrial development. Seminal studies by Davy, Faraday and Philips concerned the application of Pt sponge for catalysing combustion reactions.[2–4] One such invention, the Davy lamp with Pt gauze casing, was used in the mining industry to warn the exceeding flammable gases (e.g. methane) leading to a reduction of underground explosion and death. The Haber Process for the catalytic production for ammonia from nitrogen and hydrogen was introduced in 1903. This process used an iron based catalyst which facilitated the manufacture of artificial fertilisers, without

which the world's food production would only be able to support half of the present population.[5]

Currently, a large proportion of the chemical industry depends on the development and application of efficient catalysts. One branch of catalysis - heterogeneous catalysis is extensively used in numerous areas including the chemical, environmental, food, pharmaceutical, automobile and petrochemical industries.[6] Specific examples of the application of catalysis include catalytic oxidation to destroy pollutants in automotive exhaust systems, catalytic hydrogenation of vegetable and animal oils to form edible fats[7] and catalytic cracking and refinery processes of raw oil to produce high quality gasoline, high-octane diesel and jet fuel[6].

A catalyst is a substance that accelerates the rate of a chemical reaction without altering the reaction equilibrium, and as such, undergoes no net chemical change.[8] A catalytic process provides an alternative reaction mechanism comprising a different transition state characterized by lowering the activation energy (E_a):

$$k = Ae^{(-E_a/RT)}$$

(**Equation 1-1**)

R = molar gas constant, T = absolute temperature, A = pre-exponential factor, E_a = activation energy and k = rate constant

Figure 1-1 demonstrates the different pathways of uncatalysed and catalysed reactions, showing a distinct activation energy barrier from the reactant to product. However, no matter which pathways the reaction undergoes, the overall energy change is always the same and is the change in Gibbs free energy (ΔG) of the system. This indicates that a catalyst is able to change the intermediate process of a reaction without altering the corresponding ΔG.

There are three types of catalysts: homogenous, heterogeneous and enzymatic. A homogeneous catalyst is a catalyst in the same phase as the reaction mixture. A heterogeneous catalyst is one that is in a different phase to the reactants, and reaction(s) take place at the phase boundary. This process occurs at either solid-liquid and solid-gas interfaces, where the solid is the catalyst. Enzymes are functional proteins or nucleic acids with catalytic ability through metabolic pathways which are present in most living creatures.

The figure shows an energy diagram. Labels include:

- Reaction without catalyst
- E_{a0}
- E_{a1}
- E_{a-1}
- E_{a2}
- $E_a = E_{a1} + E_{a-1} + E_{a2}$
- $E_a < E_{a0}$
- Reaction with catalyst
- A+B
- ΔG
- C
- Energy (y-axis)
- Reaction progress (x-axis)
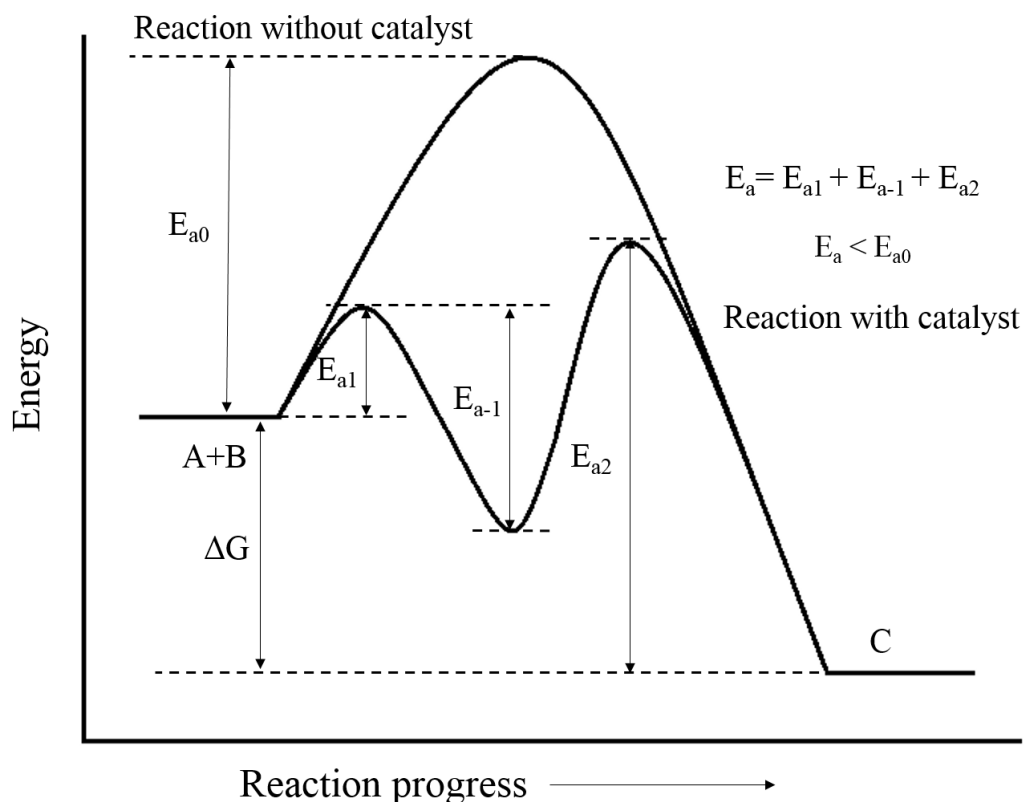
Figure 1-1: The relation between active energy and reaction progress of A+B to product C with and without catalyst.

E_a = activation energy; ΔG = change in Gibbs free energy

Heterogeneous catalysis is of vital importance to the world's economy, allowing us to convert raw materials into valuable chemicals and fuels in an economical, efficient, and environmentally benign manner[6], which is the specific area investigated in this work. One of the benefits of heterogeneous catalysis is that the catalyst can be separated from the reaction medium on completion of a given reaction. The key of a heterogeneous catalytic process is an effective adsorption of reactant onto a catalyst surface, as not all the adsorption is capable of leading to the desired target reaction. Hence, related catalyst surface for the target reactions is defined as active sites. Currently, widespread industrial applications of heterogeneous catalysis require durable catalysts that must satisfy various requirements including high selectivity and activity, thermal and mechanical stability, resistance to poisoning, and commercial feasibility,[6] which becomes the aim of current catalyst design.

1.2 Hydrogen peroxide

Hydrogen peroxide was first recognized by Thenard in 1818[9] as a simple inorganic molecule forming a clear colourless liquid at ambient conditions. Hydrogen peroxide is 100% miscible with water but can be separated by distillation. Hydrogen peroxide is a strong oxidant, possessing high oxidation potential over a wide pH range (E_o=1.763 V at pH 0, E_o=0.878 V at pH 14), which can oxidize a broad variety of inorganic and organic substances in liquid phase under mild conditions. Moreover, it also can be a strong reducing agent that reduces a number of oxidizing compounds such as $KMnO_4$, $NaClO$ and $Ce(SO_4)_2$.[9]
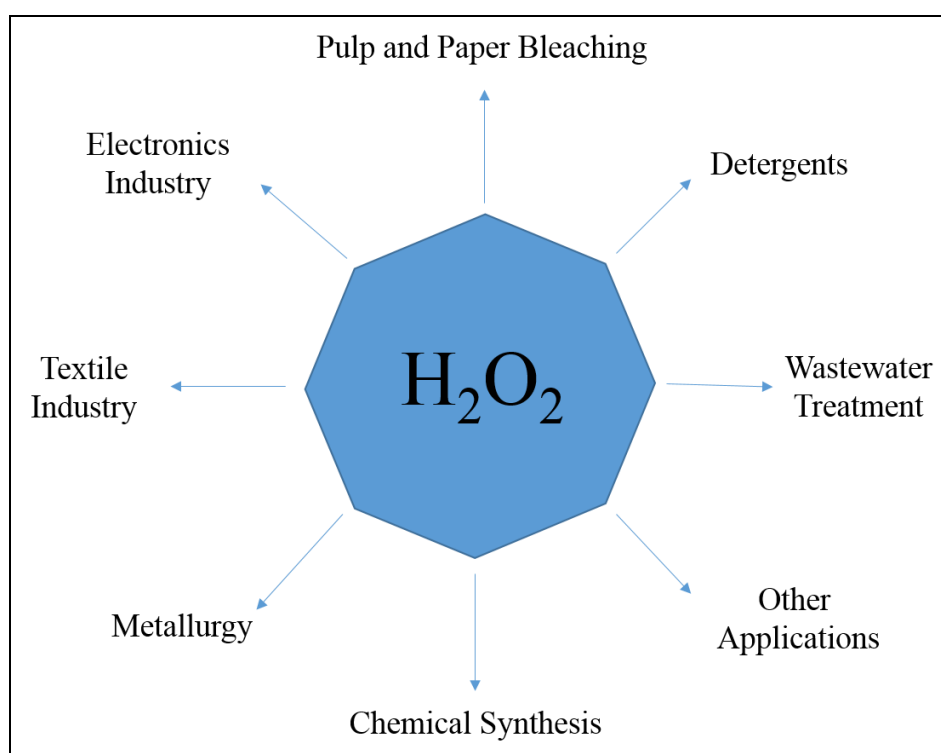
Figure 1-2: Current applications of hydrogen peroxide[9]

Due to its versatile properties, hydrogen peroxide is extensively used in both industrial and domestic sections and is recognised as an extremely important commodity chemical (Figure 1-2). Annually, global production of hydrogen peroxide stands at approximately 2.2 million metric tonnes with demand increasing at a rate of 10% per year.[10] About 50% of H_2O_2 is used for pulp and paper bleaching as an alternative to chlorine-based bleaches. The other strong area of interest for commercial hydrogen peroxide production is propene epoxidation, with two large scale plants now online and operated by Solvay/Dow/BASF.[11] H_2O_2 is also used for

the synthesis of other numerous organic and inorganic chemicals such as the oxidation of thioethers and sulfoxides,[12] and cyclohexane oxidation.[13] Another major use of H_2O_2 lies in wastewater treatment for the efficient removal of hydrogen sulphide in sewer pipes and a broad variety of chemicals in industry waste including cyanide, thiocyanate, nitrite, chloride, hypochlorite and organic substances.[14] Domestically, H_2O_2 is used in household bleaches, hair dyes and disinfectant at relatively lower concentration around 3-5 vol%.[15] H_2O_2 is considered to be an atom efficient oxidizing agent since it contains a higher activated oxygen ratio than other oxidants such as nitric acid and sodium hypochlorite. Moreover, it is also an environmentally friendly oxidant given the only by-product, namely H_2O.

1.3 Anthraquinone (AQ) auto-oxidation (AO) process

H_2O_2 can be prepared in a number of different ways such as reaction of barium peroxide with nitric acid and electrolytic processes using ammonium sulphate.[16] Currently, the majority of hydrogen peroxide production worldwide is achieved through the anthraquinone cycle.[15] After work carried out by Manchot, who noted in 1901 that hydroquinone and hydrazobenzenes are able to undergo auto-oxidation in alkaline solutions[16], Hans-Joachim Riedl and George Pfleiderer in 1939 developed[17,18] the AO process. The process involves four major steps including hydrogenation, oxidation, hydrogen peroxide extraction and treatment of the working solution.[19] A simplified flow diagram of this procedure is shown in Figure 1-3. Specifically, an anthraquinone molecule is first hydrogenated in the presence of hydrogen and a nickel or palladium catalyst to form the corresponding diol which is shown as "hydrogenation process" in the flow chat. The subsequent oxidation of anthraquinol is conducted in air, reforming the original anthraquinone and producing hydrogen peroxide, namely oxidation process, which can then be separated from the working solution through various methods.[9] The reaction is carried out between 30-60 ºC at up to 10 atmospheres pressure.

Currently, the anthraquinone (AQ) auto-oxidation process accounts for more than 95% of the world's H_2O_2 production.[9] The merits of this process include prevention of the direct contact of hydrogen and oxygen and the ability to produce H_2O_2 continuously at mild temperatures. However, the AO process suffers from several drawbacks such as mass-transport limitation in both the hydrogenation and oxidation

reaction vessels and consequently the use of operating temperatures are higher than those required for the kinetically controlled reactions intrinsic to H_2O_2 production. Moreover, side-reactions can happen because of the difficulty in controlling H_2/AQ ratio and AQ residence time, with by-products produced as a result of over-hydrogenation/degradation having to be removed on a regular basis (Figure 1-4). The non-ideal partition coefficient of H_2O_2 between water and the organic phase also leads to high energy consumption during distillation and purification of the product, which however, still cannot fully eliminate the contamination of organic chemicals. In addition, as the AO process is only economical as a large scale manufacturing process[15], there is usually a mismatch between the production scale, the H_2O_2 concentration produced and the concentration required for many applications. For instance, in order to minimize transport cost, high concentrations of up to 70 vol% H_2O_2 are produced, which are not suitable for lower concentration demands such as medical disinfectants and bleaches (3-5 vol%). Hence, for a number of reasons, smaller scale H_2O_2 manufacture at the point of use is deemed more practical.
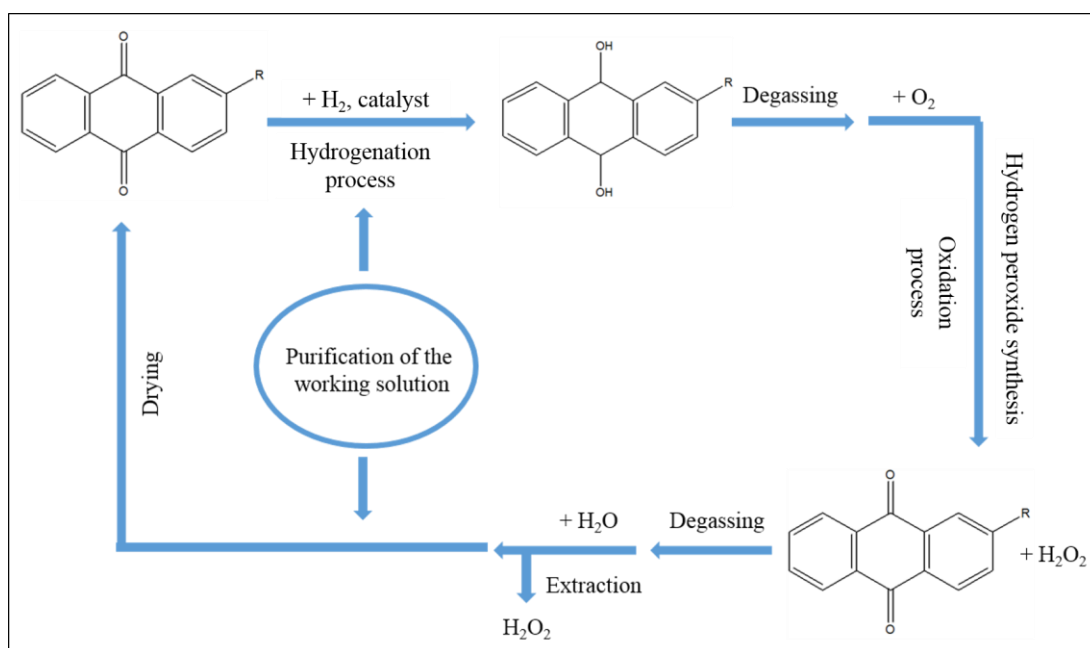
Figure 1-3: Simplified diagram of the steps involved in the anthraquinone auto-oxidation process for the synthesis of hydrogen peroxide
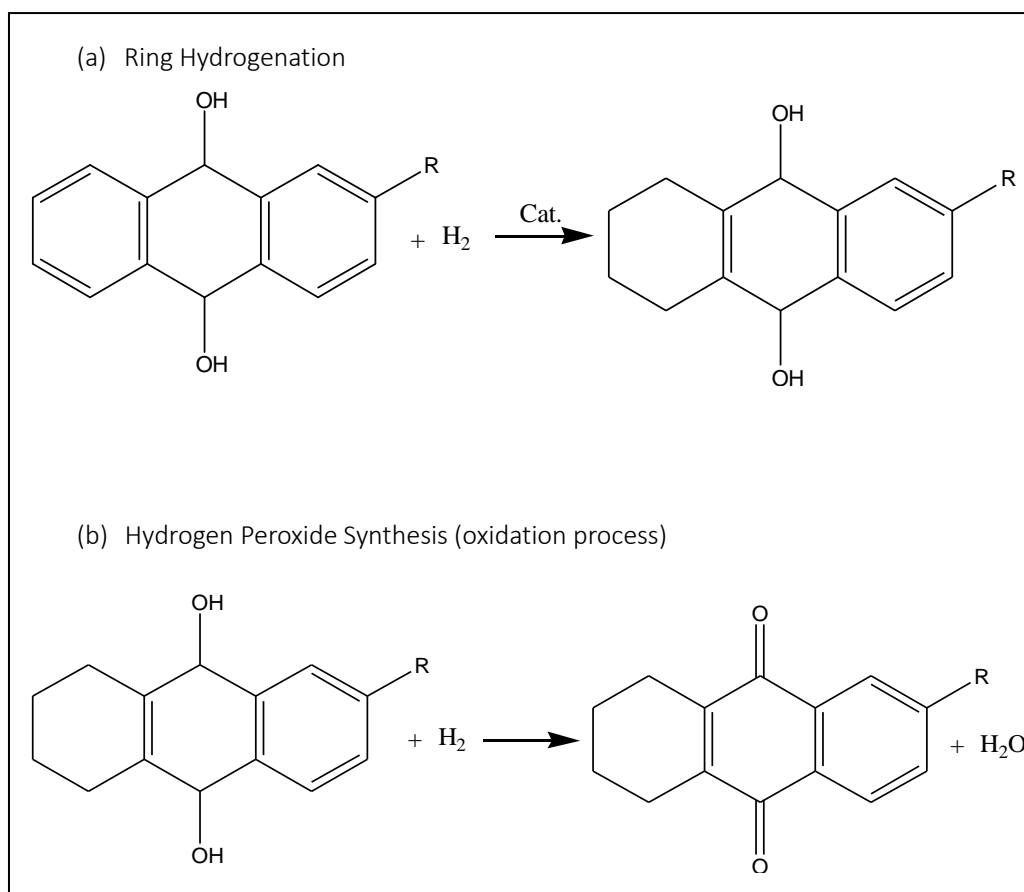
Figure 1-4: Equations used to describe some of the side reactions associated with the AO process.

In conclusion, although the AO process is being widely used in industry for the world production of hydrogen peroxide, a greener and more straightforward alternative is being investigated and developed to enable more affordable and widespread applications especially for on-site/low concentration demands.

1.4 The direct synthesis of hydrogen peroxide

The direct synthesis of hydrogen peroxide from oxygen and hydrogen is on the surface, a more straightforward alternative to the AO process. While the first patent describing the direct synthesis method was awarded to Henkel and Weber in 1914[20] this method until present has not been commercialized. In fact, moving from H_2 and O_2 mixtures to H_2O_2 unavoidably faces a number of challenges that prevent it from currently being a widespread application. First of all, a wide explosion limit for H_2 in O_2 ranging from 4% to 94% by volume exists (at 25 °C and 1 atmospheric pressure), and this range is further extended with increasing pressure.[21] In addition, for the

reaction of H_2 with O_2, more thermodynamically favourable parallel and consecutive reaction pathways than the formation of H_2O_2 exist, all of which are shown in Scheme 1-1. Unwanted reactions include the combustion of H_2 and O_2 (Route B), the hydrogenation of H_2O_2 (Route C) and the decomposition of produced H_2O_2 (Route D).
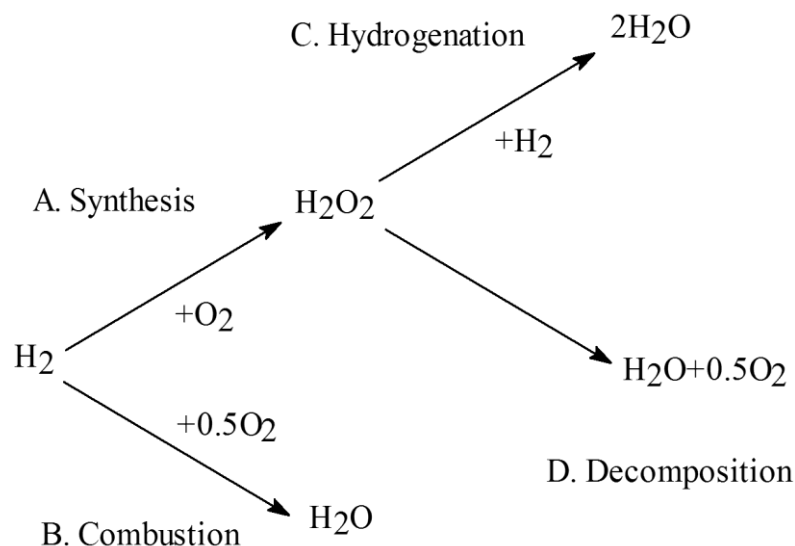
Scheme 1-1: Reaction routes, equations and corresponding thermodynamic energy during the direct synthesis of hydrogen peroxide.[22]

A. $H_2 + O_2 \rightarrow H_2O_2$ $\Delta H^o_{298\ K}$ = -135.9 kJ mol^{-1}, $\Delta G^o_{298\ K}$ = -120.4 kJ mol^{-1}

B. $H_2 + 0.5\ O_2 \rightarrow H_2O$ $\Delta H^o_{298\ K}$ = -241.6 kJ mol^{-1}, $\Delta G^o_{298\ K}$ = -237.2 kJ mol^{-1}

C. $H_2O_2 + H_2 \rightarrow 2H_2O$ $\Delta H^o_{298\ K}$ = -211.5 kJ mol^{-1}, $\Delta G^o_{298\ K}$ = -354.0 mol^{-1}

D. $H_2O_2 \rightarrow 2H_2O + O_2$ $\Delta H^o_{298\ K}$ = -105.8135.9 kJ mol^{-1}, $\Delta G^o_{298\ K}$ = -116.8 kJ mol^{-1}
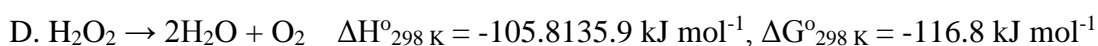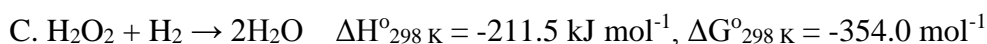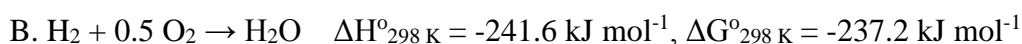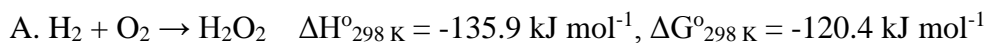
A membrane catalyst is able to solve the limitation brought about by the high flammability of H_2 that makes it possible for using pure H_2 and O_2 in this reaction. Nevertheless, the reaction rate is significantly reduced by its low mass transportation, which therefore is not applicable for industry.[22] The other way to avoid explosion is by diluting H_2 and O_2 with inert gases for instance N_2, CO_2 or Ar. The dilution of the reactants predictably leads to a lower rate of H_2O_2 production.

For the parallel combustion, hydrogenation and decomposition reactions, there are several ways to solve the H_2O_2 selectivity problem, for example, moderately decreasing reaction temperature to bring down the H_2O_2 decomposition rate, or by lowering the contact time with the catalyst to stop further formation of H_2O. Moreover, the introduction of chemical additives such as acid[23–33] and halide[80–87] in

the reaction medium can decrease the rates of subsequent and competing water forming reactions. Last but not least, successful preparation of a catalyst with 100% selectivity towards H_2O_2 infers that distinct active sites exist for both H_2O_2 synthesis and side reactions.[34] Hence, a well-designed catalyst is also of critical importance for the direct synthesis of H_2O_2.

1.4.1 Direct Synthesis of H₂O₂ using Palladium Catalysts

Palladium as a catalyst has been extensively used for hydrogenation reactions[35–39] and is also known to be excellent for a range of oxidation reactions[40–43]. The first reported experiment for the direct synthesis of H_2O_2 by Henkel and Weber was performed over a Pd catalyst.[20] Since then, the vast majority of catalytic studies have maintained interest in using Pd as the catalytic species. In an early study, H_2/O_2 compositions inside of the explosive region were used in order to achieve highly concentrated solutions of H_2O_2. Solutions of over 35 wt% H_2O_2 were manufactured from H_2 and O_2 in the presence of a Pd catalyst at elevated pressures.[44] However, operating H_2/O_2 mixtures within the explosive region is considered to be extremely dangerous, and afterwards, studies have focused on the reactions carried out with dilute gas mixtures outside the explosive regime.[45,46] Further to this, the direct synthesis of H_2O_2 involves reduction of oxygen rather than the oxidation of H_2,[47] and Pd itself with an excellent oxidation property may not be able to achieve a high selectivity of H_2O_2. A wide variety of reaction conditions have been also investigated, including the effect(s) of acid and halide addition to the reaction medium, the Pd oxidation state(s), colloidal Pd, and a number of other factors.[23,48–50]

1.4.1.1   Acid addition

H_2O_2 is unstable in alkaline solutions relative to neutral or acidic medium, and the maximum stability of H_2O_2 can be achieved between 3.5-4.2 pH.[51] H_2O_2 can be less stable towards its decomposition or hydrogenation in the presence of a catalyst such as Pd.[52] Several patents[53–61] and papers[23–25,27–33,62] have proved the beneficial role of protons present in aqueous, and non-aqueous or aqueous/organic mixtures for achieving high H_2O_2 selectivity. Although additive H^+ ions may not be essential particularly in the presence of bimetallic catalysts such as Au-Pd alloy supported catalysts[34,63], the presence of protons in the reaction medium has proved beneficial to

Pd only catalysts with respect to achieving higher selectivity and productivity towards H_2O_2.[23–25,27–33,62] Choudhary and co-workers[64] conducted H_2O_2 decomposition experiments over 5 wt% Pd/C with addition of non-coordinating acids (oxyacids) and coordinating acids (halide acids), respectively, in order to investigate the effect of the nature of acid on H_2O_2 decomposition activity. Results revealed that the moderate effect of oxyacids (acetic acid, phosphoric acid, sulfuric acid and perchloric acid) on inhibiting H_2O_2 decomposition is influence by protons, while halide acids (hydrochloric acid, hydrobromic acid and hydroiodic acid) strongly suppressed the activity of H_2O_2 decomposition because of the combined presence of protons and halide anions (site poisoning).

Hutchings and co-workers used CO_2 to dilute flammable gas-H_2[45,46,65–68] beyond its explosive limit which was also considered an *in situ* stabilizer in the form of carbonic acid in the reaction medium[15,67]. This further proved the positive effect of the protons in reaction medium on H_2O_2 selectivity and stability. However, the presence of acid in an aqueous reaction medium can lead to reactor corrosion and leaching of active components from the catalyst.[52] Through the comparison of oxyacids and halide acids, Choudhary *et al.* highlighted that phosphoric acid is less corrosive and also that phosphoric anions act as a H_2O_2 stabilizer.[69] Hence, phosphoric acid is considered to be a suitable acid promoter[29]. Using solid acid or solid super acid is another alternative to aqueous acid to avoid the corrosion of reactor and the leaching of the catalyst. Solid acid supports such as hetropolyacids[70–74], protonated forms of mordenite or MFI zeolites, and solid super-acids such as sulphuric acid supported on Al_2O_3, TiO_2 or MoO_3[75] can be used in combination with Pd to avoid the presence of acid in reaction medium. Ntainjua *et al.*[76] proved the role of the isoelectric point (IEP) of the catalyst support for the direct synthesis of peroxide through controlling the stability of produced H_2O_2. Specifically, an active carbon catalyst, which had the lowest IEP, demonstrated maximum activity and lowest hydrogenation and decomposition among TiO_2, Al_2O_3 and MgO supported catalysts. The IEP of carbon black can be modified by acid or base treatment. Hence, the IEP for raw carbon black was 6.7 which can be varied in the range from 1.3-3.0 (acid treatment) to 7.5-8.8 (base treatment).[77] Acid treatment of the active carbon support has been reported to play a significant role for H_2O_2 selectivity and productivity that generated smaller, homogeneous Au-Pd nanoparticles.[34]

1.4.1.2   Halide addition

Several patents[78–83] and papers[24,48,84–90] have claimed the positive effect of halide (in particular Cl$^-$ and Br$^-$ ions) for the direct synthesis of hydrogen peroxide from H_2 and O_2. It is found that using halides decreases the activity of Pd catalysts for H_2O_2 destruction, thereby increasing selectivity towards H_2O_2.[30] This is believed to be caused by the blockage of high energy sites which are responsible for H_2 combustion.[91] Landon *et al.*[46] compared reactions with or without the addition of HBr and proved the additive Br$^-$ responsible for the high selectivity towards H_2O_2 even up to 20 ^{o}C, indicating the poisoning of active sites responsible for H_2O formation. Experiments conducted by Choudhary and co-workers[69] revealed that the inhibiting action was influenced by the electronegativity of the anions. Results suggested I$^-$ with the highest electronegativity among the elements of F, Cl and Br, caused a complete deactivation of the catalyst and Br$^-$ and Cl$^-$ appreciably decreased H_2O_2 hydrogenation with increasing the halide concentration. Moreover, it was revealed that, in the presence of Br$^-$ and Cl$^-$, the activation energy of H_2O_2 hydrogenation was higher than that in the absence of halide. Yoshizawa's[92] group claimed a weaker interaction of reactants and metal surface achieved through the pre-treatment with strong acids or halide ions, leading to higher productivity and selectivity toward H_2O_2.

Additive halides can be introduced in the form of halide acids (HCl, HBr or HI) or alkali metal salts (Na, K or Cs salt) to the reaction medium.[52] Combination of both protons and halide anions resulted in a more enhanced improvement of catalytic performance[93] as shown in Table 1-1, which unfortunately can also cause reactor corrosion and leaching of active metal components of the catalyst. Incorporation of halide ions into the supported Pd catalysts could be an alternative among which impregnated Br$^-$ ions led to improvements in H_2 conversion, H_2O_2 yield and H_2O_2 selectivity, as shown in Table 1-2.[49]

Table 1-1: Influence of different halides (in the reaction medium) in the presence or absence of acid (0.03 M H_3PO_4) in the reaction medium on the initial rate of H_2O_2 destruction in presence and absence of hydrogen[93]

Halide	Acid in medium	Initial rate of H_2O_2 destruction (h^{-1})	
		In H_2[a]	In absence of H_2[b]
Catalyst: Pd/Al$_2$O$_3$			
None	None	Very fast	2.4
None	$H_3PO_{4(0.03 M)}$	42	0.5
KF (2.7)[c]	$H_3PO_{4(0.03 M)}$	39	0.8
KCl (2.7)	$H_3PO_{4(0.03 M)}$	5.1	0.1
KBr (2.7)	$H_3PO_{4(0.03 M)}$	3.1	<0.1
KI (2.7)	$H_3PO_{4(0.03 M)}$	0.04	0
KBr (0.9)	None	4.2	-
KBr (5.4)	None	4.1	0.3
KCl (0.9)	None	54	-
KCl (5.4)	None	45	0.4

[a] Destruction of H_2O_2 by its decomposition and/or hydrogenation.

[b] Destruction of H_2O_2 by its decomposition alone.

[c] Values in round and square brackets correspond the concentration of halide (mmol/dm^3) in the reaction medium.

Table 1-2: Results of direct synthesis of H_2O_2 in aqueous acidic (0.03 M H_3PO_4) reaction medium over ammonium halide-impregnated Pd/Al_2O_3 catalysts (flow rate of air or N_2 = 30 cm^3 g^{-1} $_{catalyst}$ min^{-1})[49]

Gas atmosphere used in heat treatment of catalyst[a]	Form of Pd[b]	H$_2$O$_2$ direct formation[c]		
		X (H$_2$) (%)	Y (H$_2$O$_2$) (%)	S (H$_2$O$_2$) (%)
Without halide modification				
No pretreatment	Pd^0	54.7	0.5	0.9
Flowing air	PdO	27.8	8.9	37.4
Flowing N$_2$	Pd^0	56.2	0	0
Catalyst halogenated by NH$_4$F (5 wt % F$^-$)				
Flowing air	PdO	38.9	11.7	29.9
Flowing N$_2$	Pd^0	67.1	0	0
Catalyst halogenated by NH$_4$Cl (5 wt % Cl$^-$)				
Flowing air	PdO	35.8	17.6	49.9
Flowing N$_2$	Pd^0	60.9	0	0
Catalyst halogenated by NH$_4$Br (5 wt % Br$^-$)				
Flowing air	PdO	32.8	18.6	53.8
Flowing N$_2$	Pd^0	45.8	23.9	52.2
Catalyst halogenated by NH$_4$I (5 wt % I$^-$)				
Flowing N$_2$	Pd^0	<2.0	0	0

X, Y and S = conversion, yield and selectivity, respectively. [a] 400 °C, 1 h; [b] XRD phase; [c] Reaction time = 3 h

1.4.1.3   Palladium oxidation state

The effect of palladium oxidation state on the direct synthesis of hydrogen peroxide has been extensively investigated by a number of groups, whereas the results are somewhat contradictory. It has been demonstrated in several publications that Pd^0 catalysts are more active but less selective than corresponding PdO catalysts for

direct H_2O_2 synthesis.[26,31,49,90,94,95] Work by Melada *et al.*[84] revealed that the oxidation of surface Pd^0 led to an enhancement of both H_2O_2 productivity and selectivity. Using $H_2/Air/N_2$ of a particular ratio as reactant mixture caused a reduction of Pd catalyst and a decrease of H_2O_2 selectivity, whereas using undiluted H_2/O_2 with a large excess of oxygen ($H_2 : O_2 = 4 : 96$) maintained a high rate of H_2O_2 synthesis and selectivity of H_2O_2 (40%) without any significant decrease even after 5 h. Work by Choudhary *et al.*[26,94] revealed that the oxidation of surface or subsurface Pd^0 to PdO by a variety of oxidizing agents such as perchloric acid, hydrogen peroxide, nitrous oxide, oxygen or air resulted in a promotion of H_2O_2 productivity and a positive increase of H_2O_2 yield and selectivity.

However, some other work suggests the superior performance of Pd^0 for achieving a high productivity and selectivity of H_2O_2.[29,86,87,96,97] For instance, as the rapid reaction of cyclohexene and H_2O_2 towards cyclohexene oxide, Hâncu *et al.*[96] determined the produced H_2O_2 indirectly by the measurement of produced cyclohexene oxide in the end. It was confirmed that Pd^0 catalysts demonstrated enhanced H_2O_2 productivity relative to PdO after 3 h reaction, and at both room temperature and elevated pressure. It was also concluded by Liu *et al.* that the partial reduction of PdO led to a two times increase of the rate of H_2O_2 formation (10.9 mol_{H2O2} kg_{Pd}^{-1} min^{-1}) in the comparison with the PdO catalyst (4.1 mol_{H2O2} kg_{Pd}^{-1} min^{-1}).

1.4.1.4 Colloidal palladium

It has been suggested that the addition of acid and halide into the reaction medium is beneficial for achieving enhanced production rates and selectivity towards H_2O_2. Work by Lunsford[27,50,88,98] revealed the formation of colloidal Pd by leaching from a silica supported Pd catalyst in the presence of concentrated HCl (0.1-1 M) combined with O_2 and H_2 mixture. Moreover, after removing solid catalyst - Pd/SiO_2, the production rate of H_2O_2 remained the same which indicates colloidal Pd as being the principal active component for the direct reaction of H_2 and O_2 to form H_2O_2. During the H_2O_2 synthesis, homogeneous catalytic process was happening through the proposed mechanism as shown in Figure 1-5. It can be noticed that in Lunsford's model, colloidal Pd acts as the active species ending up with the formation of Pd complex - $[PdCl_4]^{2-}$, which is then reduced back to colloidal Pd for a new reaction

circle. Although the colloidal Pd system is active and highly interesting for understanding the fundamentals of the H_2O_2 formation process, it is not practical from a commercial perspective since the management of Pd colloid and acid and halide additives would be a very difficult task.[22]
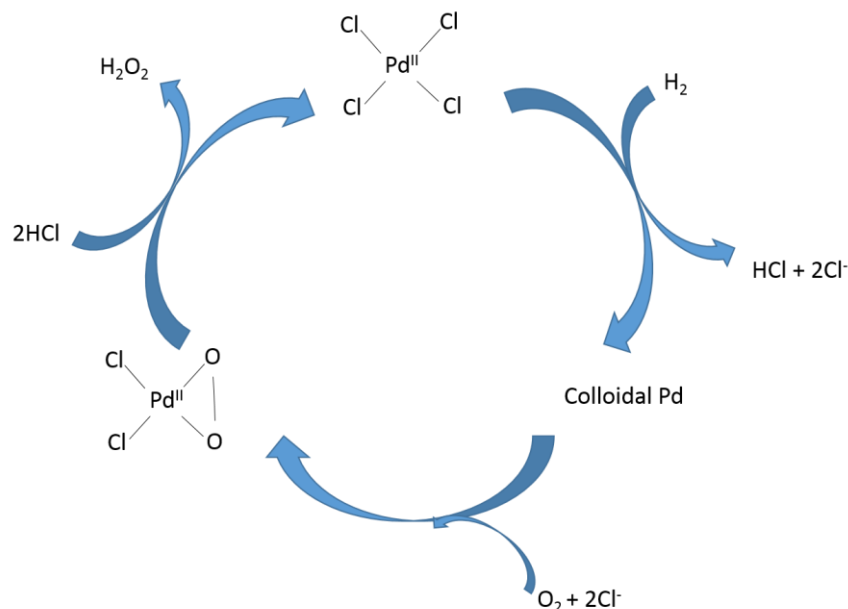
Figure 1-5: Reaction mechanism of the direct synthesis of H_2O_2 over colloidal Pd.

1.5 Active metals for H_2O_2 synthesis

Almost all of the catalysts for the direct synthesis of H_2O_2 described in literature are based on noble metals, among which palladium, gold, platinum, and silver are the most commonly employed materials.[19] Olivera *et al.*[99] concluded that palladium, gold, platinum and silver are favourable metals for H_2O_2 direct formation from theoretical studies. Through the comparison of various metals supported on a zeolite-Y support, Li *et al.*[100] claimed the attained sequence of H_2O_2 productivity with a descending order: Pd (8 mol_{H2O2} $kg_{cat.}^{-1}$ h^{-1}) > Pt (4 mol_{H2O2} $kg_{cat.}^{-1}$ h^{-1}) > Au (3 mol_{H2O2} $kg_{cat.}^{-1}$ h^{-1}) >> Ag, Cu, Rh and Ru. Au monometallic catalysts loaded on SiO_2[101,102], active carbon[103], TiO_2[65], Al_2O_3[45,104], Fe_2O_3[104], H-ZSM-5 or H-Y zeolite[105,106], SiO_2-Al_2O_3[105,106], TS-1[107] and other supports have been investigated for the direct synthesis of hydrogen peroxide. It was reported that inert supports such as SiO_2, active carbon and MCM-41 are indispensable to achieve highly dispersed Au catalysts with effective performance for hydrogen peroxide synthesis in the comparison with the Au catalysts supported on basic oxide (e.g. MgO) and acid

15

oxide (e.g. SiO_2-Al_2O_3).[103] Moreover, the supported Au catalysts prepared through impregnation method demonstrated enhanced performance than those prepared through co-precipitation or deposition-precipitation method. Corresponding results are shown in Table 1-3.[65,104]

The addition of a secondary metal such as Au, Pt, Ag, Ru, Rh and Os to Pd catalysts has also been extensively investigated in order to improve catalyst selectivity and productivity for H_2O_2 synthesis.[65,66,95,108–118] The addition of Au or Pt at an optimum concentration demonstrated a positive effect on achieving both more active and selective production of H_2O_2, whereas Ru and Rh showed an adverse effect. It was revealed that the production rate of H_2O_2 over Au-Pd bimetallic catalyst was higher than either Au or Pd monometallic catalyst (Table 1-3).[34,65,66,68,105,119–121] The beneficial role of Au was assumed as an electron promoter to Pd for the Pd-rich surface (Figure 1-6).[65,121] For homogeneous Au-Pd alloys, with the increase of additive Au, H_2O_2 production rate based on the mass of loaded Pd increased which is considered as a consequence of ensemble effect. The additive Au effectively dispersed Pd atoms and dismissed continuous Pd sites which are responsible for O_2 dissociation.[47,122] Joshi *et al.*[123] have demonstrated from DFT through Au-Pd clusters are energetically favourable for OOH and H_2O_2 formation from H_2 and O_2, and the properties of the bimetallic clusters are size and composition sensitive for H_2O_2 synthesis.

Table 1-3: The comparison of catalytic performance for direct synthesis of H_2O_2 over Au/Pd catalysts in methanol/water at 2 $^\circ$C for 0.5 h reactions[65,104]

Catalyst	Preparation method	Pre-treatment	Productivity (mol_{H2O2} kg^{-1} h^{-1})	H_2O_2 (wt%)
5% Au/α-Fe$_2$O$_3^a$	Co-precipitation	Air, 25 $^\circ$C	0.126	0.001
5% Au/α-Fe$_2$O$_3^a$	Co-precipitation	Air, 400 $^\circ$C	0.207	0.002
5% Au/α-Fe$_2$O$_3^a$	Co-precipitation	Air, 600 $^\circ$C	0.366	0.004
5% Au/α-Fe$_2$O$_3^a$	Impregnation	Air, 400 $^\circ$C	0.54	0.005
5% Au/TiO$_2^b$	Decomposition-precipitation	Air, 25 $^\circ$C	0.229	0.002
5% Au/TiO$_2^b$	Decomposition-precipitation	Air, 120 $^\circ$C	0.482	0.005
5% Au/TiO$_2^b$	Decomposition-precipitation	Air, 400 $^\circ$C	0.388	0.004
5% Au/TiO$_2^b$	Impregnation	Air, 400 $^\circ$C	7.1	0.014
5% Au/α-Fe$_2$O$_3^a$	Impregnation	Air, 400 $^\circ$C	0.54	0.005
2.5% Au-2.5% Pd / α-Fe$_2$O$_3^a$	Impregnation	Air, 400 $^\circ$C	16	0.161
5% Pd/α-Fe$_2$O$_3^a$	Impregnation	Air, 400 $^\circ$C	3.6	0.036
5% Au/Al$_2$O$_3^b$	Impregnation	Air, 400 $^\circ$C	3.1	0.006
2.5% Au-2.5%Pd / Al$_2$O$_3^b$	Impregnation	Air, 400 $^\circ$C	18	0.036
5% Pd/Al$_2$O$_3^b$	Impregnation	Air, 400 $^\circ$C	12	0.024
5% Au/TiO$_2^b$	Impregnation	Air, 400 $^\circ$C	7.1	0.014
4% Au-1%Pd / TiO$_2^b$	Impregnation	Air, 400 $^\circ$C	28	0.057
2.5% Au-2.5%Pd / TiO$_2^b$	Impregnation	Air, 400 $^\circ$C	64	0.128
5% Pd/TiO$_2^b$	Impregnation	Air, 400 $^\circ$C	31	0.061

Mass of catalyst for H_2O_2 synthesis: [a] 50 mg, [b] 10 mg
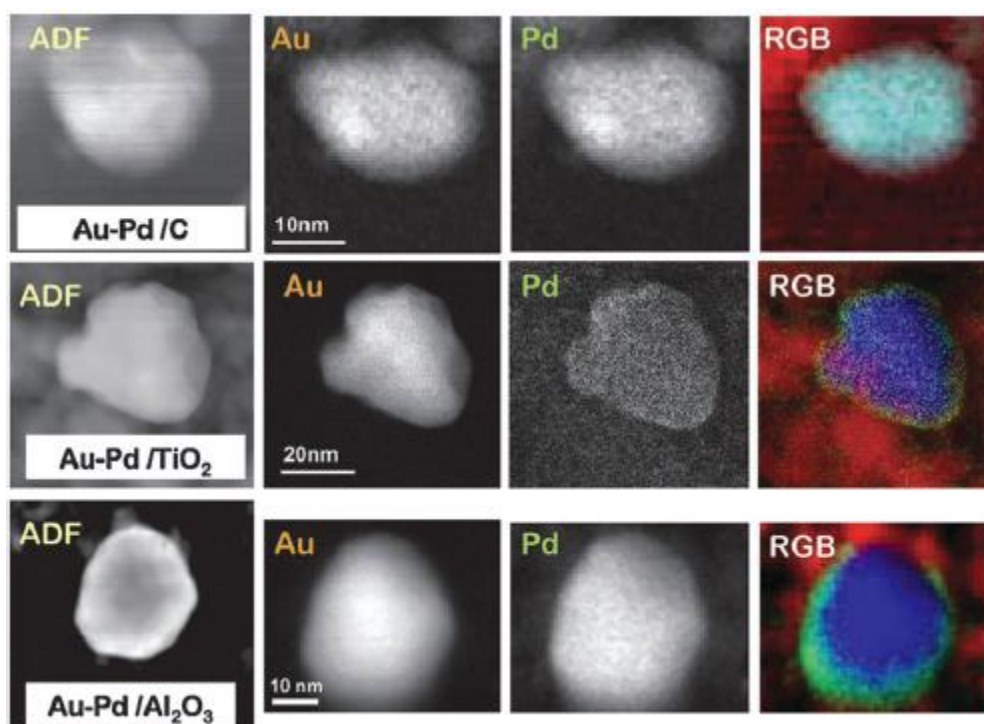
Figure 1-6: High-Angle Dark-Field (HAADF) imaging (column 1), Au map (column 2), Pd map (column 3) and RGB reconstructed overlap map (column 4) (Blue: Au; Green: Pd) for calcined Au-Pd/C (row 1), calcined Au-Pd/TiO$_2$ (row 2) and calcined Au-Pd/Al$_2$O$_3$ (row 3). Note that Au-Pd particles on TiO$_2$ and Al$_2$O$_3$ supported catalysts demonstrate a Au rich core-Pd rich shell morphology, which however are homogeneous on active carbon supported catalyst. [121]

The positive effect of additive Pt to Pd has been proved in the respect of enhancing the productivity and selectivity towards H$_2$O$_2$ once an optimum ratio of Pd/Pt is employed.[108,124,125] Melada *et al.*[124] suggested that the optimum ratio of Pd/Pt ratio is in the range of the one with a high content Pd. The work by Wang and co-workers[125] revealed that the production rate of H$_2$O$_2$ reduced drastically with the increase of Pt/Pd ratio over the optimum value. Hölderich and co-workers[126,127] claimed the optimum level of Pt as a beneficial effect for achieving a desirable increase of surface Pd^{2+} which is considered as a selective species for H$_2$O$_2$ formation. Melada *et al.*[124] demonstrated through TEM that the addition of Pt to Pd changed particle shape from spherical to irregular shaped. Results from Xu *et al.*[128] suggests that Pd$_{16}$Pt$_1$ demonstrated the best catalytic performance for H$_2$O$_2$ synthesis with a rate of 1.77 mol h^{-1} g$_{Pd}^{-1}$ and 60% selectivity which were both drastically higher than those for the Pd-only catalyst. Nevertheless, excess Pt (Pd/Pt < 8) in alloys compromised

catalytic performance remarkably. It was assumedly concluded that charge transfer between Pt and Pd might be responsible for the enhanced productivity and selectivity.

Until now, majority of the catalysts in the investigation for the direct synthesis of hydrogen peroxide have been focused on noble metals, whereas the considerable cost of precious metals to some extent sets an obstacle for commercialization. Take the most utilized metal-Pd for instance, its price per kilogram has increased drastically in the last two decades from 2100 $ per kg in 1990 to nearly 52000 $ per kg currently.[19] According to Garcia-Serna *et al.,*[19] theoretically, for producing 10 kt 17 wt% H_2O_2 per year from direct synthesis over a catalyst (5 wt% Pd/C) with a productivity of 30 $mol_{H_2O_2}$ $kg_{cat.}^{-1}$ h^{-1}, at least 10.5 kg of pure palladium will be needed which consequently will cost approximately 0.54 million $. Hence, including high activity, the catalyst life-time is crucial for industry which however strongly depends on the operational conditions including temperature, pH, promoters, flow rate etc.[19] Using active and selective materials with much lower price is also an alternative for minimizing the cost. One of the options is using a cheap additive metal to Pd that increases catalyst productivity and H_2O_2 selectivity, and consequently decreases the amount of utilized Pd. This is one of the general aims this thesis.

1.6 A brief summary of other effects for the direct synthesis of H_2O_2 (H_2/O_2 ratio, reaction medium, time, pressure and temperature)

During the direct synthesis of H_2O_2, according to Lunsford *et al.*[129], the net formation rate of the reaction is first order with respect to H_2 and zero order with respect to O_2. However, H_2O_2 is less stable in the presence of hydrogen towards its hydrogenation than in the presence of oxygen. Hence, H_2/O_2 ratio has a significant effect on the direct synthesis of hydrogen peroxide. Lunsford *et al.*[129] demonstrated that at the large ratio of H_2/O_2, non-selective hydrogen consumption through H_2O_2 hydrogenation was enhanced that resulted in an increase of H_2 conversion and decrease of H_2O_2 selectivity. Tuning the ratio of H_2/O_2, Choudhary *et al.*[130] claimed that an optimized production rate of H_2O_2 can be achieved at the H_2/O_2 ratio of 1. When protons and Br^- were added to the reaction medium with a continuous flow of H_2 and O_2, the optimum ratio of H_2/O_2 became 0.5. In fact, an appropriate composition of H_2/O_2 significantly depends on the utilized catalyst, reaction medium, additive promoters and the type of reactor.[67,107,125,130]

Reaction period of H_2O_2 direct synthesis can strongly influence H_2 conversion, H_2O_2 selectivity and surface/sub-surface oxidation state of the catalyst especially in batch-mode operation.[22] The ratio of H_2/O_2 in the reaction system changes with the reaction time and possibly results in modifications of the surface/sub-surface oxidation state of the catalyst, consequently altering catalytic behaviour. Moreover, in an enclosed system, the rate of subsequent reactions - H_2O_2 decomposition and hydrogenation associated with the production becomes significant with the accumulation of H_2O_2 as the reaction proceeds.
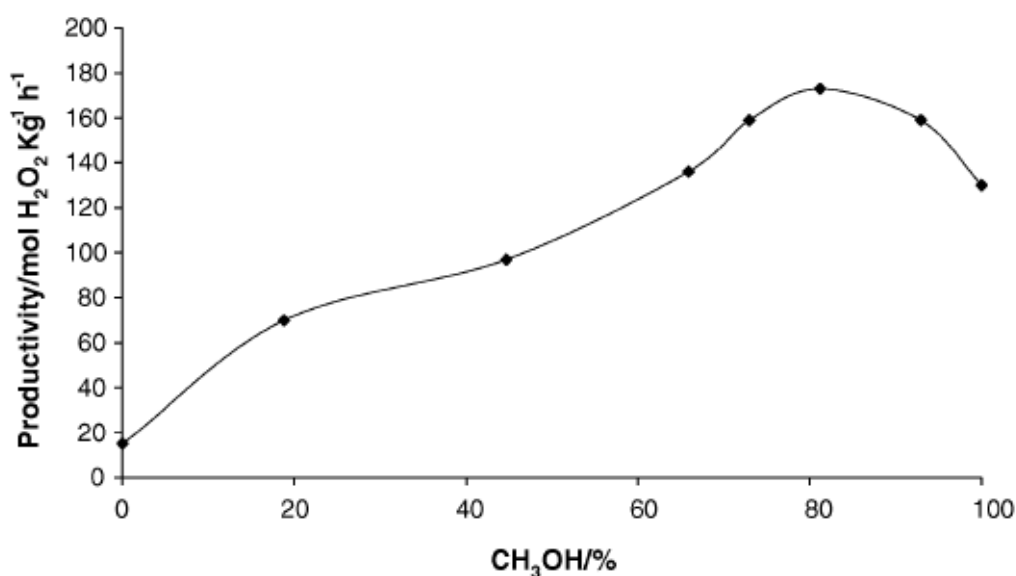
Figure 1-7: Production rate of H_2O_2 as a function of methanol/water composition.[67] Reaction conditions: 10 mg 2.5%Au-2.5%Pd/TiO$_2$ catalyst, total pressure 580 psi, H_2/O_2 ratio = 0.525, 1200 rpm, 0.5 h, total mass of solvent = 8.5 g.

Since the direct synthesis of hydrogen peroxide takes place in a three phase system, the mass transfer rate of gaseous reactants to the catalyst surface plays a crucial role on hydrogen peroxide productivity. According to Samanta[22], using proper solvents with high gas solubility, low viscosity and low surface tension is an effective way to increase the mass transfer. Water is considered as the most desirable solvent because of its wide availability and low cost relative to other solvents, which however is not particularly effective for H_2O_2 formation as its low solubility of H_2 and O_2 (Figure 1-7 and Table 1-4). The addition of water soluble alcohol such as methanol or ethanol can significantly increase H_2O_2 productivity, H_2 conversion and H_2O_2 selectivity.[67,112,131] However, using alcohol as the reaction medium can lead to a promoted hydrogenation of H_2O_2 at long reaction time due to the high concentration

of H_2 in the solvent. Moreover, water also plays an important role as its higher solubility of H_2O_2 than alcohols. Hence, in order to effectively produce H_2O_2, careful control of the water/alcohol composition and reaction time is necessary.

Table 1-4: solubility of H_2 and O_2 in water and various alcohol at room temperature.[87]

Solvent	Solubility of H_2 (mg/L)	Solubility of O_2 (mg/L)
Water	1.62	40
Methanol	7.91	324
Ethanol	7.50	320
Isopropanol	6.92	323

Gas phase pressure is another factor directly related to the mass transfer of the reactants to the liquid phase for H_2O_2 direct synthesis. The increase of total pressure of the system increases gas solubility and decreases bubble size that is able to enhance the efficiency of mass transfer. The more H_2 and O_2 molecules dissolved in the solvent, the higher the concentration of reactants on the catalyst surface and consequently, the reaction rate is therefore enhanced.[19] Voloshin *et al.*[132], Piccinini *et al.*[67] and Freakley *et al.*[133] all observed the enhanced catalytic performance through the increase of total pressure of the system in the respect of productivity, yield and selectivity towards H_2O_2 in both flow reactor and batch mode over Au-Pd catalyst or Pd monometallic catalyst. With respect to industrial scale-up, an optimum pressure will be a compromise of equipment expense, process volume and efficiency of H_2O_2 production.

In addition, reaction temperature is another important factor for H_2O_2 direct synthesis as it is related to mass transfer of the reactants and the reaction rate of both target and side reactions. Blanco-Brieva *et al.*[134] found that operating the direct synthesis of H_2O_2 in water-methanol system with HBr as a promoter, reaction at 40 °C demonstrated more than twice yield of H_2O_2 (4.1 wt% H_2O_2) than that of the reaction conducted at 20 °C (1.7 wt% H_2O_2). In contrast, for a promoter-less system, Biasi *et al.*[135,136] demonstrated that the concentration of H_2O_2 reached the maximum at -5 °C and a minimum at 40 °C. Furthermore, Piccinini *et al.*[67] reported that in

water-methanol system, the solubility of O_2 decreases in the reaction medium and H_2 increases in methanol with the increase of reaction temperature, and hence, a higher hydrogenation rate of H_2O_2 results (Figure 1-8). Moreover, H_2O_2 is more stable at low temperature that elevated reaction temperature can lead to a decomposition of H_2O_2 towards H_2O.
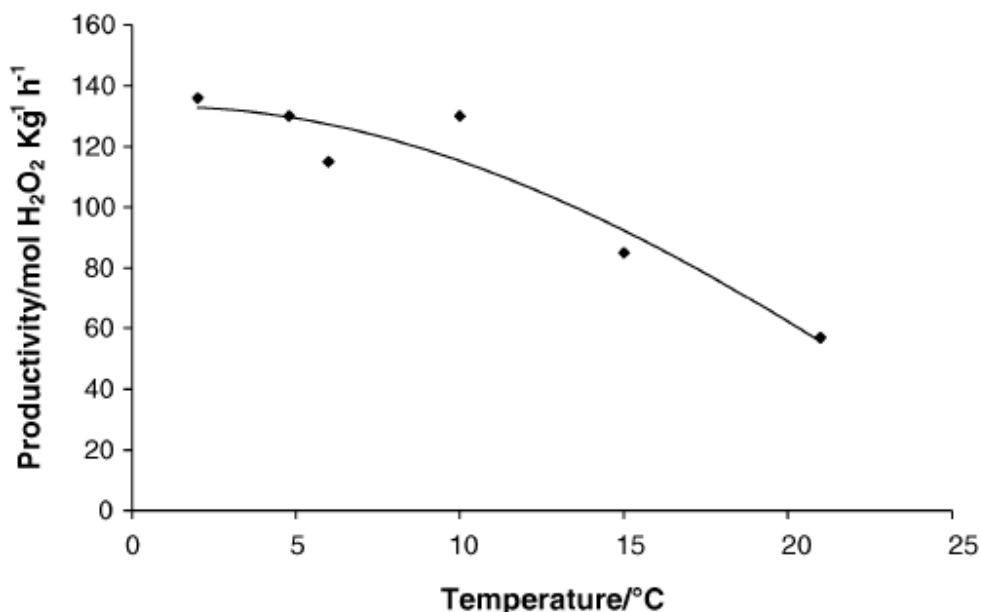
Figure 1-8: H_2O_2 productivity as a function of reaction temperature.[67] Reaction conditions: 10 mg 2.5%Au-2.5%Pd/TiO_2 catalyst, total pressure 580 psi, H_2/O_2 ratio = 0.525, 1200 rpm, 0.5 h, total mass of solvent = 8.5 g.

1.7 A summary of the mechanism studies for the direct synthesis of hydrogen peroxide

Hutchings and Moulijn proposed kinetic mechanisms for the direct production of hydrogen peroxide (Reaction equations (1)-(5)), the parallel hydrogen combustion and consecutive hydrogenation/decomposition of H_2O_2 (Reaction equations (6)-(10)) which are shown in Scheme 1-2.[67] It can be noticed that the formation of OOH is an elementary step for H_2O_2 formation. On the other hand, the dissociation of O_2 molecules into oxygen atoms will lead to the combustion of H_2 to H_2O. Through using a mixture of $^{18}O_2/^{16}O_2$ for H_2O_2 direct synthesis, Lunsford[98] demonstrated that H_2O_2 is derived from a diatomic form of oxygen as nearly no $H_2^{18}O^{16}O$ could be observed through Raman spectra. Calculations by Li *et al.*[92] for Au-Pd and Pd surface revealed that Pd [111] led to the dissociation of the O-O bond and non-

selective formation of H_2O, whereas the addition of Au inhibits dissociative adsorption of O_2. This is in agreement with the theoretical study by Ham *et al.*[137,138] that the sites of Pd surrounded by inactive Au atoms play an important role for selective formation of H_2O_2 by inhibiting the scission of the O-O bond.

(1) $\quad H_2 + 2^* \rightarrow 2H^*$ $\qquad$ (6) $\quad O_2 + 2^* \rightarrow 2O^*$

(2) $\quad O_2 + ^* \rightarrow O_2^*$ $\qquad$ (7) $\quad O^* + H^* \rightarrow OH^* + ^*$

(3) $\quad H^* + O_2^* \rightarrow OOH^* + ^*$ $\qquad$ (8) $\quad OH^* + H^* \rightarrow H_2O^* + ^*$

(4) $\quad OOH^* + H^* \rightarrow H_2O_2^* + ^*$ $\qquad$ (9) $\quad H_2O^* \rightarrow H_2O + ^*$

(5) $\quad H_2O_2^* \rightarrow H_2O_2 + ^*$ $\qquad$ (10) $\quad H_2O_2^* + ^* \rightarrow H_2O^* + O^*$
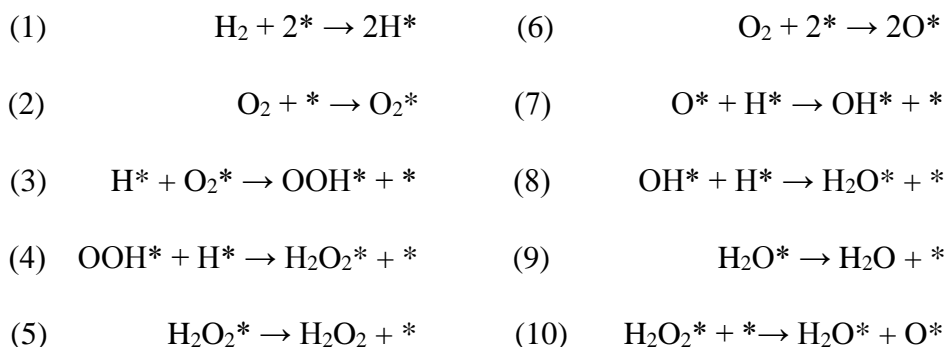
Scheme 1-2: Plausible mechanism of hydrogen peroxide synthesis from H_2 and O_2[67]

1.8 Thesis aims and outlines

1.8.1 Thesis aims

According to the statements above, one question can be raised here that if Au atoms isolated Pd towards individual Pd sites that lead to an enhanced catalytic performance, whether another inactive material alloyed with Pd also works for selective and active formation of H_2O_2? Can less expensive catalytic materials prepared through a simple method have an excellent performance for the synthesis of H_2O_2? Research into new approaches to catalyst design using cheaper materials and simpler preparation methods may help the commercialisation of the process.

The aim of the thesis is to find a cheap metal which is able to enhance the catalytic performance of supported Pd catalysts in a comparable manner to that of Au and Pt. The effect of secondary cheap metal for the direct synthesis of hydrogen peroxide also needs to be understood. Moreover, there are different drawbacks of the current, existing catalyst preparation methods for hydrogen peroxide direct synthesis. A simple effective preparation method for catalytic materials will also be investigated in this thesis.

1.8.2 Thesis outlines

First, active carbon (G60) supported Ni-Pd catalysts were prepared whose activity however interestingly increased with the time of use and over storage. Hence, an explanation of this interesting phenomenon will be pursued. Moreover, the role of Ni to Pd for the direct synthesis of H_2O_2 will also be briefly discussed through the understanding of catalytic performance and characterisations of Ni/Pd catalysts (including carbon supported 2.5 wt%Ni, 2.5 wt%Pd and 2.5 wt%Ni-2.5 wt%Pd catalysts).

The role of Ni to Pd will be further investigated through the experiments over TiO_2 (P-25) supported Ni-Pd catalysts. H_2 conversion, H_2O_2 selectivity and H_2O_2 productivity over Ni/Pd monometallic and bimetallic catalysts will be investigated in order to understand the effect of Ni to Pd for H_2O_2 direct synthesis. X-ray photoelectron spectroscopy, scanning transmission electron microscopy, temperature programmed reduction and in-situ diffuse reflectance infrared fourier transform spectroscopy with CO adsorption will be employed for both Ni-Pd and Pd only catalysts to understand the morphology change with the addition of Ni. Hence, the relation between catalytic performance and catalyst structure will be understood and the active sites for H_2O_2 will also be heuristically comprehended.

Moreover, an innovative catalyst preparation method-modified impregnation was developed by Hutchings' group[68] which is on the basis of the conventional impregnation method with excess Cl⁻ in the preparation followed by high temperature reduction to remove Cl on catalyst surface. Au-Pd catalysts prepared through this new method demonstrated outstanding activity and stability for H_2O_2 direct synthesis and prepared Au-Pd particles have been proved to be homogeneous alloys with small particle size and tight particle distribution. In this thesis, through tuning Au-Pd composition, a group of H_2O_2 synthesis results will be achieved through the whole range of Au/Pd ratio. According to the results, the effect of excess Cl⁻ can be further understood in the comparison of conventional impregnation counterpart. Furthermore, the actual active sites for the direct synthesis of H_2O_2 will be further predicted.

1.9 References

1.   J. A. Moulijn, P. W. N. M. Van Leeuwen, and R. A. Van Santen, in *Catalysis-An integrated approach to homogeneous, heterogeneous and industrial catalysis*, Elsevier, 1993, 3–21.

2.   J. Z. Fullmer, in *Sir Humphry Davy's Published Works*, Harvard University Press, Cambridge, 1969.

3.   M. Faraday, *Phil Trans.*, 1834, **124**, 55.

4.   Phillips, *GP6069*, 1831.

5.   V. Smil, *Nature*, 1999, **400**, 415.

6.   G. Ertl, H. Knözinger, F. Schüth, and J. Weitkamp, in *Handbook Of Heterogeneous Catalysis*, Wiley-VCH Verlag GmbH& Co., 2008, 1–56.

7.   G. Rothenberg, in *Catalysis-Concepts and Green Applications*, Wiley-VCH Verlag GmbH& Co., 2008, 1–35.

8.   P. Atkins and J. D. Paula, in *Atkins' Physical Chemistry*, Oxford University Press, Oxford, Seventh Ed., 2010, pp. 876–908.

9.   J. M. Campos-Martin, G. Blanco-Brieva, and J. L. G. Fierro, *Angew. Chem. Int. Ed. Engl.*, 2006, **45**, 6962–8694.

10. R. Hage and A. Lienke, *Angew. Chem. Int. Ed. Engl.*, 2005, **45**, 206–222.

11. Solvay, *http://interactivedocument.labrador-company.com/Labrador/EN/Solvay/2013AnnualReport/*, 2013.

12. D. Robinson, L. Davies, N. McGuire, D. Lee, P. McMorn, D. Willock, P. Page, D. Bethell, and G. Hutchings, *Phys. Chem. Chem. Phys.*, 2000, 1523–1529.

13. U. Schuchardt, D. Cardoso, R. Sercheli, R. Pereira, R. S. da Cruz, M. C. Guerreiro, D. Mandelli, E. V. Spinacé, and E. L. Pires, *Appl. Catal. A Gen.*, 2001, **211**, 1–17.

14. K. Kosaka, H. Yamada, K. Shishida, S. Echigo, R. A. Minear, H. Tsuno, and S. Matsui, *Water Res.*, 2001, **35**, 3587–94.

15. G. J. Hutchings, *Chem. Commun. (Camb).*, 2008, **7345**, 1148–1164.

16. C. W. Jones, in *Applications of Hydrogen Peroxide and Derivatives*, The Royal Society of Chemistry, Cambridge, 1999, 1–34.

17. H. J. Riedl, G. Pfleiderer, and I. G. Farbenindustrie, *Prod. Hydrog. Peroxide*, 1936.

18. H. J. Riedl and G. U. S. Pfleiderer, *Chem. Abstr*, 1941, **35**, 5297.

19. J. García-Serna, T. Moreno, P. Biasi, M. J. Cocero, J.-P. Mikkola, and T. O. Salmi, *Green Chem.*, 2014, **16**, 2320.

20. H. Henkel and W. Weber, in *Patent 774054*, Henkel & CIE, Germany, 1914.

21. B. Lewis and G. Von Elbe, in *Combustion, Flames and Explosion of Gases, Academic Press*, Academic Press, New York, 1961.

22. C. Samanta, *Appl. Catal. A Gen.*, 2008, **350**, 133–149.

23. T. A. Posepelova, *Russ. J. Phys. Chem.*, 1961.

24. F. Fu, K. T. Chuang, and R. Fiedorow, *Stud. Surf. Sci. Catal.*, 1992, **71**, 33–41.

25. K. P. Reis, V. K. Joshi, and M. E. Thompson, *J. Catal.*, 1996, **67**, 62–67.

26. V. Choudhary, A. Gaikwad, and S. Sansare, *Catal. Letters*, 2002, **83**, 235–239.

27. D. P. Dissanayake and J. H. Lunsford, *J. Catal.*, 2002, **206**, 173–176.

28. Y. Han and J. Lunsford, *J. Catal.*, 2005, **230**, 313–316.

29. R. Burch and P. R. Ellis, *Appl. Catal. B Environ.*, 2003, **42**, 203–211.

30. V. Choudhary and C. Samanta, *J. Catal.*, 2006, **238**, 28–38.

31. C. Samanta and V. R. Choudhary, *Chem. Eng. J.*, 2008, **136**, 126–132.

32. V. Choudhary and P. Jana, *J. Catal.*, 2007, **246**, 434–439.

33. V. R. Choudhary, C. Samanta, and P. Jana, *Appl. Catal. A Gen.*, 2007, **317**, 234–243.

34. J. K. Edwards, B. Solsona, E. N. Ntainjua, A. F. Carley, A. A Herzing, C. J. Kiely, and G. J. Hutchings, *Science*, 2009, **323**, 1037–41.

35. L. ĈERVENÝ, *Chem. Eng. Commun.*, 1989, **83**, 31–63.

36. F. Delbecq and P. Sautet, *J. Catal.*, 1995, **152**, 217-236.

37. M. Zhao and R. Crooks, *Angew. Chem. Int. Ed. Engl.*, 1999, **38**, 364–366.

38. A. Wright, A. Wong, and L. Diosady, *Food Res. Int.*, 2003, **36**, 1069–1072.

39. T. Ueno, M. Suzuki, T. Goto, T. Matsumoto, K. Nagayama, and Y. Watanabe, *Angew. Chemie*, 2004, **116**, 2581–2584.

40. S. S. Stahl, *Science*, 2005, **309**, 1824–1826.

41.   D. I. Enache, J. K. Edwards, P. Landon, B. Solsona-Espriu, A. F. Carley, A. A Herzing, M. Watanabe, C. J. Kiely, D. W. Knight, and G. J. Hutchings, *Science*, 2006, **311**, 362–365.

42.   W. Wu and H. Jiang, *Acc. Chem. Res.*, 2012, **45**, 1736–1748.

43.   L. A. Parreira, L. Menini, and E. V. Gusevskaya, *Catal. Sci. Technol.*, 2014, **4**, 2016-2022.

44.   B. Zhou and L. K. Lee (Hydrocarbon Technologies USA Inc.), *US Pat. 6,168,775*, 2001.

45.   P. Landon, P. J. Collier, A. J. Papworth, C. J. Kiely, and G. J. Hutchings, *Chem. Commun.*, 2002, 2058–2059.

46.   P. Landon, P. J. Collier, A. F. Carley, D. Chadwick, A. J. Papworth, A. Burrows, C. J. Kiely, and G. J. Hutchings, *Phys. Chem. Chem. Phys.*, 2003, **5**, 1917–1923.

47.   F. Gao and D. W. Goodman, *Chem. Soc. Rev.*, 2012, **41**, 8009–8020.

48.   S. Abate, G. Centi, S. Melada, S. Perathoner, F. Pinna, and G. Strukul, *Catal. Today*, 2005, **104**, 323–328.

49.   C. Samanta and V. R. Choudhary, *Appl. Catal. A Gen.*, 2007, **330**, 23–32.

50.   D. Dissanayake, *J. Catal.*, 2003, **214**, 113–120.

51.   W. T. Hess, in *Kirk-Othmer Encyclopedia of Chemical Technology*, Wiley, New York, Fourth Ed., 1995, 961.

52.   C. Samanta, *Appl. Catal. A Gen.*, 2008, **350**, 133–149.

53.   G. W. Hooper (ICI), *US Pat. 3,336,112*, 1967.

54.   G. W. Hooper (ICI), *US Pat. 3,361,533*, 1968.

55.   Y. Izumi, H. Miyazaki, and S. Kawahara (Tokuyama Soda KK.), *Pat. 2,528,601*, 1976.

56.   A. I. Dalton and R. W. Skinner (Air Products & Chemicals Inc.), *US Pat. 4,336,239*, 1982.

57.   L. W. Gosser (Du Pont), *EP Pat. 0 132,294 A1*, 1985.

58.   L. W. Gosser (Du Pont), *US Pat. 5,135,731*, 1992.

59.   K. T. Chuang and B. Zhou (EKA Nobel AB), *US Pat. 5,846,898*, 1998.

60.   G. Paparatto, F. Rvetti, P. Andrigo, and G. Alberti (Eni S.p.A.), *US Pat. 6,649,140*, 2003.

61.   G. Paparatto, F. Rivetti, P. Andrigo, G. Alberti, and U. Romano (Eni S.p.A.), *US Pat. 7,048,905*, 2006.

62.   V. R. Choudhary, A. G. Gaikwad, and S. D. Sansare, 2002, **83**, 235–239.

63.   J. K. Edwards and G. J. Hutchings, *Angew. Chem. Int. Ed. Engl.*, 2008, **47**, 9192–9198.

64.   V. R. Choudhary, C. Samanta, and T. V. Choudhary, *J. Mol. Catal. A Chem.*, 2006, **260**, 115–120.

65.   J. K. Edwards, B. E. Solsona, P. Landon, A. F. Carley, A. A. Herzing, C. J. Kiely, and G. J. Hutchings, *J. Catal.*, 2005, **236**, 69–79.

66.   B. E. Solsona, J. K. Edwards, P. Landon, A. F. Carley, A. Herzing, C. J. Kiely, and G. J. Hutchings, *Chem. Mater.*, 2006, **18**, 2689–2695.

67.   M. Piccinini, E. Ntainjua, J. K. Edwards, A. F. Carley, J. A. Moulijn, and G. J. Hutchings, *Phys. Chem. Chem. Phys.*, 2010, **12**, 2488–2492.

68.   M. Sankar, Q. He, M. Morad, J. Pritchard, S. J. Freakley, J. K. Edwards, S. H. Taylor, D. J. Morgan, A. F. Carley, D. W. Knight, C. J. Kiely, and G. J. Hutchings, *ACS Nano*, 2012, **6**, 6600–6613.

69.   V. R. Choudhary, C. Samanta, and P. Jana, *Ind. Eng. Chem. Res.*, 2007, **46**, 3237–3242.

70.   S. Park, S. Lee, S. Song, D. Park, S. Baeck, T. Kim, Y. Chung, S. Oh, and I. Song, *Catal. Commun.*, 2009, **10**, 391–394.

71.   S. Park, D. R. Park, J. H. Choi, T. J. Kim, Y.-M. Chung, S.-H. Oh, and I. K. Song, *J. Mol. Catal. A Chem.*, 2010, **332**, 76–83.

72.   D. R. Park, S. Park, Y. Bang, and I. K. Song, *Appl. Catal. A Gen.*, 2010, **373**, 201–207.

73.   E. N. Ntainjua, M. Piccinini, S. J. Freakley, J. C. Pritchard, J. K. Edwards, A. F. Carley, and G. J. Hutchings, *Green Chem.*, 2012, **14**, 170-175.

74.   S. J. Freakley, R. J. Lewis, D. J. Morgan, J. K. Edwards, and G. J. Hutchings, *Catal. Today*, 2014, 1–8.

75.   Y. Hiramatsu, Y. Ishiuchi, and H. Nagashima (Mitsubishi Gas Chemical Company), *US Pat. 5,236,692*, 1993.

76. E. Ntainjua N., J. K. Edwards, A. F. Carley, J. A. Lopez-Sanchez, J. A. Moulijn, A. A. Herzing, C. J. Kiely, and G. J. Hutchings, *Green Chem.*, 2008, **10**, 1162.

77. M. L. Toebes, J. A. Van Dillen, and K. P. De Jong, *J. Mol. Catal. A Chem.*, 2001, **173**, 75–98.

78. L. W. Gosser (Du Pont), *US Pat. 4,681,751*, 1987.

79. K. T. Chuang and B. Zhou (EKA Nobel AB), *WO Pat. 9,314,025*, 1993.

80. U. Luckoff, H. Paucksch, and G. Luft (Solvay Interox), *US Pat. 5,505,921*, 1996.

81. G. Paparatto, G. De Alberti, and R. Buzzoni (Eni S.p.A.), *US Pat. 6,630,118*, 2003.

82. T. Hass, G. Stochniol, and J. Rollmann (Degussa AG), *US Pat. 6,764,671*, 2004.

83. G. Paparatto, G. De Alberti, and R. Buzzoni (Eni S.p.A.), *US Pat. 7,122,501*, 2006.

84. S. Melada, R. Rioda, F. Menegazzo, F. Pinna, and G. Strukul, *J. Catal.*, 2006, **239**, 422–430.

85. V. R. Choudhary, S. D. Sansare, and A. G. Gaikwad, *Catal. Letters*, 2002, **84**, 81–87.

86. S. Chinta, *J. Catal.*, 2004, **225**, 249–255.

87. V. Krishnan, *J. Catal.*, 2000, **196**, 366–374.

88. Q. Liu and J. Lunsford, *J. Catal.*, 2006, **239**, 237–243.

89. C. Burato, P. Centomo, M. Rizzoli, A. Biffis, S. Campestrini, and B. Corain, *Adv. Synth. Catal.*, 2006, **348**, 255–259.

90. C. Samanta and V. R. Choudhary, *Catal. Commun.*, 2007, **8**, 73–79.

91. F. Menegazzo, P. Burti, M. Signoretto, M. Manzoli, S. Vankova, F. Boccuzzi, F. Pinna, and G. Strukul, *J. Catal.*, 2008, **257**, 369–381.

92. J. Li, T. Ishihara, and K. Yoshizawa, *J. Phys. Chem. C*, 2011, 25359–25367.

93. V. R. Choudhary, C. Samanta, and P. Jana, *Appl. Catal. A Gen.*, 2007, **332**, 70–78.

94. V. R. Choudhary, A. G. Gaikwad, and S. D. Sansare (Council of Scientific and Industrial Research), *US Paten 6,534,440*, 2003.

95.   C. Samanta and V. R. Choudhary, *Appl. Catal. A Gen.*, 2007, **326**, 28–36.

96.   D. Hâncu and E. J. Beckman, *Green Chem.*, 2001, **3**, 80–86.

97.   Q. Liu, K. Gath, J. Bauer, R. Schaak, and J. Lunsford, *Catal. Commun.*, 2009, **132**, 342–348.

98.   J. Lunsford, *J. Catal.*, 2003, **216**, 455–460.

99.   P. P. Olivera, E. M. Patrito, and H. Sellers, *Surf. Sci.*, 1994, **313**, 25–40.

100. G. Li, J. Edwards, A. F. Carley, and G. J. Hutchings, *Catal. Commun.*, 2007, **8**, 247–250.

101. T. Ishihara, Y. Ohura, S. Yoshida, Y. Hata, H. Nishiguchi, and Y. Takita, *Appl. Catal. A Gen.*, 2005, **291**, 215–221.

102. C. A. Jones and R. A. Grey (Arco Chemical), *US Pat. 6,468,496*, 2002.

103. M. Okumura, Y. Kitagawa, K. Yamagcuhi, T. Akita, S. Tsubota, and M. Haruta, *Chem. Lett.*, 2003, **32**, 822–823.

104. J. K. Edwards, B. Solsona, P. Landon, A. F. Carley, A. Herzing, M. Watanabe, C. J. Kiely, and G. J. Hutchings, *J. Mater. Chem.*, 2005, **15**, 4595-4600.

105. G. Li, J. Edwards, A. F. Carley, and G. J. Hutchings, *Catal. Today*, 2006, **114**, 369–371.

106. G. Li, J. Edwards, A. F. Carley, and G. J. Hutchings, *Catal. Today*, 2007, **122**, 361–364.

107. S. Ma, G. Li, and X. Wang, *Chem. Lett.*, 2006, **35**, 428–429.

108. L. W. Gosser and J. A. T. Schwartz (Du Pont), *US Pat. 4,832,938*, 1989.

109. J. Wanng.ang.rd (EKA Chemicals AB), *US Pat. 5,961,948*, 1999.

110. B. Zhou and L. Lee (Hydrocarbon Technologies USA Inc.), *US Pat. 6,168,775*, 2001, **1**.

111. B. Zhou, M. Rueter, and S. Parasher (Headwaters Nanokinetix Inc.), *US Pat. 7,011,807*, 2006.

112. M. Rueter, B. Zhou, and S. Parasher (Headwaters Nanokinetix Inc.), *US Pat. 7,144,565*, 2006.

113. T. Danciu, E. J. Beckman, D. Hancu, R. N. Cochran, R. Grey, and D. M. Hajnik, *Angew. Chem. Int. Ed. Engl.*, 2003, **42**, 1140–1142.

114. E. N. Ntainjua, S. J. Freakley, and G. J. Hutchings, *Top. Catal.*, 2012, **55**, 718–722.

115. S. Abate, S. Melada, G. Centi, S. Perathoner, F. Pinna, and G. Strukul, *Catal. Today*, 2006, **117**, 193–198.

116. S. Abate, G. Centi, S. Perathoner, and F. Frusteri, *Catal. Today*, 2006, **118**, 189–197.

117. G. Bernardotto, F. Menegazzo, F. Pinna, M. Signoretto, G. Cruciani, and G. Strukul, *Appl. Catal. A Gen.*, 2009, **358**, 129–135.

118. V. R. Choudhary, C. Samanta, and T. V. Choudhary, *Appl. Catal. A Gen.*, 2006, **308**, 128–133.

119. S. Kondrat, G. Shaw, S. J. Freakley, Q. He, J. Hampton, J. K. Edwards, P. J. Miedziak, T. E. Davies, A. F. Carley, S. H. Taylor, C. J. Kiely, and G. J. Hutchings, *Chem. Sci.*, 2012, **3**, 2965-2971.

120. J. Pritchard, L. Kesavan, M. Piccinini, Q. He, R. Tiruvalam, N. Dimitratos, J. A. Lopez-Sanchez, A. F. Carley, J. K. Edwards, C. J. Kiely, and G. J. Hutchings, *Langmuir*, 2010, **26**, 16568–16577.

121. J. K. Edwards, A. F. Carley, A. A. Herzing, C. J. Kiely, and G. J. Hutchings, *Faraday Discuss.*, 2008, **138**, 225-239.

122. L. Ouyang, G. Da, P. Tian, T. Chen, G. Liang, J. Xu, and Y.-F. Han, *J. Catal.*, 2014, **311**, 129–136.

123. A. Joshi, *J. Phys. Chem. C*, 2007, 7384–7395.

124. S. Melada, F. Pinna, G. Strukul, S. Perathoner, and G. Centi, *J. Catal.*, 2006, **237**, 213–219.

125. X. Wang, Y. Nie, J. L. C. Lee, and S. Jaenicke, *Appl. Catal. A Gen.*, 2007, **317**, 258–265.

126. R. Meiers, U. Dingerdissen, and W. F. Holderich, *J. Catal.*, 1998, **386**, 376–386.

127. R. Meiers and W. F. Holderich, *Catal. Letters*, 1999, **59**, 161–163.

128. J. Xu, L. Ouyang, G.-J. Da, Q.-Q. Song, X.-J. Yang, and Y.-F. Han, *J. Catal.*, 2012, **285**, 74–82.

129. Q. Liu and J. H. Lunsford, *Appl. Catal. A Gen.*, 2006, **314**, 94–100.

130. V. R. Choudhary, C. Samanta, and P. Jana (Council of Scientific and Industrial Research), *US Pat. 7,288,240*, 2007.

131. Y. Han and J. Lunsford, *Catal. Letters*, 2005, **99**, 13–19.

132. Y. Voloshin and A. Lawal, *Appl. Catal. A Gen.*, 2009, **353**, 9–16.

133. S. J. Freakley, M. Piccinini, J. K. Edwards, E. N. Ntainjua, J. A. Moulijn, and G. J. Hutchings, *ACS Catal.*, 2013, **3**, 487-501.

134. G. Blanco-Brieva, E. Cano-Serrano, and J. M. Campos-Martin, *Chem. Commun.*, **10**, 2004, 1184–1185.

135. P. Biasi and N. Gemo, *Ind. Eng. Chem. Res.*, 2012, **51**, 8903–8912.

136. N. Gemo, P. Biasi, P. Canu, and T. O. Salmi, *Chem. Eng. J.*, 2012, **207-208**, 539–551.

137. H. Ham, G. Hwang, and J. Han, *J. Phys. Chem. C*, 2009, **113**, 12943–12945.

138. H. C. Ham, J. A. Stephens, G. S. Hwang, J. Han, S. W. Nam, and T. H. Lim, *Catal. Today*, 2011, **165**, 138–144.

Chapter 2

Experimental

2.1 Outline

A series of mono- and bi-metallic Ni, Au and Pd catalysts supported on active carbon (G60), TiO_2, SiO_2, CeO_2 and graphite were synthesized and evaluated for the direct synthesis of hydrogen peroxide. In this chapter, catalyst precursors, reaction reagents, catalyst preparation, reaction procedure and characterization techniques are discussed.

2.2 Reagents

2.2.1 Catalyst Precursors

Table 2-1 Summary of catalyst precursors

Compound	Chemical Formula	Purity / Assay	Manufacturer
Nickel nitrate hexahydrate	$Ni(NO_3)_2 \cdot 6H_2O$	99.99% trace metals basis	Sigma Aldrich
Nickel chloride hexahydrate	$NiCl_2 \cdot 6H_2O$	99.99% trace metals basis	Sigma Aldrich
Palladium chloride	$PdCl_2$	99.99% trace metals basis	Sigma Aldrich
Palladium nitrate	$Pd(NO_3)_2$	Pd assay: 40%	Sigma Aldrich
Hydrogen tetrachloroauric acid	$HAuCl_4 \cdot 3H_2O$	Au assay: 41.21%	Johnson Matthey

2.2.2 Supports

Table 2-2 Summary of supports for catalyst preparation

Support	Type	Manufacturer
Carbon	G-60 / Activated	Darco
TiO_2	P-25	Degussa
SiO_2	200-500 µm particles, 60A^o pore size	Acros Organics
CeO_2	<5 µm particles	Aldrich

2.2.3 Reaction liquids (provided by Sigma Aldrich)

Table 2-3 Summary of reaction solvents, liquids and relevant details

Reagent	Details
Water	HPLC grade
MeOH	HPLC grade
50% H_2O_2 (aq)	Stabilised
$(NH_4)_2Fe(SO_4)_2 \cdot 6H_2O$	98% purity

2.2.4 Gases

All gases were obtained from BOC Gases or Air Products Ltd. Gas purities are listed below:

Table 2-4: Summary of utilized gases and associated purities.

Gas	Purity
25% O_2/CO_2	99.99%
5% H_2/CO_2	99.99%
5% H_2/Ar	99.95%
10% H_2/Ar	99.95%
N_2	99.95%

2.3 Catalyst preparation

2.3.1 Conventional Impregnation

The procedure to prepare 0.5 g of a 2.5 wt% Ni-2.5 wt% Pd catalyst is outlined as follows, 0.0313 g $Pd(NO_3)_2$ (Pd assay: 40%) and 0.0619 g $Ni(NO_3)_2 \cdot 6H_2O$ (or 0.0506 g $NiCl_2 \cdot 6H_2O$) were dissolved in deionized water while stirring at 80 ºC until the salts dissolved completely. 0.475 g support was then added to the solution with constant stirring at 80 ºC until slurry formed. The material was dried at 110 ºC for 16 h and subsequently heat-treated in various atmospheres at 400 ºC or higher temperature for 3 h with a ramp rate of 20 ºC/min. Ni or Pd monometallic catalysts were synthesized using the same method. 1 wt% Au-Pd/TiO_2 conventional impregnation catalysts in Chapter 5 were also prepared by the stated method, yet $PdCl_2$ salt dissolved in $HAuCl_4 \cdot 3H_2O$ as a clear solution was used as the precursor. Any changes of the preparation for particular catalysts will be specified in result chapters.

2.3.2 Modified Impregnation

The procedure to prepare 1 g of catalyst by the modified impregnation method is outlined as follows; 0.2810 ml $HAuCl_4 \cdot 3H_2O$ (8.9 mg/ml) and 0.05 ml $PdCl_2$ (6.0 mg/ml) solutions were added to a 50 ml round bottom flask. Herein, $PdCl_2$ solution was made of $PdCl_2$ dissolved in 0.58 M HCl with a final concentration of 6 mg/ml.

The volume of the mixture of Au-Pd solution was then adjusted with deionised water to a total volume of 8 ml. The solution was stirred (1000 rpm) at a temperature of 60 °C for 10 minutes. 0.99 g support was added slowly into the solution over 8-10 mins with constant stirring followed by a 15 min additional stirring at 60 °C. The temperature was raised to 95 °C with the constant stirring at 1000 rpm for 16 h in order to dry the slurry thoroughly. Subsequently, the solid was carefully ground to a uniform fine mixture using a mortar and pestle. A 0.4 g portion of this mixture was then reduced under a flow of 5% H_2/Ar at 400 °C for 4 h with a ramp rate of 10 °C/min.

2.4 Catalyst Evaluation

2.4.1 Hydrogen Peroxide Synthesis

Catalysts were tested in Parr stainless steel autoclave with maximum working condition of 100 ml volume and 14 MPa pressure, which was equipped with an overhead stirrer, a cooling system and a real time monitor for the measurement of temperature and pressure. For standard reaction conditions for the direct synthesis of hydrogen peroxide, the autoclave was charged with 10 mg catalyst, 2.9 g HPLC grade water and 5.6 g MeOH resulting in 8.5 g reaction solvent in total. 3 MPa 5% H_2/CO_2 was purged three times followed by 2.9 MPa 5% H_2/CO_2 and 1.1 MPa 25% O_2/CO_2 as reactants. 30 min stirring with a 1200 rpm speed was started when the reactor was cooled down to 2 °C. After the reaction, reactant gases were purged into a gas analysis bag and subsequently analysed by Gas Chromatography (GC) in order to determine both the H_2 conversion and H_2O_2 selectivity. The calculations involved in this step are described in detail in chapter 2.4.4. The reaction solution was immediately filtered, aliquots weighed and titrated by acidified $Ce(SO_4)_2$ standard solution, using $(NH_4)_2Fe(SO_4)_2 \cdot 6H_2O$ ferroin indicator for hydrogen peroxide yield determination. H_2O_2 molarity and catalyst productivity were determined for each reaction using the following equations:

$$2Ce^{4+} + H_2O_2 \rightarrow 2Ce^{3+} + 2H^+ + O_2 \qquad \textbf{(Equation 2-1)}$$
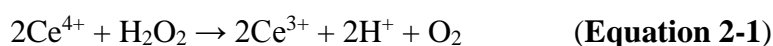
$$\text{Volume } Ce(SO_4)_2 \text{ to titrate whole reaction solution (ml)} = \frac{V_{Ce(SO_4)_2} \text{ for part of the solution (ml)} \times 8.5g}{\text{the mass of the part of the solution (g)}}$$

$\qquad\qquad\qquad\qquad\qquad\qquad\qquad\qquad\qquad\qquad$ **(Equation 2-2)**

$$\text{Moles Ce(SO}_4)_2 = \frac{V_{\text{Ce(SO}_4)_2}(\text{ml}) \times [\text{Ce(SO}_4)_2]}{1000}$$

(**Equation 2-3**)

$$\text{Moles H}_2\text{O}_2 = \frac{\text{Moles Ce(SO}_4)_2}{2}$$

(**Equation 2-4**)

$$\text{H}_2\text{O}_2 \text{ Productivity } \left(\text{mol}_{\text{H2O2}} \text{ kg}_{\text{catalyst}}^{-1} \text{h}_{\text{reaction}}^{-1}\right) = \frac{\text{Moles H}_2\text{O}_2}{10 \times 10^{-6} \text{ kg} \times 0.5 \text{ h}}$$

(**Equation 2-5**)

2.4.2 Hydrogen Peroxide Hydrogenation

For hydrogen peroxide hydrogenation rate, catalysts were also tested in a stainless steel autoclave which was identical to the one used for the direct synthesis. The reactor was charged with 10 mg catalyst, 0.68 g 50 wt% H_2O_2, 2.22 g H_2O and 5.6 g MeOH. 3 MPa 5% H_2/CO_2 was purged three times followed by 2.9 MPa 5% H_2/CO_2. 30 min stirring with a 1200 rpm speed was started when the reactor was cooled down to 2 °C. The concentration of H_2O_2 in solvent before and after reaction was determined by acidified $Ce(SO_4)_2$ solution with $(NH_4)_2Fe(SO_4)_2 \cdot 6H_2O$ ferroin indicator for hydrogenation productivity determination.

2.4.3 Catalyst Stability Tests

The autoclave was charged with 50 mg catalyst, followed by a standard synthesis procedure. Reacted catalyst was filtered, washed with deionised water, dried at room temperature overnight, and lastly placed into the oven and heated at 110 °C for 1 h. The catalytic performance of the used catalyst was tested and compared with that of the fresh catalyst to determine reusability.

2.4.4 Gas Chromatography (GC) for the analysis of H_2 conversion and H_2O_2 selectivity

Chromatography based on differences in partitioning behaviour between a flowing mobile phase and stationary phase is a technique for separating and analysing a mixture of chemical substances. Gas Chromatography (GC) is one of the most common analytical techniques used to analyse gaseous mixtures or compounds that

can be easily vaporized. It is able to provide both qualitative and quantitative information about the mixture and also identify impurities.[1]

A GC system typically involves a mobile phase, a stationary phase, detector and a computer data system. A carrier gas as the mobile phase containing the mixture to be separated is passed through a sample loop and injected into the stationary phase known as a column which is held at a specific temperature by an oven. Due to the distinct interaction between different species and the column, the components leave the column at different times (known as the retention time), and enter the detector. A thermal conductivity detector (TCD) is the most commonly used detector for GC, and records differences between the thermal conductivities of the carrier gas and the component being eluted from the column. A schematic of a typical GC system is shown in Figure 2-1.
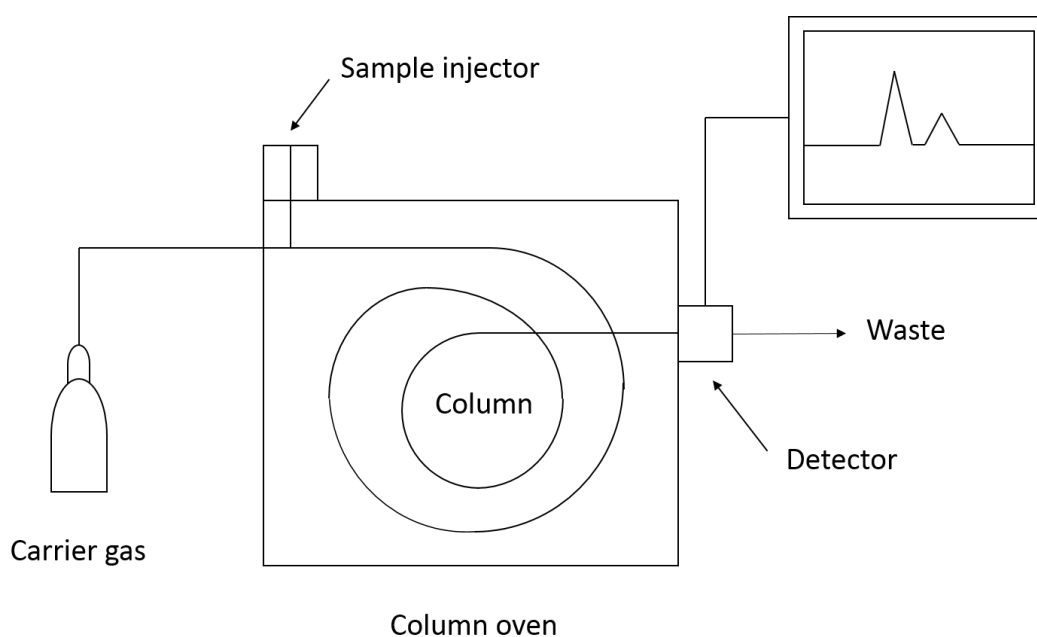
Figure 2-1: Diagram of a gas chromatograph

A Varian 3800 GC fitted with a TCD was used to analyse the gas mixture obtained from H_2O_2 direct synthesis. The GC was equipped with a 4 m molecular sieve 5 Å column, using Ar as the carrier gas, with a flow rate of 30 ml/min. Given CO_2 does not directly participate in H_2O_2 synthesis (the amount both before and after reaction is constant), it was used as the internal standard for the integration of the change in H_2 concentration. The column oven was held at 40 $^{\circ}$C for 15 mins to allow separation of H_2, O_2 and CO_2, and then increased to 200 $^{\circ}$C at 25 $^{\circ}$C/min to

effectively eliminate the moisture from the column. The retention time of the components analysed for hydrogen peroxide synthesis is shown in Table 2.5.

Table 2-5: Summary of the retention time of the components for the direct synthesis of hydrogen peroxide

Component	Retention time (min)
H_2	1.4
O_2	2.7
CO_2	7.2

An average area ratio of H_2 and CO_2 attained from more than three blank standard reactions without catalyst (namely blank $ratio_{H2/CO2}$) were first determined as the basis for the calculation of both H_2 conversion and H_2O_2 selectivity. The relevant equations are described below, and the total moles of H_2 was calculated according to the ideal gas law − $P\,V = n\,R\,T$, (where P is the absolute pressure of the gas, V is the volume of the gas, n is the moles of substance of gas, R is the ideal gas constant, and T is the absolute temperature of the gas.)

$$H_2 \text{ conversion (\%)} = \frac{\text{Blank ratio}_{H2/CO2} - \text{ratio}_{H2/CO2}}{\text{Blank ratio}_{H2/CO2}} \times 100\%$$

(**Equation 2-6**)

$$H_2O_2 \text{ selectivity (\%)} = \frac{\text{moles } H_2O_2}{H_2 \text{ conversion (\%)} \times \text{total moles of } H_2} \times 100\%$$

(**Equation 2-7**)

2.5 Catalyst Characterization

2.5.1 Thermo-Gravimetric Analysis (TGA)

Thermo-gravimetric analysis (TGA) can be used to track the variation of physical and chemical properties of a material as a function of increasing temperature, or a function of time, in an atmosphere of air, nitrogen, helium or under a vacuum. TGA can provide the information about physical phenomena including vaporization, absorption and desorption, and also can reflect the information of chemical

variations including chemisorption, decomposition and oxidation.[2] In this thesis TGA was used to evaluate the thermal stability of a material as negligible mass loss indicates the thermal stability of a species in a desired temperature range.

TGA was performed using a Seteram TG-DTA, 30-40 mg of sample was placed in an aluminium crucible which was heated to 400 $^{\circ}$C for 3 hours at a ramp rate of 20 $^{\circ}$C/min under air or nitrogen atmosphere. Mass variation, temperature and heat flow were measured to a high degree of accuracy by a detector within the instrument.

2.5.2 Microwave Plasma-Atomic Emission Spectrometer (MP-AES)

Microwave plasma-atomic emission spectrometry (MP-AES) is used to determine the concentration of a particular element in a sample. MP-AES is based on atomic emission techniques used for the quantitative determination of a specific wavelength of a given element emitted from microwave plasma. The microwave magnetically excited nitrogen plasma provides high frequency electromagnetic radiation in the GHz range that is capable for exiting electrodeless gas discharge. Excited atoms subsequently transit back to lower energy states (including the ground state) that are able to emit redundant energy in the form of a photon. Different elements provide the radiation with specific wavelengths and frequencies, and the intensity of the spectral line is directly proportional with atomic concentration in the sample. The detector determines the particular wavelength and a computer data system converts the attained spectral line into quantified information. Concentration measurements are usually determined from a working curve after calibrating the instrument with standards of known concentrations. Figure 2-2 demonstrates a schematic of a MP-AES.
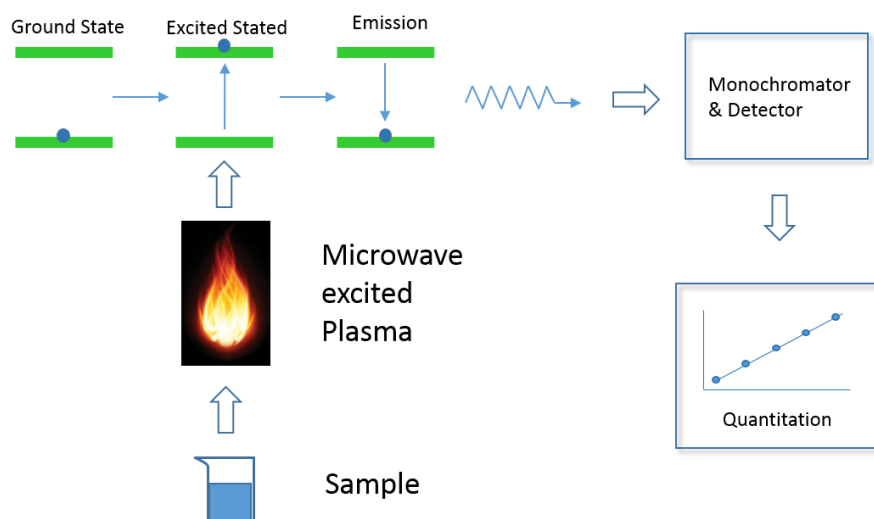
Figure 2-2: Schematic of a microwave plasma-atomic emission spectrometer.

MP-AES was performed on an Agilent 4100 MP-AES. Ni- and Pd-containing samples were determined by average results at the wavelengths of 341.48, 352.45 and 361.94 nm for Ni and 340.46, 360.96 and 363.47 nm for Pd. 30 mg samples were digested in concentrated nitric acid, followed by a dilution with deionised water to a total volume of 50 ml. MP-AES was used to determine the wt% of the metal loaded on the support after impregnation, and also the Ni and Pd content of the used catalysts in order to determine the amount of metal leaching during reaction by comparison against the values obtained for fresh catalysts.

2.5.3 Temperature programmed reduction (TPR)

Temperature programmed reduction (TPR) is a technique to analyse the reduction kinetics of oxide species. Through heating the sample with a linear temperature ramp in a flow of hydrogen, the consumption of hydrogen will be monitored simultaneously by a TCD. Fingerprint profiles (usually the TCD signal plotted against temperature) can be obtained to indicate the reducibility of oxide species, as a positive peak in the TCD signal means H_2 consumption. TPR can give an indication of the initial species present on the catalyst. In addition, it can also provide information on the extent of interaction between species such as the interaction between individual metal oxide components and the support through analysing the shape of the peaks and the shift of the maximum.[3]

TPR profiles were recorded using a Micromeritics Autochem 2910. The sample (0.1 g) was loaded into a quartz tube and pre-treated in He (40 ml/min) up to a temperature of 300-400 $^\circ$C (depended on the catalyst studied) for 1 h before cooling back to room temperature. After the stabilization of TCD signal under testing atmosphere – 10% H_2/Ar (10 ml/min) the sample was then reduced under the same atmosphere and flow rate while increasing the temperature using a ramp rate of 10 $^\circ$C/min until it reached 1000 $^\circ$C. The profile was recorded using a TCD with positive polarity.

2.5.4 X-ray photoelectron spectroscopy (XPS)

X-ray photoelectron spectroscopy (XPS) is a highly-sensitive quantitative spectroscopic technique that measures chemical and electronic state of the elements that exist on the surface of a material. By irradiating a material with X-ray beam, XP spectra can be attained while simultaneously measuring the kinetic energy and the number of electrons that escape from the top layers (0 to 10 nm depth) of the material. The basic components of XPS are demonstrated in Figure 2-3.

With a monochromatic beam of X-rays of given frequency (ν), photons are absorbed by an atom in a molecule or solid, leading to ionization and the emission of a core (inner shell) electron. The kinetic energy distribution of the emitted photoelectrons can be measured by an electron energy analyser and then a photoelectron spectrum can be recorded. Using the equation as follows (Equation 2-8), binding energy can be obtained which is characteristic information associated with each core atomic orbital of each and every element. The presence of peaks at particular energies therefore indicates the presence of a specific element on the surface of a material of particular electronic environment, and moreover, the intensity of the peaks is related to the concentration of the element within the sampled region.

$$\text{Binding energy} = h\nu - \text{kinetic energy} \qquad (\textbf{Equation 2-8})$$

h = Planck's constant; ν = X-ray frequency.[4]
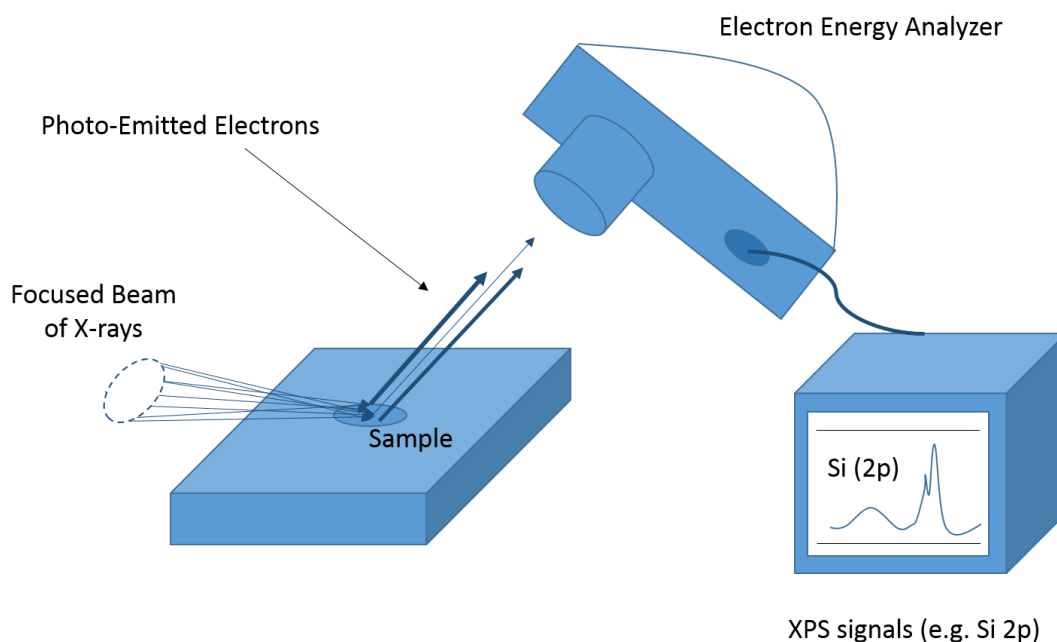
Figure 2-3: Basic components of a monochromatic XPS system.

XPS was performed by a VG EscaLab 220i spectrometer, using a standard Al-K_α X-ray source (300W) and analyzer pass energy of 20 eV. Double-side adhesive tape was used for sample mounting, and the binding energy of C (1s) was used as reference, which was determined as 284.7 eV.

2.5.5 Powder X-ray Diffraction (XRD)

X-ray Diffraction (XRD) is a technique for providing information of bulk crystallite structure including phase identification, unit cell size determination, crystallite size and morphological analysis, which can be achieved by measuring the angles and intensities of diffracted X-ray beams. X-rays are generated from bombarding a copper target with high energy electrons. Generated X-rays are passed through a monochromator to achieve a particular wavelength and directed at the packed sample. With the spinning of the sample plate at a degree of Ө, the detector are moved at twice speed - 2 Ө which is demonstrated in Figure 2-4.
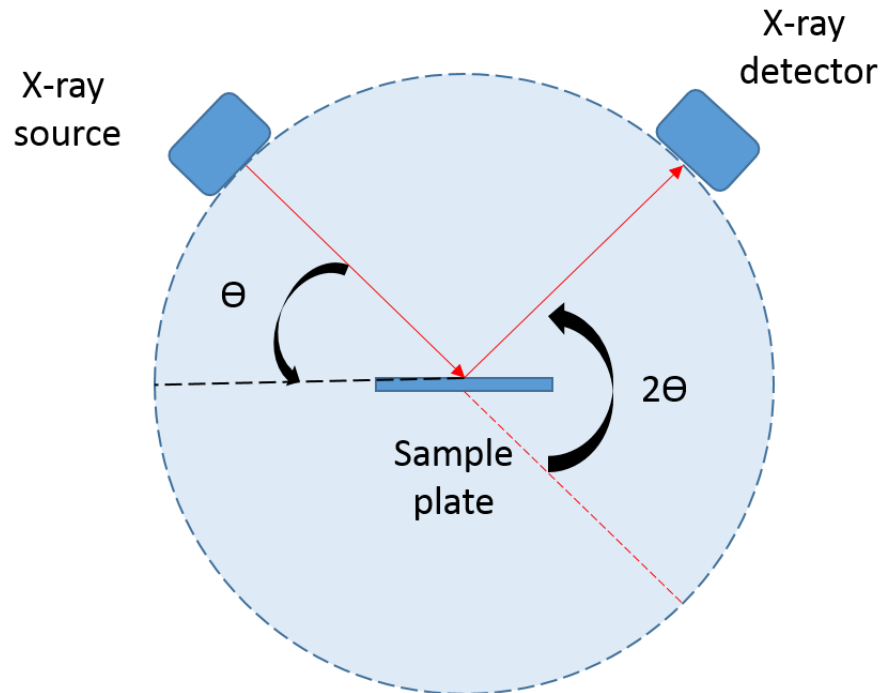
Figure 2-4: Diagram for an X-ray diffractometer setup.[5]

When the monochromatic source hits the sample, it will be scattered by the atomic planes. The X-rays scattered from adjacent planes will constructively interfere when the distance of the angle θ between the plane and the X-ray is equal to an integer number of wavelengths, namely AB + BC = nλ, which is shown in Figure 2-5. Hence, it is possible to calculate the lattice spacing of the crystallite using the Bragg relationship (Equation 2-9). Each different crystallite has reflections at a unique set of angles, θ.

$$n\lambda = 2d_{hkl}\sin\theta \qquad\qquad (\textbf{Equation 2-9})$$

n = an integer, λ = X-ray wavelength, d = lattice spacing, θ = angle between incident and normal to the plane.
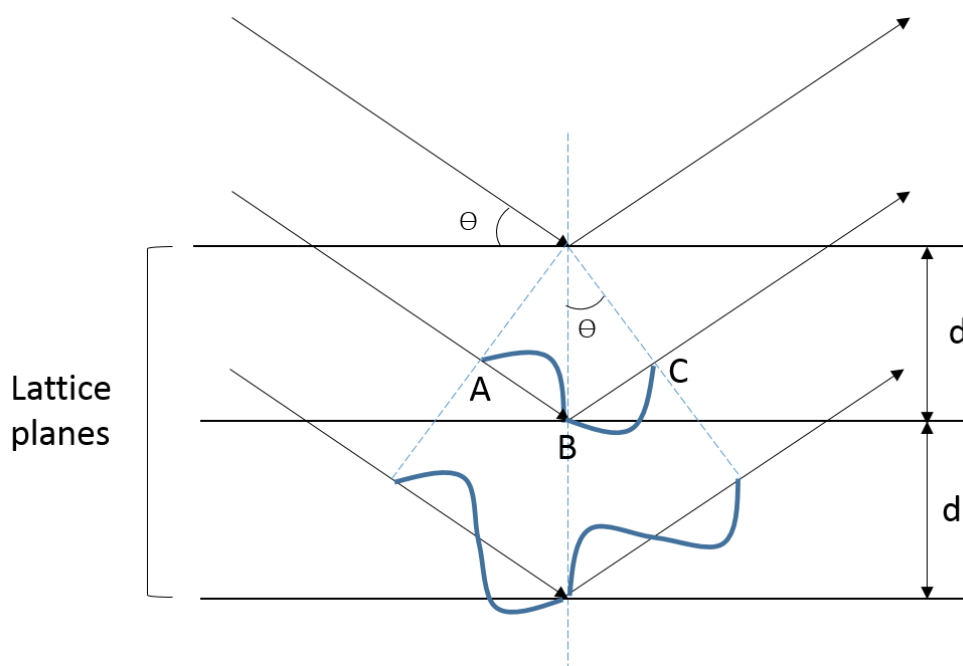
Figure 2-5: Scheme describing the Bragg relationship.

For small crystallite, incomplete destructive interference gives rise to line broadening. Hence, the information about crystallite size can be integrated from the shape of the peaks as an inverse relation between average crystallite size and the peak broadening. Using the Scherrer equation, shown as Equation 2-10, an average crystallite size can be estimated:

$$\tau = \frac{K\lambda}{\beta \cos\theta}$$ (**Equation 2-10**)

τ = the mean size of the ordered (crystalline) domains; K = dimensionless shape factor; λ = X-ray wavelength; β = the line broadening at half the maximum intensity (FWHM); θ = the Bragg angle.

Investigation of the bulk structure of the catalytic materials was carried out using a (θ-θ) PANalytical X'Pert Pro powder diffractometer using a Cu K$_\alpha$ radiation source operating at 40 KeV and 40 mA. Standard analysis was performed using a 40 minute scan between 2θ values of 10-80°, with the samples supported on an amorphous silicon wafer. Diffraction patterns of phases were identified using the ICDD database.

2.5.6 CO Chemisorption

Pulse chemisorption is a technique based on the adsorption of a molecule such as CO on metals without chemisorption taking place on the surface of the support material, and therefore the number of the exposed metal atoms on a supported catalyst can be selectively determined. The metal dispersion can be calculated through dividing the number of adsorbed molecules by the total number of metal atoms:

$$\text{Dispersion (\%)} = \frac{n \times \text{moles of adsobed CO}}{\text{moles of total metal atoms}} \times 100\%$$

(Equation 2-11)

n = stoichiometric number of CO and metal atom

Chemisorption analysis was performed using a Micromeritics Autochem 2910. The surface of the catalyst was cleaned in-situ at 300 ^{o}C for 1 h using He (40 ml/min). The sample was then cooled to 150 ^{o}C and exposed to 10% H_2/Ar (20 ml/min) for 1 h in order to reduce the surface. This was followed by flowing He (40 ml/min) through the sample at a temperature of 150 ^{o}C for 1 h in order to get rid of the excess adsorbed H_2 on the metal. The catalyst was then cooled to room temperature and again under a flow of He (30 ml/min), CO was sequentially injected in the system every 10 minutes using a 70 µL loop once the TCD signal was stable. After a certain number of pulses, no amount of the injected gas was adsorbed and peaks with the same area were recorded. The number of surface metal sites was then calculated assuming stoichiometric factor of absorption equal to 1 for CO and Pd, for instance. The loop volume was calibrated by manual injections.

2.5.7 *In situ* Diffuse Reflectance Infrared Fourier Transform Spectroscopy (DRIFTS) for CO adsorption

Infrared (IR) spectroscopy is based on the principle that molecules absorb radiation with specific frequencies which are characteristic of their structure. These absorptions match the frequency of i.e. the transition energy of the bond or group that vibrates whose energy is determined by the shape of the molecule, the masses of the atoms and the vibronic coupling.[6] A basic IR spectrum is a function of IR absorbance/transmittance on the vertical axis and frequency/wavelength on the horizontal axis.

Infrared Fourier Transform Spectroscopy (DRIFTS)[7] is a special application of IR which is suitable for heterogeneous samples or powders and solids. In comparison to other IR techniques, only the diffusely scattered radiation from the sample is collected by a mirror, and by this, the surface species of a material can be investigated. To record the infrared spectrum of a given sample, it is necessary to measure both the sample and a reference. This is because each measurement is affected by not only the light-absorption properties of the sample, but also the properties of the instrument.

DRIFTS combined with CO adsorption was conducted since CO binds spontaneously to many surfaces, with C-O bond stretching typically giving rise to intense and sharp infrared absorption peak(s).[8] From the absorption frequency of this band, the location of the adsorbate at either: on-top, two-fold or multi-fold adsorption sites can be deduced, and hence, it is a powerful technique for the investigation of metal morphology on the surface of a material.

A reference or sample was mounted in a test chamber followed by N_2 (15 ml/min) pretreatment at 110 ^{o}C for 1 h to desiccate the sample. The adsorption experiment was then conducted at room temperature, and the measurements started with exposure to the background gas (N_2, 12 ml/min), followed by the test gas (CO, 3 ml/min). An IR spectrum was recorded on a TENSOR27 Bruker IR instrument every 60 s until the shape of the spectrum did not change, indicating that the metal surface was saturated with CO. The spectrum recorded during exposure to the background gas was used as the reference spectrum.

2.5.8 Scanning Transmission Electron Microscopy (STEM)

Scanning Transmission Electron Microscopy (STEM) is a high-performance technique for studying nanostructures and providing a range of different imaging modes with the ability to yield information on elemental composition and electronic environment of atoms to a high degree of sensitivity. It is a form of Transmission Electron Microscopy (TEM), where a highly accelerated electron beam is transmitted through a sufficiently thin specimen. STEM, however, is distinguished from conventional transmission electron microscopes by focusing the electron beam into a narrow spot which is scanned over the sample. This allows for simultaneous

operation of elemental analysis techniques, including mapping by X-ray Energy Dispersive Spectroscopy (XEDS) and High Angle Annular Dark Field (HAADF) imaging.[9]

XEDS identifies an element through detecting the precise amount of energy produced by an X-ray caused by the movement of excited electrons from an outer atomic shell to the inner shell (Figure 2-6). It allows elemental analysis since this energy difference is elemental specific. A detector measures the energy values of the characteristic X-rays generated within the microscope before an X-ray microanalysis system converts X-ray energy into an electron count. A spectrum based on the chemical analysis of the sample can be formed using this electron count data, indicating which elements are present from a given k_α value.
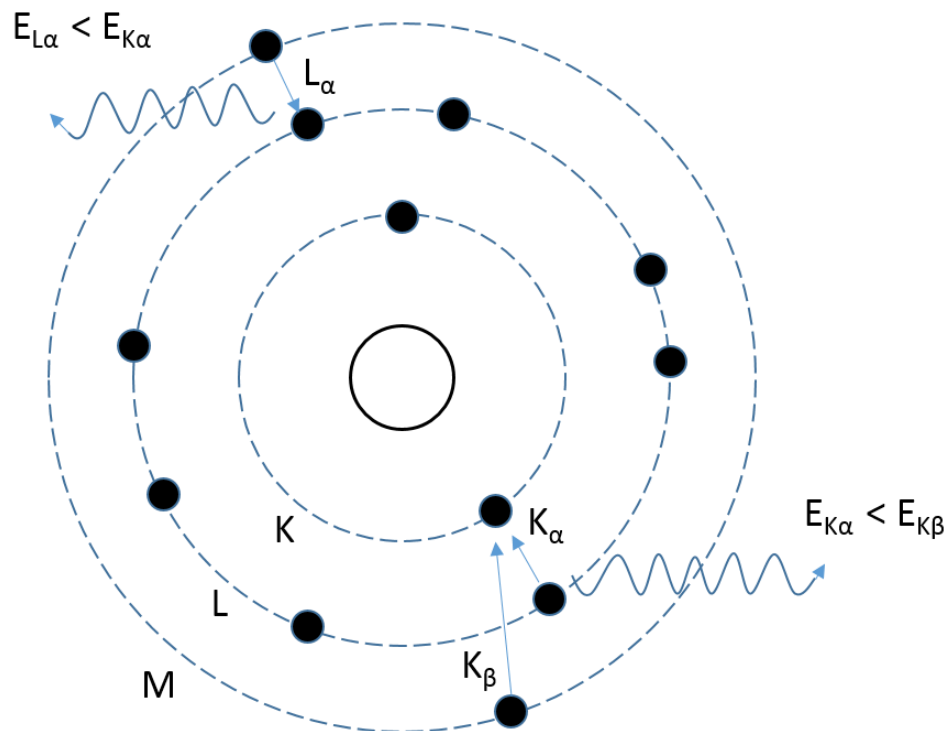
Figure 2-6: Diagram illustrating the principles of XEDS.

Figure 2-7 demonstrates the principle of the formation of bright field (BF), dark field (DF) and high angle annular dark field (HAADF) images. Referring to the figure, a BF image is formed by both unscattered electrons from the incident beam and scattered electrons, while a DF image can be only formed from scattered electrons results. DF images give rise to a higher level of contrast than that produced in BF

although longer exposure time to the incident beam is required. By using a STEM and a high-angle detector, the contrast of HAADF images is directly related to the atomic number of atoms, as a result, it is possible to form atomic resolution images where the contrast is highly dependent on the atomic number (Z-contrast image).
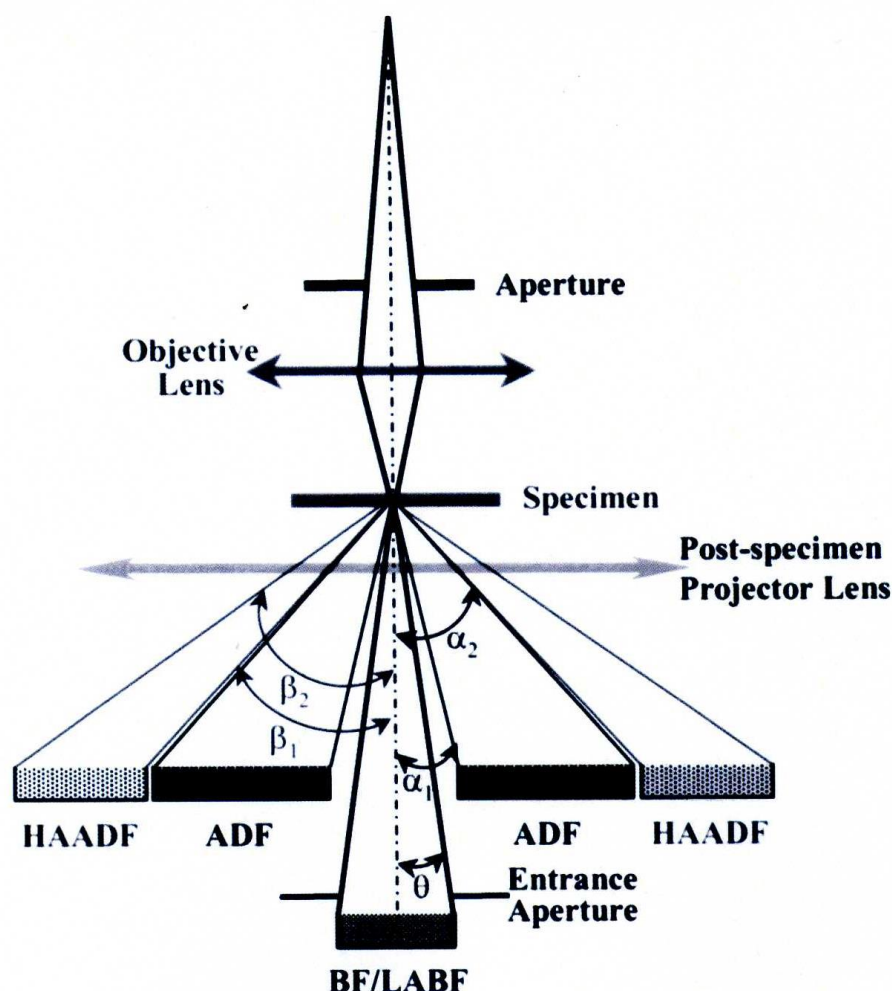
Figure 2-7: Scheme of BF and DF of a STEM.[10]

All the STEM analysis was conducted by Li Lu and Sultan Althahban at Lehigh University, Pennsylvania, USA. Samples for TEM and STEM analysis were prepared by dispersing the catalyst in high-purity ethanol onto a holey carbon film supported by a 300-mesh copper grid. Samples were then subjected to BD diffraction contrast imaging and XEDS using a JEOL 2200 FS TEM operating at 200 kV. The further characterization using HAADF was conducted for the detection of any highly dispersed metallic species in JEOL 2200 FS TEM operating at 200 kV and equipped with a CEOS probe corrector. A sub-set of samples were examined in an aberration

corrected JEOL 2200 FS TEM operated in STEM-HAADF imaging and STEM-XEDS modes at 200 kV for the analysis of the structural and compositional details of individual nanoparticles.

2.6 References

1.   G. Schwedt, *Essential Guide To Analytical Chemistry*, Wiley and Sons, 1997.

2.   A. Coats and J. Redfern, *Analyst*, 1963, **1**.

3.   R. Bochum, T. Chemie, and D.- Bochum, 2001, 4633–4638.

4.   T. L. Barr, in *Modern ESCS: The Principles and Practice of X-ray Photoelectron Spectroscopy*, CRC Press, 1994.

5.   S. Lowell, *An Introduction to Power Surface Area*, John Wiley & Sons Ltd., 1979.

6.   D. A. Skoog, F. J. Holler, and S. R. Crouch, in *Principles of Instrumental Analysis*, David Harris, 6th edn., 2007, 430.

7.   C.-P. S. Hsu, *Handbook of Instrumental Techniques for Analytical Chemistry*, Prentice-Hall, 1997.

8.   Y. Wong and R. Hoffmann, *J. Phys. Chem.*, 1991.

9.   M. T. Otten, *Journal of electron microscopy technique*, 1991, **17**, 221.

10.   M. Watanabe, D. W. Ackland, C. J. Kiely, D. B. Williams, M. Kanno, R. Hynes, and H. Sawada, *JEOL news*, 2006, **41**, 2–7.

Chapter 3

Carbon supported Ni-Pd catalysts for the direct synthesis of hydrogen peroxide

3.1 Outline

All the supported catalysts described in this chapter were prepared on active carbon (G60) by the conventional impregnation method described in Chapter 2 using water soluble precursors. H_2O_2 synthesis and hydrogenation tests were carried out according to the testing procedures outlined in Chapter 2 unless otherwise stated. A summary of the testing conditions has been given below:

- Rate of H_2O_2 production determined after reaction using the standard reaction conditions: 5% H_2/CO_2 (2.9 MPa) and 25% O_2/CO_2 (1.1 MPa) , 8.5 g solvent (5.6 g MeOH and 2.9 g H_2O), 0.01 g catalyst, 2 $^{\circ}$C, 1200 rpm, 30 mins.

- Rate of hydrogenation of H_2O_2 calculated from the amount of H_2O_2 hydrogenated using standard reaction conditions: 2.9 MPa 5%H_2/CO_2, 8.5 g solvent (5.6 g MeOH, 2.22 g H_2O and 0.68 g 50%H_2O_2), 0.01 g catalyst, 2 $^{\circ}$C, 1200 rpm, 30 mins.

3.2 Screening of metal additives to Pd catalysts for the direct synthesis of hydrogen peroxide

Transition metals demonstrate outstanding catalytic properties for hydrogenation and oxidation reactions.[1] The aim of this study is to find an alternative to gold as an additive to Pd for the direct synthesis of hydrogen peroxide. The direct formation of H_2O_2 is in fact a hydrogenation reaction of O_2 rather than an oxidation reaction of H_2 as there is no scission of the O–O bond.[1] Hence, three non-noble transition metals - Cu, Zn and Ni were first selected, as they have been reported to be active for particular hydrogenation reactions[2–5], and also they sit in the same or neighbouring group to active precious metals Au and Pd. Cu and Zn as a secondary metal in Pd catalysts have been reported to be active and selective for hydrogenation reactions such as the hydrogenation/isomerization of but-1-ene,[2] the hydrogenation of CO_2 to C1-C7 hydrocarbons[3] and acrylonitrile to acrylamide.[6] Ga was also investigated, since it demonstrated excellent hydrogenation reactivity in some cases.[7–9] Moreover, Ni is able to activate and dissociate H_2 for a number of hydrogenation reactions.[5,10,11] In addition, M. Nystrom et al. stated that less active material for instance Ni is able to increase the selectivity of the direct synthesis of hydrogen peroxide in some processes.[12]

In this work, a group of M-Pd/C (M = Cu, Zn, Ga or Ni) bimetallic catalysts and M/C (M = Cu, Zn, Ga, Ni or Pd) monometallic catalysts were first screened to find out active catalysts or effect secondary metal to Pd. The Pd precursor used was a solution of $PdCl_2$ dissolved in HCl acidified water with final metal concentration of 6 mg/ml. All the other metal precursors used were metal nitrates, as they are soluble salts in water. Samples

were calcined at 400 °C for 3 h in air and evaluated for the direct synthesis of hydrogen peroxide in high pressure autoclaves under standard reaction conditions described previously.

Table 3-1 shows the productivity and hydrogenation rate of hydrogen peroxide over the catalysts described above, among which Cu, Zn and Ga monometallic catalysts demonstrated limited productivity for hydrogen peroxide synthesis. With the introduction of Pd, all the bimetallic catalysts - M-Pd/C (M = Cu, Zn or Ga) demonstrated lower H_2O_2 productivity relative to that of Pd monometallic sample. Moreover, the hydrogenation activities of H_2O_2 over the bimetallic samples were also lower than that of Pd only catalyst. Hence, a conclusion can be made here that none of Cu, Zn or Ga was active material for the direct synthesis of hydrogen peroxide prepared through the stated method and the evaluation under the described reaction conditions.

Pure Ni catalyst was active for generating H_2O_2 but at a very limited rate, and also it was not active for one of the side reactions-H_2O_2 hydrogenation as which demonstrated half activity of that over carbon support. With the addition of Pd, the bimetallic catalyst demonstrated a greater production rate than that of either Ni or Pd monometallic catalysts. In addition, according to Table 3-1, the addition of Ni to Pd suppressed hydrogenation rate of H_2O_2 from 503 mol $kg_{cat.}^{-1}$ h^{-1} for the monometallic Pd catalyst to 241 mol $kg_{cat.}^{-1}$ h^{-1}. Hence, Ni was chosen as additive metal to Pd for further investigation as a catalyst for the synthesis of hydrogen peroxide synthesis in this thesis.

Table 3-1: Results summary of several supported catalysts on carbon for the direct synthesis of hydrogen peroxide

Catalyst	H_2O_2 productivity [c] $(mol_{H2O2}\,kg_{cat.}^{-1}\,h^{-1})$	Hydrogenation productivity $(mol_{H2O2}\,kg_{cat.}^{-1}\,h^{-1})$
C	0	80
5 wt% Pd[a]/C	90	503
2.5 wt% Pd[a]/C	65	473
5 wt% Cu/C	0	-
2.5 wt% Cu[b]-2.5 wt% Pd[a]/C	0	141
5 wt% Zn/C	2	-
2.5 wt% Zn[b]-2.5 wt% Pd[a]/C	48	141
5 wt% Ga/C	3	60
2.5 wt% Ga[b]-2.5 wt% Pd[a]/C	59	100
5 wt% Ni[b]/C	4	40
2.5 wt% Ni[b]-2.5 wt% Pd[a]/C	104	241

[a] Pd precursor was $PdCl_2$ dissolved in HCl.

[b] The precursors of additive metals were nitrate salts.

[c] Production rate was based on catalyst weight otherwise stated.

Heat treatment: 20 °C/min, 400 °C, 3 h, static air

3.3 The standardisation of the preparation method for supported Ni on carbon

In order to standardise the preparation conditions, studies into various precursors and heat treatments were investigated as follows.

3.3.1. Precursors

For initial studies, the Pd precursor used for the preparation of monometallic and bimetallic catalysts was $PdCl_2$ dissolved in HCl. However, according to our previous work[13] which will be discussed in detail in Chapter 5, the addition of HCl in the impregnation procedure can assist the solubility of $PdCl_2$ and metal dispersion after the heat treatment. The concentration of HCl can also affect stability of the catalyst. In order to simplify the investigation and remove the effect of residual chloride, a water soluble precursor - $Pd(NO_3)_2$ was chosen as $PdCl_2$ has very limited solubility in water.

3.3.2. Heat treatments

As has been previously reported, heat treatment is an essential step in the catalyst preparation procedure,[14,15] which are crucial in optimising the decomposition of metal precursors and also can enhance metal-metal and metal-support interactions, thereby, enhancing catalytic performance and stability. Moreover, different utilized atmosphere of heat treatments may result in various oxidation states of the particles whose effect on the direct synthesis of hydrogen peroxide will be discussed in this thesis later. In order to compare the performance of Ni-Pd catalysts with that of Au-Pd catalysts under the same conditions as our previous publications,[16] 400 ºC calcination under static air was used (Table 3-1) which was high enough for the decomposition of Ni and Pd precursors.[17,18] Metals such as Pd and Ni can however act as catalysts which are able to catalyse the combustion of carbon during calcinations.[19] Hence, TGA was used to investigate the catalyst weight loss during heating, which was carried out under static air at 400 ºC for 3 hours with a ramp rate of 20 ºC/min. According to the attained results in Figure 3-1, the bimetallic sample demonstrated 75% mass loss under static air, however, nearly no mass loss could be observed for active carbon. This infers Ni and Pd did act as catalysts for carbon ignition during calcination. When TGA of the bimetallic catalyst was carried out under N_2 at 400 ºC for 3 hours with a ramp rate of 20 ºC/min, 10% mass

loss was observed. Hence, in order to avoid ignition happening during the heat treatment with loss of the carbon support, N_2 was chosen as an inert atmosphere which can protect the carbon support at 400 ^{o}C.

It is worth noting that the results in Table 3-1 are eligible because no catalyst demonstrated over 10 wt% weight loss after calcination was tested for the reaction, nevertheless TGA over carbon supported Ni-Pd catalyst proved that static air was not suitable for the heat treatment over 400 ^{o}C relative to N_2. 10 wt% was calculated from the mass difference between nitrate salts with metal oxides after decomposition in 2.5 wt% Ni-2.5 wt% Pd catalyst.
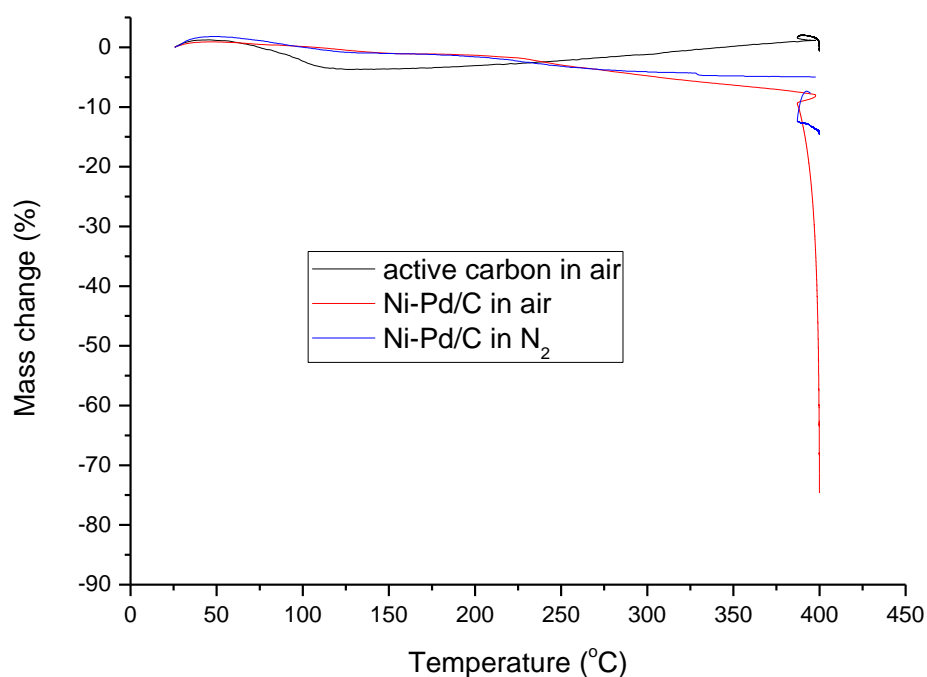
Figure 3-1: TGA results for Ni-Pd/C catalysts which were treated under static air or N_2 (precursors: $Ni(NO_3)_2$ and $Pd(NO_3)_2$)

In conclusion, to simplify our investigation, $Pd(NO_3)_2$ was chosen as the Pd precursor and soluble salts - $Ni(NO_3)_2$ would be used as the nickel precursor. For carbon-supported catalysts, a N_2 heat treatment at 400 ^{o}C was chosen which is sufficient for the decomposition of precursors without the combustion of the carbon support.[17,18]

3.4 The "synergistic effect" of Ni and Pd for the direct synthesis of hydrogen peroxide

3.4.1. Ni-Pd catalysts for the direct synthesis of hydrogen peroxide

Ni, Pd monometallic and bimetallic catalysts were prepared through the procedure stated in Chapter 2, and tested for the direct synthesis of H_2O_2 and H_2O_2 hydrogenation reactions. As we can see in Table 3-2, 2.5 wt% Pd/C was active for H_2O_2 synthesis; whereas very limited activity for peroxide synthesis was demonstrated over Ni monometallic catalyst. When Ni was used a secondary metal to Pd giving a 5 wt% bimetallic catalyst, an enhanced H_2O_2 productivity was observed, which was more active than either 2.5 wt% Ni/C or 2.5 wt% Pd/C monometallic samples. Furthermore, for hydrogenation productivity, the addition of Ni to Pd suppressed the activity from 766 mol kg^{-1} h^{-1} to 642 mol kg^{-1} h^{-1}. In summary of the results in Table 3-2, Ni as a second metal added to Pd, improved the production rate of hydrogen peroxide direct synthesis, and simultaneously, suppressed the activity of one side reaction-H_2O_2 hydrogenation.

Table 3-2: Results summary of C supported Ni/Pd monometallic and bimetallic catalysts for the direct synthesis of hydrogen peroxide

Catalyst*	H_2O_2 productivity (mol$_{H2O2}$ kg$_{cat.}^{-1}$ h^{-1})	Hydrogenation productivity (mol$_{H2O2}$ kg$_{cat.}^{-1}$ h^{-1})
2.5wt%Ni/C	1	39
2.5wt%Pd/C	18	766
2.5wt%Ni 2.5wt%Pd/C	40	642

*Heat treatment: 20 °C/min, 400 °C, 3 h under N_2

3.4.2. Characterisation

3.4.2.1. Microwave Plasma-Atomic Emission Spectrometer (MP-AES)

The metal loadings of the catalysts reported in the previous tables were theoretical values based on calculations, but during the preparation process it is possible that the whole amount of precursors were not loaded onto supports. Hence, MP-AES was used

to investigate the actual metal loading of the catalysts. 30 mg of 2.5 wt% Ni-2.5 wt% Pd/C, 2.5 wt% Pd/C and 2.5 wt% Ni/C were digested in concentrated nitric acid and then diluted to 50 ml solutions for the analysis. The concentrations determined from the analysis are listed in Table 3-3. According to the results, the actual Ni loading was similar as the theoretic amount, but for Pd there was around 50% mass loss during the impregnation. Hence, one possible reason to explain this phenomena is part of Pd remained in the containers during the preparation. In addition, the actual loading of Pd in both bimetallic and monometallic catalysts is similar which indicates that the enhanced productivity for hydrogen peroxide synthesis over bimetallic catalyst was not caused by the variation of Pd loading. This result further demonstrates the positive effect of adding Ni to Pd catalysts for hydrogen peroxide direct synthesis.

Table 3-3: Summary of actual metal loadings on active carbon support according to MP-AES

Catalyst	Productivity (mol kg$_{cat.}$$^{-1}$ h^{-1})	Theoretical value (wt%)		Actual loading (wt%)	
		Ni	Pd	Ni	Pd
Ni-Pd/C fresh	40	2.5	2.5	2.35	1.28
Pd/C fresh	18	-	2.5	-	1.36
Ni/C fresh	1	2.5	-	2.23	-

3.4.2.2. X-Ray Diffraction (XRD)

X-ray diffraction was used to determine the presence of crystalline materials in the catalysts. The active bare carbon support, 2.5 wt% Ni/C, 2.5 wt% Pd/C and 2.5 wt% Ni-2.5 wt% Pd/C were analysed after 400 °C heat treatment under N$_2$ for 3 h. As shown in Figure 3-4, no reflections assigned to Ni species could be observed in the mono and bimetallic samples that suggests no crystalline Ni species were formed after 400 °C heat treatment. For both Pd mono and bimetallic samples, the pattern showed sharp reflections indexed as [111], [200], [220] and [311] at a Bragg angle of 40.3°, 46.8°,

68.3° and 82.4° respectively, which indicates crystalline metallic Pd was formed after the heat treatment.[20] The reflections of Pd in the bimetallic catalyst were broader than those of Pd monometallic sample. According to Scherrer Equation, a broader full width half maximum represents a smaller mean size of crystals. Calculated mean size and corresponding phases are summarized in Table 3-4. With the addition of Ni, the mean size of Pd(0) was decreased from 32 nm to 19 nm suggesting that Ni helped to disperse Pd particles in the comparison with Pd monometallic catalyst. Powder XRD has a limitation of being able to detect average crystal size from 5 nm to 100 nm. So the mean size determined in this case does not include the crystals/particles smaller than 5 nm; however, the results obtained still suggest the addition of Ni to some extent, resulted in a greater dispersion of Pd.
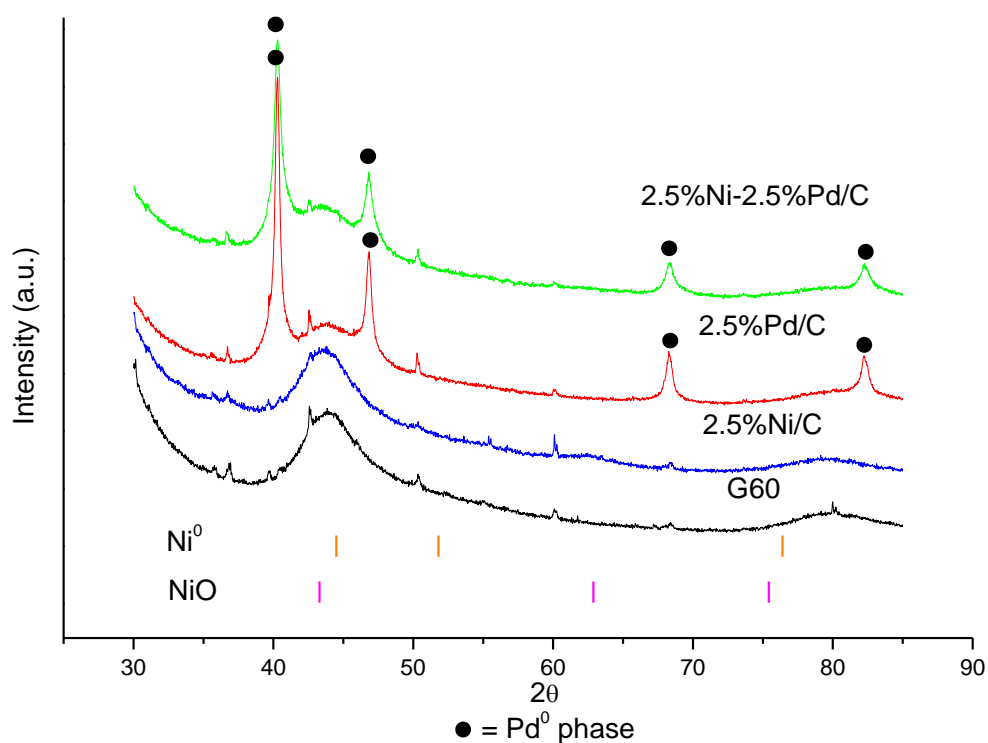

Figure 3-2: XRD patterns for Ni and Pd monometallic and bimetallic catalysts including the principle reflections of Ni^0 and NiO.[21,22]

Table 3-4: Average crystallite size for the crystals in carbon supported Ni/Pd catalysts

Sample	Metal phase	Average crystallite size (nm)
2.5 wt% Ni/C	Ni	not detected
2.5 wt% Pd/C	Pd^0	32
2.5 wt%Ni-2.5 wt% Pd/C	Pd^0	19

3.4.2.3. X-ray Photoelectron Spectroscopy(XPS)

XPS analysis was used to determine the oxidation state and atomic ratio of the elements on the catalyst surface. Figure 3-3 shows Pd 3d and Ni 2p XPS spectra of the mono and bimetallic samples, and corresponding binding energy and atomic ratio on the surface are listed in Table 3-5 and 3-6. As seen in Figure 3-3, the Ni 2p spectra for both Ni/C and Ni-Pd/C show a complex structure with an intense satellite signal for high binding energy adjacent to the main peaks, which is attributed to multi-electron excitation (shake-up peaks).[23] For the bimetallic Ni-Pd/C sample, the Ni $2p_{3/2}$ spectrum can be fitted into three distinguishable peaks at binding energies of 856.4 eV, 854.6 eV and 852.9 eV which correspond to NiOOH, NiO and Ni(0) respectively.[24] For Ni/C, the Ni $2p_{3/2}$ can be fitted to two distinguishable peaks at binding energies of 856.2 and 854.4 eV and assigned to NiOOH and NiO. The calculated atomic ratio of these Ni species are shown in Table 3-5.

For the Pd 3d spectrum of both Pd/C and Ni-Pd/C samples (Figure 3-4), two peaks relating to the Pd $3d_{5/2}$ and $3d_{3/2}$ states, respectively were observed as a result of spin-orbital splitting.[23] The binding energy of ca. 335.5 eV is attributed to Pd(0), suggesting that the Pd species were present in the metallic form in these catalysts. In the Pd $3d_{5/2}$ spectrum, the binding energy ascribed to Pd(0) was centred at 335.5 and 335.7 eV respectively.
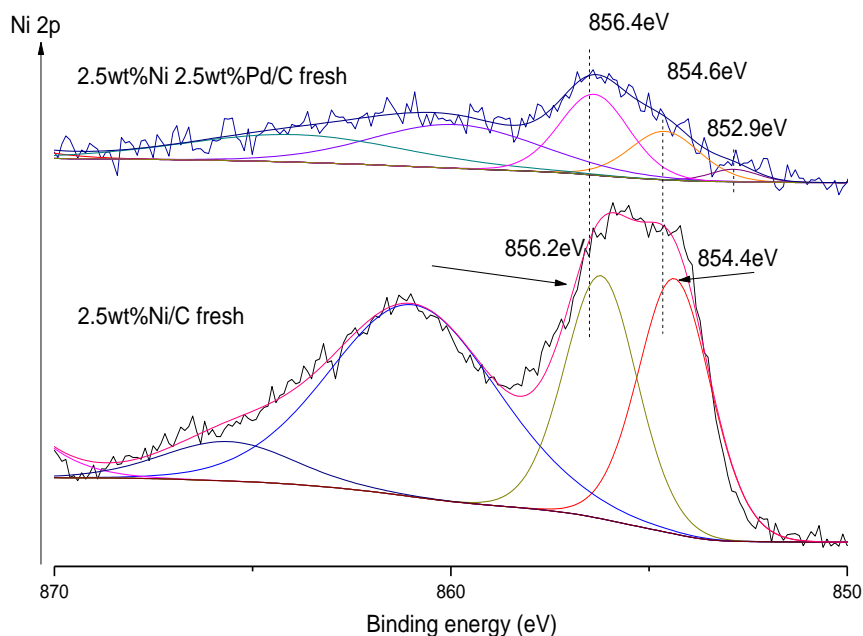
Figure 3-3: The Ni 2p spectra of Ni, Pd monometallic and bimetallic catalysts

It is worth noting that in the bimetallic sample, both binding energies of Ni^{3+} in NiOOH and Ni^{2+} in NiO shifted to higher values compared with those of monometallic sample. The binding energy 852.9 eV of Ni^0 in the bimetallic sample is higher than that of previous research-852.6 eV.[25] This is consistent with the results obtained from the Pd 3d XPS that the binding energy of Pd shifted to lower values compared with the spectra of monometallic catalysts, implying the possibility of electron transfer from Ni to Pd. Since the electronegativity of Pd is 2.3 which is higher than 1.8 of Ni by the Gordy and Thomas scale.[25]

The intensity of the Ni spectrum in the bimetallic catalyst is lower than that of the monometallic catalyst (Figure 3-3 (right)). In addition, the surface Ni/Pd molar ratio for Ni-Pd/C sample was much lower than the total Ni/Pd ratio determined by MP-AES analysis (Table 3-6). Integrated with XRD result - no reflection assigned to crystallite Ni could be observed, it suggests that in the Ni-Pd particles, amorphous Ni was present below the surface and Pd metal enriched outside of the particles. According to Table 3-6, a small amount of Cl species was detectable on the surface of all these three samples.

Since both precursors were nitrate salts which were dissolved in deionized water, this trace amount of Cl was only possible the impurity from carbon support.
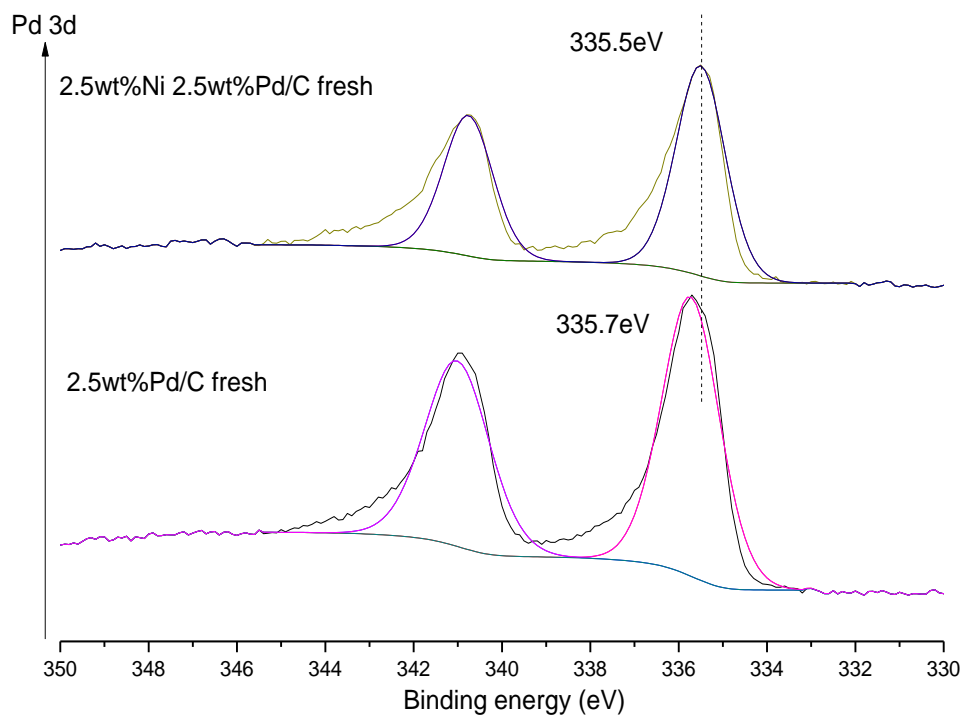
Figure 3-4: The Pd 3d spectra of Ni, Pd monometallic and bimetallic catalysts

Table 3-5: Ni and Pd oxidation states on the catalyst surface according to XPS analysis

Catalyst	H_2O_2 productivity $(mol_{H2O2}kg_{cat.}^{-1}h^{-1})$	B.E. / eV			
		Pd(3d)	Ni(2p) including at%		
		Pd^0	Ni^{3+}	Ni^{2+}	Ni^0
2.5%Ni/C Fresh	1	---	856.2	854.4	-
			51.0%	49.0%	-
2.5%Pd/C Fresh	18	335.7	---		
2.5%Ni2.5%Pd/C Fresh	40	335.5	856.4	854.6	852.9
			56.0%	34.5%	9.5%

Table 3-6: Summary of surface atom percentage for Ni-Pd catalysts

Catalyst	2.5 wt% Ni/C		2.5 wt% Pd/C		2.5 wt% Ni-2.5 wt% Pd/C fresh	
	Peak	At%	Peak	At%	Peak	At%
	Pd 3d	-	Pd 3d	3.12	Pd 3d	1.28
	Ni 2p	3.39	Ni 2p	-	Ni 2p	0.67
XPS Information	O 1s	11.00	O 1s	8.55	O 1s	7.33
	C 1s	85.52	C 1s	88.2	C 1s	90.63
	Cl 2p	0.08	Cl 2p	0.13	Cl 2p	0.09
Ni/Pd atomic ratio (bulk)	-		-		7:2*	
Ni/Pd atomic ratio (surface)	-		-		1:2	

*Determined by MP-AES

In summary of XPS analysis over Ni/C, Pd/C and Ni-Pd/C samples, it is suggested that i) for Pd content catalysts, metallic Pd existed on the sample surface, ii) integrated with MP-AES and XRD results, the surface ratio of Ni/Pd over the bimetallic catalyst indicates the Pd metal could be present on the top of the particles with amorphous Ni beneath, and the Ni species were present in multiple oxidation states. Metallic Ni was detected in the bimetallic sample whereas in the monometallic samples only oxidised Ni species were observed. Moreover, electron transfer from Ni to Pd may occur according to the spectra of Ni 2p and Pd 3d. Both imply that there is probably dissolution of Ni in Pd to some extent.

3.4.2.4. Temperature Programmed Reduction (TPR)

TPR has been used to analyse the reducibility of the species in carbon supported catalysts. The Ni/Pd monometallic and bimetallic catalysts were investigated and the

results are shown in Figure 3-5. Observed in all of the TPR profiles was a broad H_2 consumption peak between 600 °C and 800 °C, which were attributed to the reduction of the functional groups on carbon support[26] and gasification of active carbon respectively.[27,28]
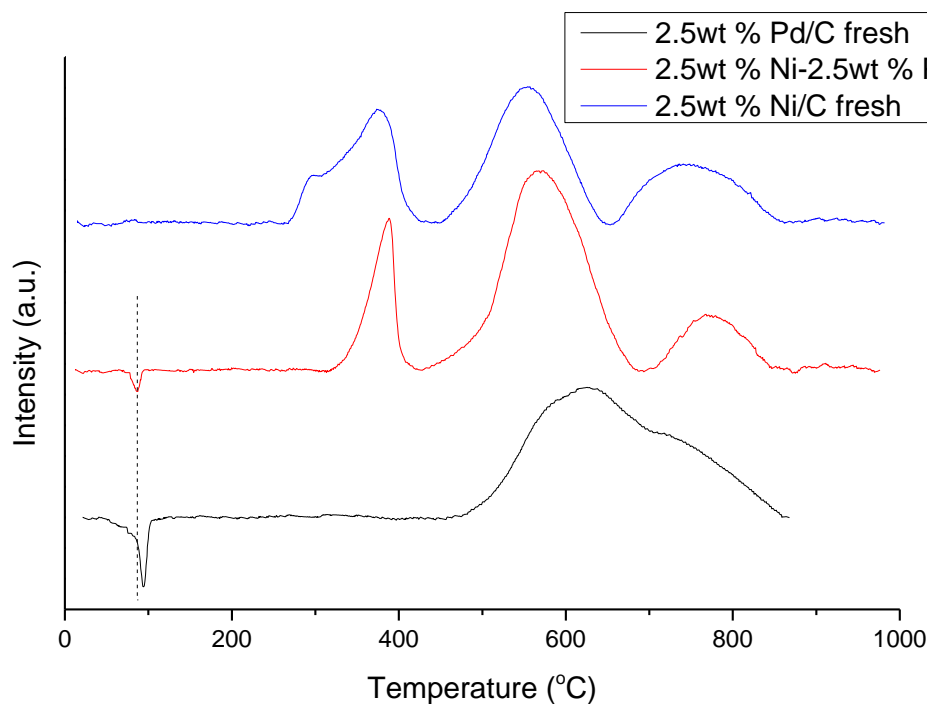

Figure 3-5: TPR results for Ni/Pd monometallic and bimetallic samples

The signals centred lower than 500 °C provide the information of the supported metals- Ni and Pd. For the profile of the Ni-Pd bimetallic sample, a single positive peak with a maximum at 387 °C is observed in the H_2 TPR pattern of NiO whereas that of Ni monometallic sample shows two adjacent peaks, one of which centred near 300 °C was assigned to the reduction of Ni^{3+} to Ni^{2+} and the other at 377 °C corresponded to the reduction of NiO to metallic nickel.[29] According to the integrated information in Table 3-7, with the addition of Pd, the peak area of the NiO_x reduction in the bimetallic catalyst was supressed by 42% in the comparison with that of monometallic sample indicating the existence of metallic Ni in the Ni-Pd catalyst. This is in agreement with XPS results which shows the existence of metallic Ni in the bimetallic sample whereas only oxidised Ni species were observed in the monometallic samples. It also can be

noticed that the peak assigned to Ni^{3+} disappeared after adding Pd to Ni. Both of the observations infer the interaction of Ni and Pd in the bimetallic catalyst.

Table 3-7: Integrated information of the TPR results over 2.5 wt% Ni/C, 2.5 wt% Pd/C and 2.5 wt% Ni-2.5 wt% Pd/C catalysts

Catalyst	Sample weight (mg)	NiO$_x$	β-PdH$_x$	
		Peak area	Peak position (^{o}C)	Peak area
2.5 wt% Ni/C	50	759	-	-
2.5 wt% Pd/C	50	-	95.0	90
2.5 wt% Ni-2.5 wt% Pd/C	50	443	85.4	18

For the Pd content catalysts, no reduction signals for Pd species can be observed in the corresponding patterns indicating the metallic state of Pd in these two samples. This observation is consistent with the results from XRD and XPS.

Furthermore, negative signals centred below 100 ^{o}C can be observed in the patterns of Ni-Pd/C and Pd/C samples which corresponded to the decomposition of β-PdH$_x$. However, obviously suppressed intensity and dissociation temperature of the β-PdH$_x$ signal were demonstrated in the pattern of the bimetallic sample. According to the integrated results shown in Table 3-7, with the addition of Ni to Pd, the decomposition of β-PdH$_x$ demonstrated 9.6 ^{o}C negative shift from 95.0 ^{o}C and 80% area loss on the basis of TCD signal. According to our present knowledge of the β-PdH$_x$ phase in supported palladium suggests that the position, shape and intensity of the peak should depend on different variables, among which Pd dispersion, type of support and modifying additives play a dominant role.[30] The same kind of support was used which can be excluded for explaining the difference here. However, the lower shifting of decomposition temperature indicates the interaction of Ni and Pd.[5] This is consistent with several investigations that Pd hydrides are not stable when Pd is present as alloys with another metals, and more prone to decompose at lower temperature than the

hydrides of pure Pd.[31,32] As for the suppressed intensity of Pd hydride decomposition, it can be explained in two ways. Firstly, better dispersed palladium absorbs lower amount of H_2 than large palladium particles which was proved by different techniques.[33,34] For instance, F. Pinna and co-workers[35] proved that with the increase of Pd dispersion, x in β-PdH$_x$ decreases which was determined from the shift of XRD Pd [111] peak after hydride formation. The study by XRD has shown Pd crystals in the bimetallic sample are smaller than those in Pd only sample which provides a support of this hypothesis.

In summary of the TPR analysis, reducible Ni species in the monometallic sample contained Ni^{3+} and NiO species, whereas, in the bimetallic sample, only NiO was detected. Moreover, H_2 consumption of NiO_x in the bimetallic catalyst was significantly suppressed compared with that in Ni monometallic catalyst indicating the formation of metallic Ni after adding Pd. In addition, Pd in both samples was metallic. The decomposition peaks of Pd hydride also strongly indicate the interaction of Ni and Pd in these catalysts.

3.5 The stability of carbon catalyst

3.5.1. Catalyst performance for the direct synthesis of hydrogen peroxide

Due to the nature of catalyst preparation method and hydrogen peroxide synthesis system, heterogeneous catalysts were operated in three phase mixture that catalyst components can leach into the reaction solvent leading to changes in catalytic activity. In order to investigate catalyst stability, fresh, usedX1 and usedX2 catalysts were prepared and tested under standard conditions for H_2O_2 synthesis and hydrogenation, and obtained results are shown in Figure 3-6. As we can see, with increasing number of uses for hydrogen peroxide synthesis, the productivity increased substantially from 40 mol kg^{-1} h^{-1} to 81 mol kg^{-1} h^{-1}. Simultaneously, side reaction rate-hydrogenation productivity was suppressed from 642 mol kg^{-1} h^{-1} to 352 mol kg^{-1} h^{-1}.

When we stored the materials in sealed containers in the dark for 12 months under ambient conditions, superior catalytic performance was also achieved compared with the fresh samples as shown in Table 3-8. As seen, both aged Ni-Pd bimetallic catalyst and

Pd only catalyst demonstrated superior H_2O_2 productivity and suppressed hydrogenation rate relative to their fresh analogues.
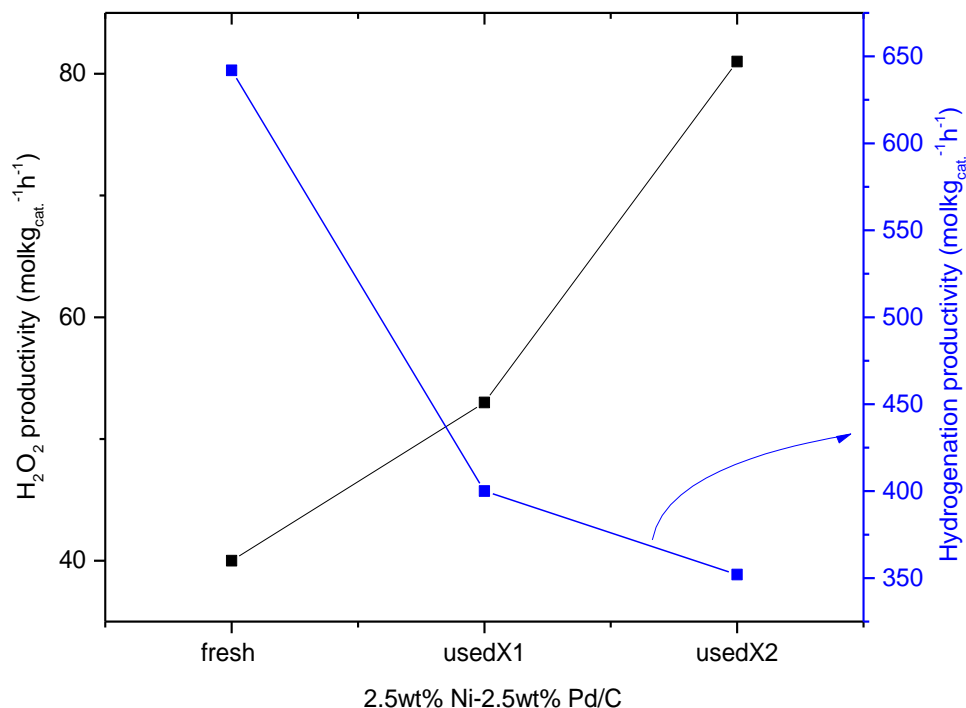

Figure 3-6: Reusability test for Ni-Pd/C fresh and used catalysts: (**Black**: productivity for hydrogen peroxide formation; **Blue:** hydrogenation rate for hydrogen peroxide)

Pd monometallic catalysts with various metal loadings were also prepared and tested for the hydrogenation rate based on the weight of Pd. As shown in Figure 3-7, with the increase of metal loading, hydrogenation rate decreases remarkably from 4.2×10^4 to 2.3×10^4 mol $kg_{Pd}^{-1} h^{-1}$.

It was observed that both the use for hydrogen peroxide synthesis and storage of the catalyst enhanced the catalytic performance of monometallic and bimetallic Ni:Pd carbon catalysts. Moreover, with the increase of Pd metal loading, the hydrogenation rate of H_2O_2 based on the weight of Pd was suppressed substantially. MP-AES, XRD, XPS and CO-chemisorption results will be discussed in detail below to explain the interesting phenomena.

Table 3-8: Productivity summary of fresh and stored catalysts for the direct synthesis of hydrogen peroxide

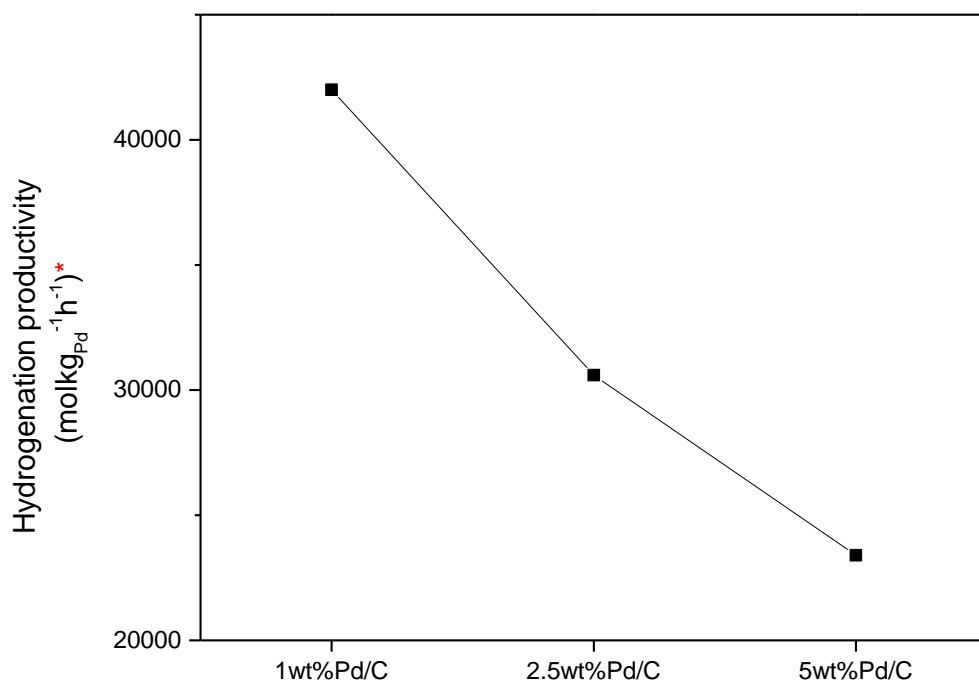| Catalyst	H_2O_2 productivity ($mol_{H2O2}\,kg_{cat.}^{-1}\,h^{-1}$)	Hydrogenation productivity ($mol_{H2O2}\,kg_{cat.}^{-1}\,h^{-1}$)
2.5%Ni2.5%Pd/C fresh	40	642
2.5%Ni2.5%Pd/C stored for 12 months	70	193
2.5%Pd/C fresh	18	766
2.5%Pd/C stored for 12 months	35	401

Figure 3-7: Results summary of hydrogenation productivity over Pd only catalysts with different metal loadings

*The hydrogenation productivity was calculated based on the weight of Pd.

3.5.2. Characterization

3.5.2.1. Microwave Plasma-Atomic Emission Spectrometer (MP-AES)

Table 3-9: Summary of metal leaching during reactions according to MP-AES

Catalyst	Remaining metal on carbon support (wt%)		Leaching (%)	
	Ni	Pd	Ni	Pd
2.5 wt% Ni-2.5 wt% Pd/C fresh	2.35	1.28	-	-
2.5 wt% Ni-2.5 wt% Pd/C used×1	1.82	0.85	45.53	33.59
2.5 wt% Ni-2.5 wt% Pd/C used×2	0.90	0.79	50.55	7.06
1 wt% Pd/C	-	0.50	-	-
2.5 wt% Pd/C	-	1.36	-	-
5 wt% Pd/C	-	2.62	-	-

MP-AES was first used for the investigation of the actual metal loading in the catalysts which is essential as a reference for other characterizations, for instance XPS and CO-chemisorption. All the catalysts as stated in 3.5.1 were digested and analysed through this technique and attained results were calculated into actual metal loadings listed in Table 3-9. It can be noticed that merely around half of the Pd remained on carbon support for all the Pd contained catalysts indicating a partial Pd stayed in the containers during impregnation. The comparison of fresh and used catalysts revealed that both Ni and Pd leached into the reaction solvent during the synthesis of hydrogen peroxide even after the second use. Moreover, in the comparison of 1, 2.5 and 5 wt% Pd samples, the actual metal loading increased proportionally which was as expected.

3.5.2.2. X-ray Diffraction (XRD)

XRD analysis was used for fresh, used×1 and used×2 samples of 2.5 wt% Ni-2.5 wt% Pd/C to compare the change in crystallite structure during hydrogen peroxide synthesis. According to Figure 3-8, the same as previously seen for the fresh sample, no reflection

attributed to Ni species could be observed in the patterns after use. Moreover, the reflections corresponding to metallic Pd were observed in all these three patterns which were indexed as [111], [200], [220] and [311] at Bragg angle around 40.3°, 46.8°, 68.3° and 82.4° respectively[20]. Average crystallite sizes have been calculated from the reflection [111] and shown in Table 3-10 that the average crystallite size of Pd increased from 19 nm to 32 nm after one use of hydrogen peroxide synthesis and remained as 32 nm after the second use.

Figure 3-8: XRD patterns for fresh and used Ni-Pd bimetallic catalysts.

Table 3-10: Average crystallite size for the crystals in Ni Pd catalysts

Sample	Metal phase	Average crystallite size (nm)
2.5%Ni-2.5%Pd/C fresh	Pd^0	19
2.5%Ni-2.5%Pd/C used×1	Pd^0	32
2.5%Ni-2.5%Pd/C used×2	Pd^0	32

The comparison of fresh and stored samples was also investigated through XRD for both Ni-Pd bimetallic and Pd only catalysts. As seen in Figure 3-8 and 3-9, very similar

as previous XRD results, the patterns of stored samples did not show obvious Ni reflections, and the Pd reflections at Bragg angles of 40.3º, 46.8º, 68.3º and 82.4º indexed as [111], [200], [220] and [311] of metallic Pd respectively. However, for both aged samples, Pd reflections were sharper and corresponding FWHMs were narrower than those of their fresh analogues which indicates the agglomeration of Pd particles over time. This phenomenon was consistent with our earlier observations that the storage of the catalysts leads to an increase of the whole range of particles.[36]

XRD patterns for Pd monometallic catalysts with various metal loadings are shown in Figure 3-11. The phase of Pd in these three samples was all metallic whose reflections centred at 40.3º, 46.8º, 68.3º and 82.4º. It can be noticed that with the increase of metal loading, the reflections of Pd were sharper indicating the increase of particle size. Calculated average crystallite size is summarized in Table 3-12 which proved that relatively large particles were possessed in the sample with high metal loading.
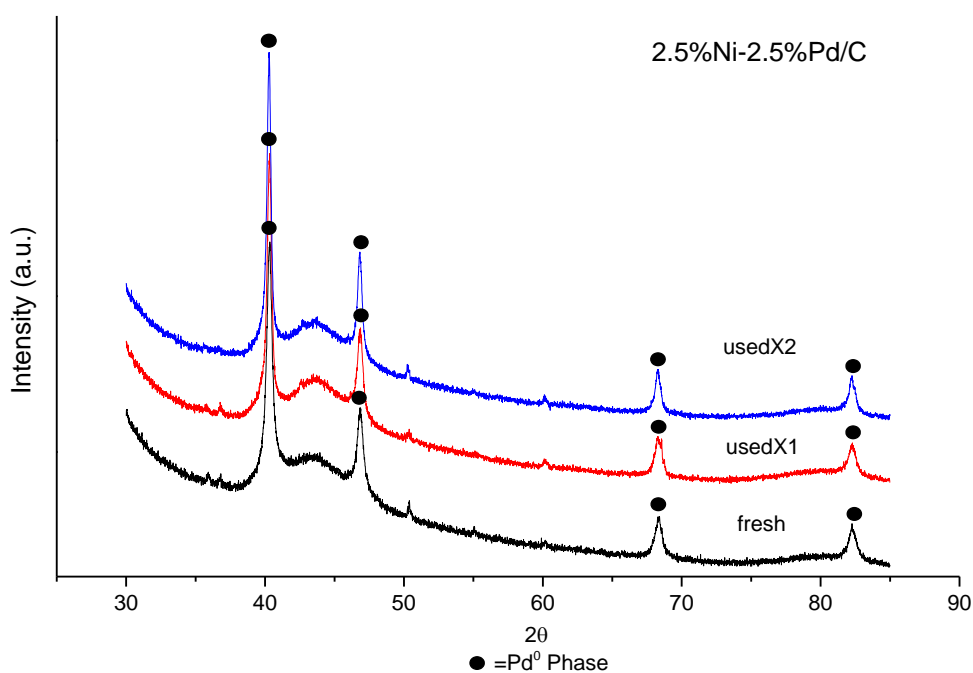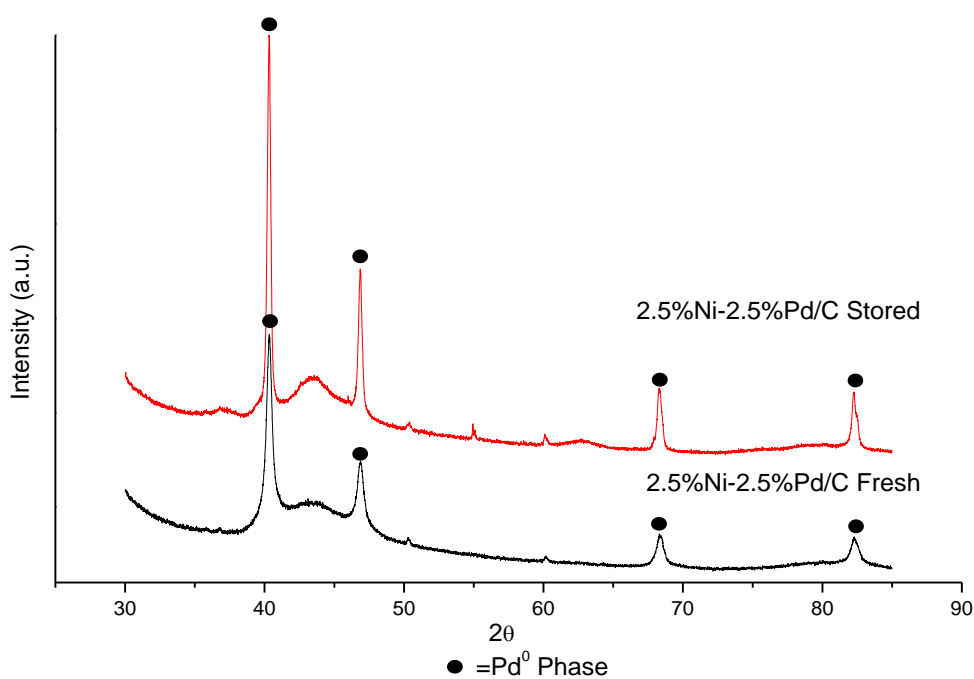

Figure 3-9: XRD patterns for fresh and stored Ni/Pd bimetallic catalysts.

Table 3-10: Average crystallite size of Pd(0) for the crystals in carbon supported Ni-Pd catalysts

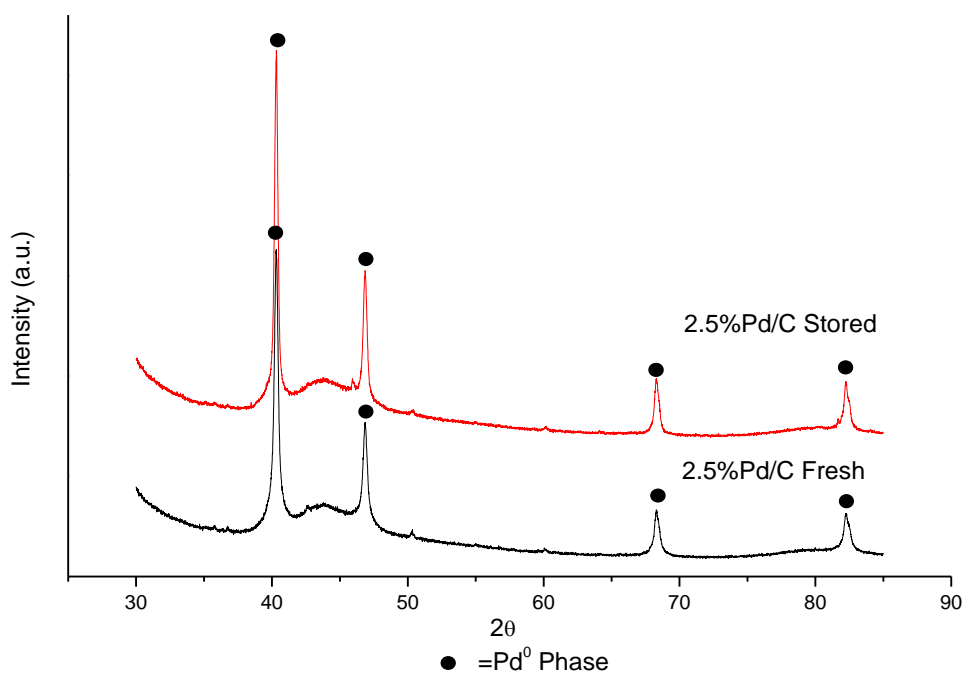| Sample	Metal phase	Average crystallite size (nm)
2.5%Ni-2.5%Pd/C fresh	Pd^0	19
2.5%Ni2.5%Pd/C stored	Pd^0	49

Figure 3-9: XRD patterns for fresh and stored Pd monometallic catalysts.

Table 3-11: Average crystallite size of Pd(0) for the crystals in carbon supported Pd monometallic catalysts

Sample	Metal phase	Average crystallite size (nm)
2.5%Pd/C fresh	Pd^0	32
2.5%Pd/C stored	Pd^0	43
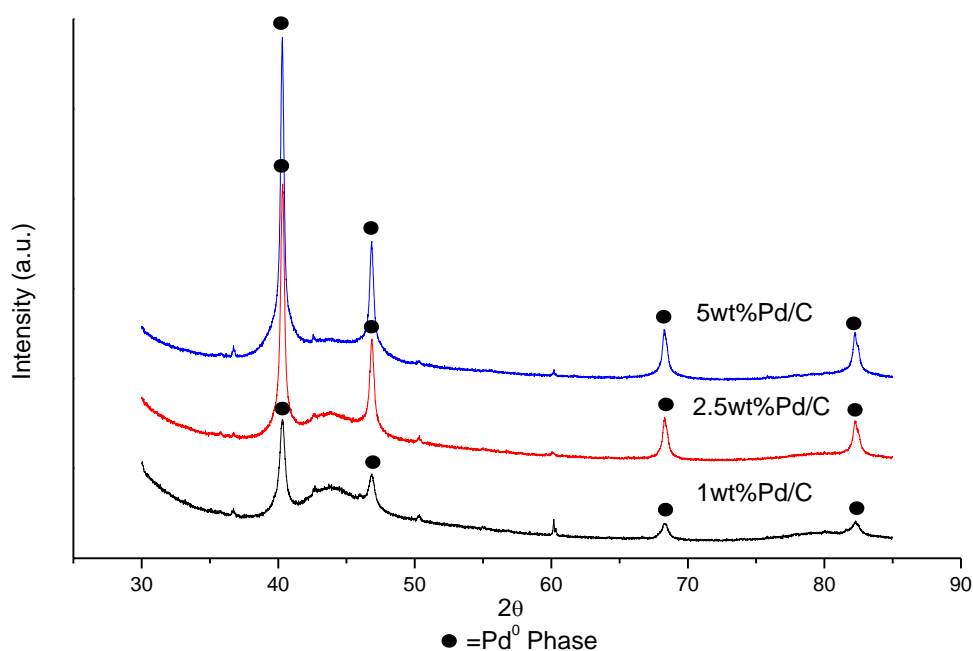
Figure 3-10: XRD patterns for Pd monometallic catalysts with different metal loadings

Table 3-12: Average crystallite size of Pd(0) for Pd monometallic catalysts with various metal loading

Sample	Metal phase	Average crystallite size (nm)
1%Pd/C	Pd^0	19
2.5%Pd/C	Pd^0	32
5%Pd/C	Pd^0	55

In conclusion, both reactions for hydrogen peroxide synthesis and storage leaded to particle agglomeration of Pd particles. Moreover, average crystallite size of Pd increased with metal loading from 1 wt% to 5 wt% on active carbon support.

3.5.2.3.   X-ray Photoelectron Spectroscopy (XPS)

All the catalysts above were investigated through XPS for surface chemical analysis. Fresh, used×1 and used×2 samples of the bimetallic catalyst were first tested. The attained spectra and calculated atomic ratio on the surface are shown in Figure 3-11, Figure 3-12 and Table 3-13 respectively. For both Ni and Pd, the binding energy did not show substantial shifts after reactions that Ni therefore stayed as mainly Ni oxides, and Pd remained as Pd(0) on the surface. It can be noticed that lower intensity of both Ni 2p and Pd 3d reflections were observed in the used×1 sample, however higher intensity of the reflections observed for the used×2 sample. According to Table 3-13, calculated atomic ratios demonstrated that Pd concentration on the surface kept decreasing with increasing number of uses, yet for Ni, it decreased after the first use but increased after the second use. MP-AES demonstrated Pd leaching during the two subsequent uses. Moreover, XRD proved that Pd particle size grew from 19 to 32 nm after the reactions. Both of the observations are able to induce the decrease of Pd atomic ratio on the surface by the analysis of XPS. In addition, the relatively higher atomic ratio of Ni on the surface for the used×2 sample infers that well dispersed Ni appeared on the surface possibly because of (i) the leaching of large amorphous Ni on the top of well dispersed Ni which is consistent with MP-AES results that 51 wt% of Ni was washed off during the second use or (ii) the leaching of Pd particles on the top of Ni before the second use of peroxide synthesis. Or possibly the lower atomic ratio of Pd demonstrated on the surface shifted up the relative atomic ratio of Ni.
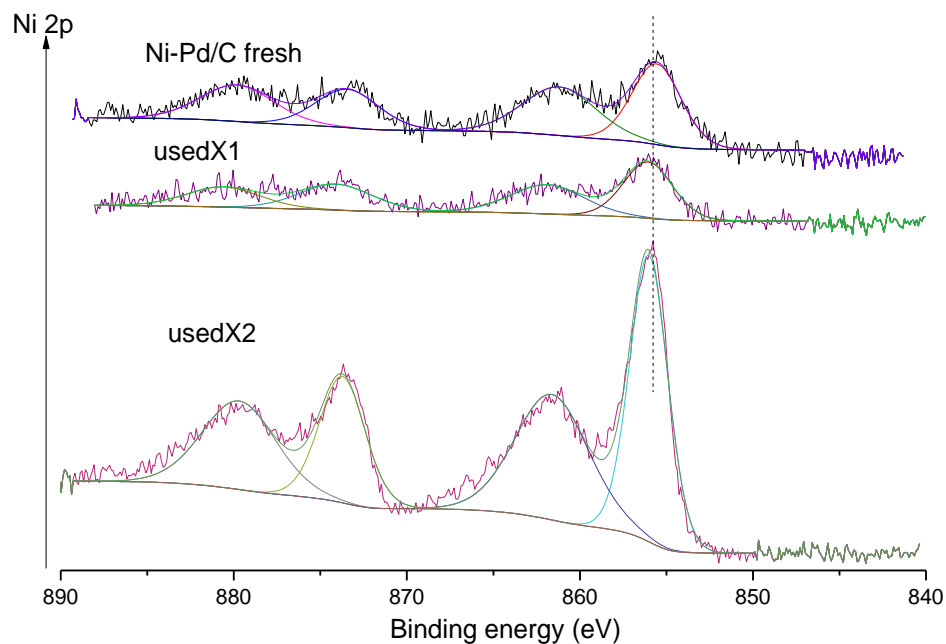
Figure 3-11: The Ni 2p spectra of fresh, used×1 and used×2 Ni-Pd bimetallic catalysts

Figure 3-12: The Pd 3d spectra of fresh, used×1 and used×2 Ni-Pd bimetallic catalysts

Table 3-13: Summarized atomic ratio on the surface of fresh and used Ni-Pd bimetallic catalysts

Catalyst	2.5%Ni2.5%Pd/C fresh		2.5%Ni2.5%Pd/C used×1		2.5%Ni2.5%Pd/C used×2	
	Peak name	at%	Peak name	at%	Peak name	at%
XPS information	Pd 3d	1.47	Pd 3d	0.73	Pd 3d	0.67
	Ni 2p	0.57	Ni 2p	0.42	Ni 2p	1.44
	O 1s	7.33	O 1s	5.64	O 1s	7.64
	C 1s	90.14	C 1s	93.09	C 1s	90.13
	Cl 2p	0.09	Cl 2p	0.13	Cl 2p	0.13

For the comparison of fresh and aged bimetallic samples shown in Figure 3-13 and Figure 3-14, Ni also still stays as mainly Ni oxides overtime, and aged Pd is still metallic. However, the intensity of the reflections of Ni and Pd and calculated surface atom ratio decrease remarkably especially for Pd which changed from 1.47 at% to 0.48 at% which indicates the particle agglomeration happened over time.

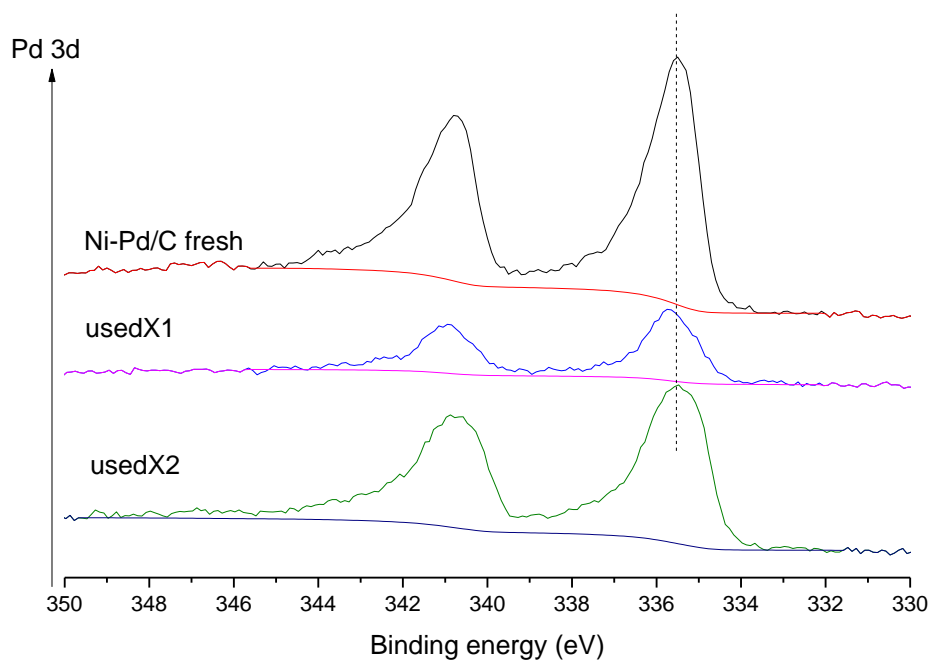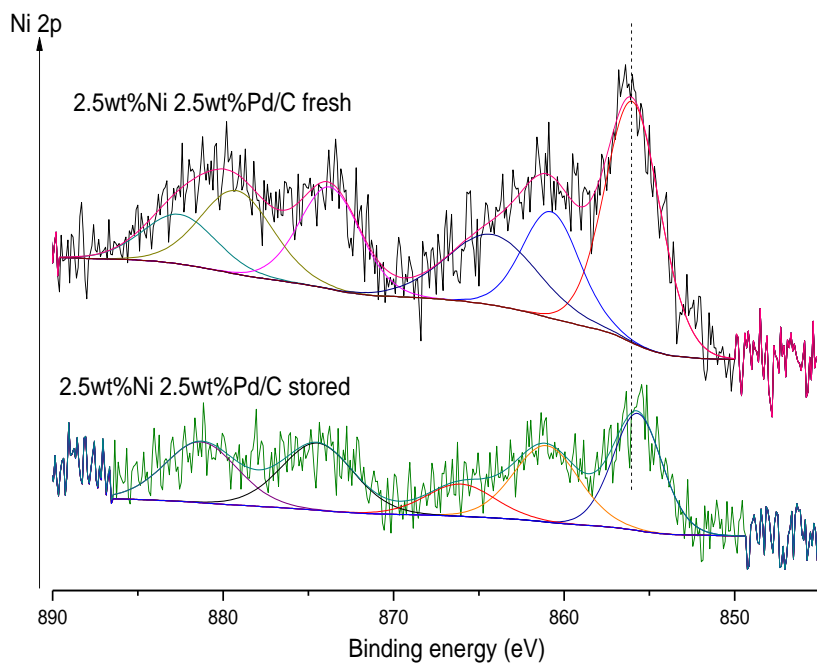**Figure 3-13:** The Ni 2p spectra of fresh and stored Ni-Pd bimetallic catalysts

Figure 3-14: The Pd 3d spectra of fresh and stored Ni-Pd bimetallic catalysts

Table 3-14: Summarized atomic ratio on the surface of fresh and stored Ni-Pd bimetallic catalysts

Catalyst	Peak name	at%
2.5%Ni-2.5%Pd/C fresh	Ni 2p	0.57
	Pd 3d	1.47
	O 1s	7.24
	C 1s	90.59
	Cl 2p	0.092
2.5%Ni-2.5%Pd/C stored	Ni 2p	0.44
	Pd 3d	0.48
	O 1s	4.28
	C 1s	94.72
	Cl 2p	0.089

For fresh and aged Pd only catalysts (Figure 3-15 and Table 3-15), a similar phenomenon can be observed whose Pd surface atom ratio suppressed from 2.42 at% to 0.52 at%. Both of them indicate that the storage of the catalysts leaded to a lower metal dispersion over time.
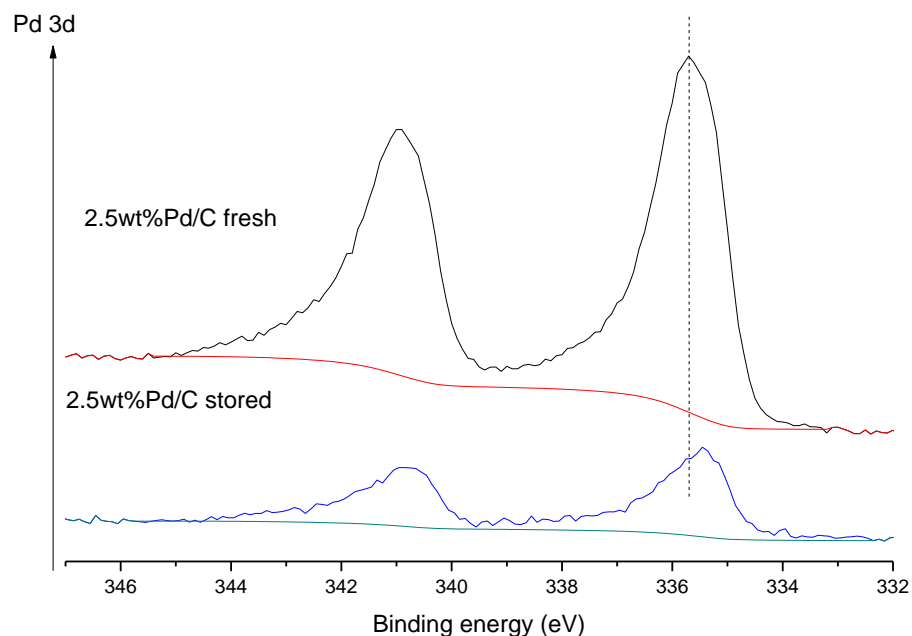
Figure 3-15: Pd 3d spectra of fresh and stored Pd monometallic catalysts

Table 3-15: Summarized atomic ratio on the surface of fresh and stored Pd monometallic catalysts

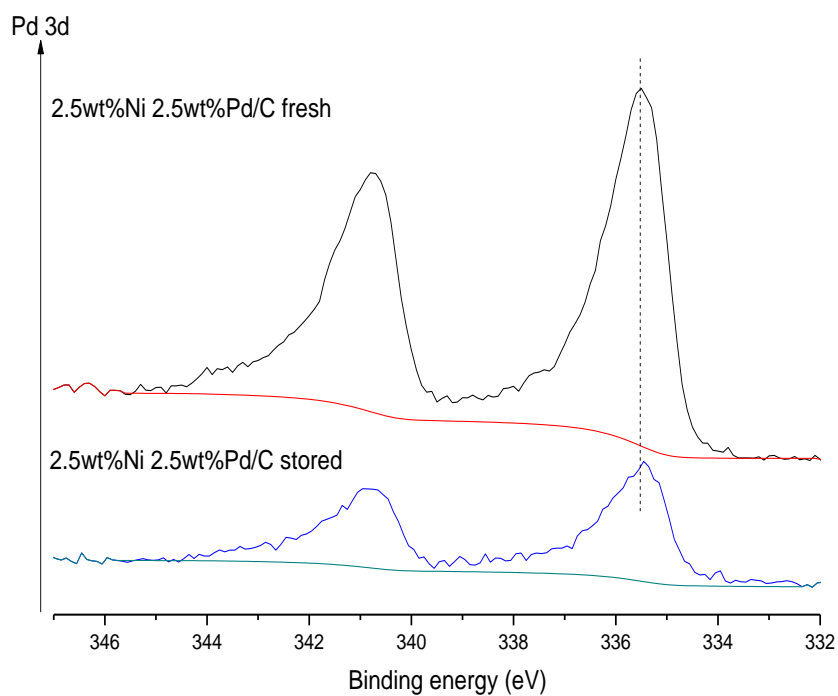| Catalyst	Peak name	at%
2.5%Pd/C fresh	Pd 3d	2.42
	O 1s	8.57
	C 1s	88.84
	Cl 2p	0.17
2.5%Pd/C stored	Pd 3d	0.52
	O 1s	4.35
	C 1s	95.08
	Cl 2p	0.055

Pd monometallic samples with different metal loadings including 1 wt%, 2.5 wt% and 5 wt% Pd were also investigated through XPS analysis and comparison results are shown in Figure 3-16 and Table 3-16. According to the binding energy and the shape of Pd

spectra, only Pd(0) existed on the surface of these three catalysts. Moreover, with the increase of metal loading, the intensity of Pd 3d reflections increased and calculated atomic ratio increased simultaneously. If we use the surface atomic ratio based on the actual metal loading (according to attained results from MP-AES) as an estimation of Pd metal dispersion, it can be noticed that with the increase metal loading the calculated result demonstrated a lower value in the comparison of the catalyst with low metal loading (Table 3-16). This is consistent with the XRD results of these three catalysts (Table 3-12) that the catalyst with higher metal loading had lower metal dispersion.
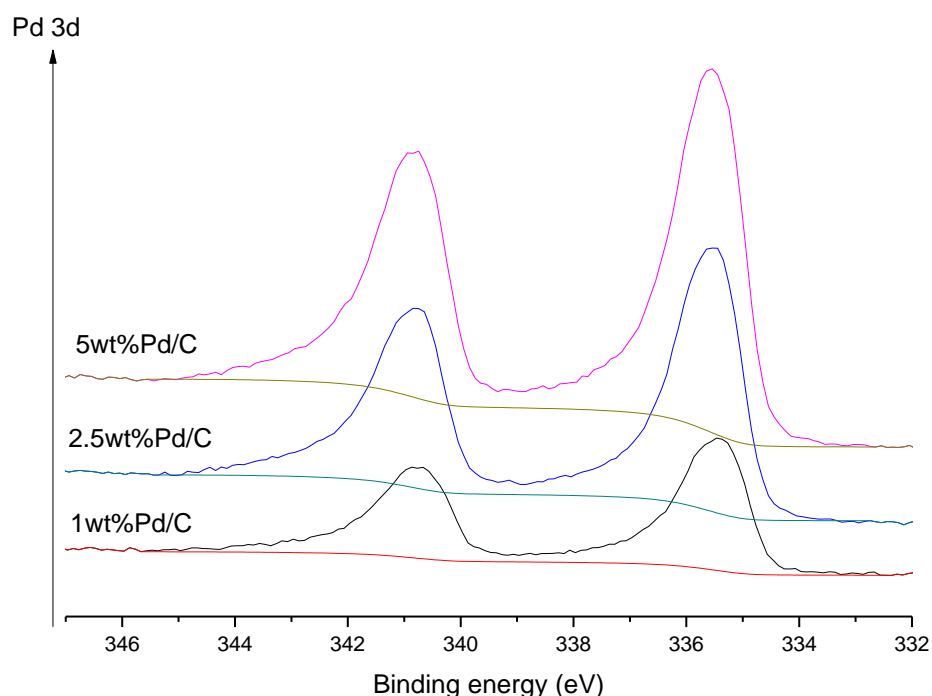
Figure 3-16: Pd 3d spectra of Pd monometallic catalysts with different metal loadings

Hence, according to XPS analysis, both the synthesis of hydrogen peroxide and storage of the catalysts can cause lower surface atomic ratio of active components. According to the results of MP-AES and XRD, particle growth and metal leaching were both possibly responsible for this phenomenon after reactions. For the aged catalysts, particle agglomeration over the time of storage was the only explanation of the lower atomic ratio of Ni and Pd on the surface of the catalysts. Moreover, with the increase of metal

loading, lower metal dispersion was achieved which necessary to be further is supported by CO-chemisorption.

Table 3-16: Atom ratio on material surface of Pd monometallic samples

Catalyst	Peak name	at%	at%/metal loading
1 wt% Pd/C		1.12	2.24
2.5 wt% Pd/C	Pd 3d	2.42	1.78
5 wt% Pd/C		3.08	1.17

3.5.2.4. CO-chemisorption

Although the results of XRD and XPS can to some extent provide qualitative information of the metal dispersion, neither of them is able to determine a precise value of the overall particles. Hence, CO-chemisorption was used for metal dispersion analysis of all the Pd only samples mentioned above and attained results are listed in Table 3-17. As we can see, the stored sample demonstrated a lower Pd dispersion relative to the fresh sample. Moreover, an inverse trend of metal loading and particle dispersion can be noticed according to the attained results.

Table 3-17: The summary of Pd dispersion of different Pd only samples

Catalyst	Pd dispersion (%)
2.5 wt% Pd/C fresh	13.25
2.5 wt% Pd/C stored	5.02
1 wt% Pd/C	16.75
2.5 wt% Pd/C	13.25
5 wt% Pd/C	4.01

3.6 Discussion

3.6.1. The effect of Ni in Pd for the direct synthesis of hydrogen peroxide

The first point of discussion is a better comprehension of the role of Ni in Pd catalysts for hydrogen peroxide synthesis. In fact the main effect of the secondary metal in catalysis is to modify the geometric structure or electronic structure of the single metal respectively called ensemble and ligand effect.[1] Moreover, the additive metal may also be able to provide active sites for the reaction. However, according to the results shown in Table 3-2, Ni monometallic samples demonstrated very limited activity for H_2O_2 synthesis, which indicates that Ni itself may not be an active species for the hydrogen peroxide formation under stated conditions.

The ensemble effect is due to the dilution of active sites with relatively inactive atoms, and therefore the surface metals keep a certain degree of individuality. The ligand effect instead is attributed to the change of electronic structure between the atoms on the surface, consequently resulted in altering the heat of adsorption of reactants or products. Here, there is no evidence which directly proves an increase of individuality of Pd atoms on the surface of the Ni-Pd bimetallic catalyst. Whereas, XRD results demonstrated a better dispersion of the Pd particles with the addition of Ni which was to some extent supported by TPR analysis – a lower intensity of Pd-H_x decomposition peak over bimetallic catalyst than the Pd only sample. The combination of XRD, MP-AES and XPS indicates that metallic Pd sits on the top of amorphous Ni oxides. The existence of metallic Ni according to XPS and TPR analysis in Ni-Pd bimetallic catalyst and the decrease of decomposition temperature of Pd-H_x with the addition of Ni imply that there may be some dissolution of Ni(0) in metallic Pd phase. STEM analysis is necessary to support the assumption of the particle morphology in Ni-Pd bimetallic catalyst.

XPS results also showed negative shifting of Pd 3d corresponding to positive shifting of Ni 2p over the bimetallic catalyst indicating a possible electron transfer from Ni to Pd. This assumption will be further investigated by EXAFS in the future. Moreover, the role of the additive metal-Ni in Pd will be further investigated in Chapter 4. Aspects including the mechanism of hydrogen peroxide synthesis and morphology of the catalysts will be discussed in detail in order to understand the relation between catalyst
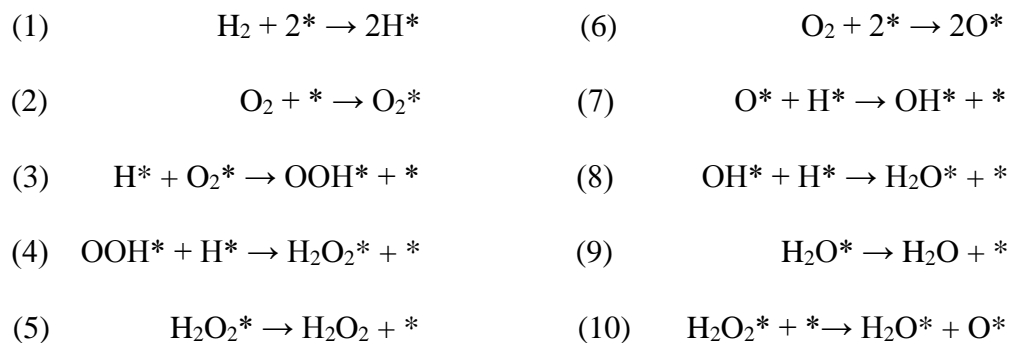
structure and corresponding catalytic performance, and also the active sites for the direct formation of H_2O_2.

3.6.2.   The effect of Pd dispersion on the direct synthesis of H_2O_2

It is well-known that unlike metal oxides for instance TiO_2 which is able to provide strong metal support interaction effects (SMSI), active carbon can only demonstrate very weak interaction between the support and supported metal particles.[37] Hence, well dispersed Pd on carbon support with high energy are less energetically favoured and less stable than large particles, and as a consequence, has a strong tendency to agglomerate into large particles by an Ostwald Ripening mechanism.[38] In this thesis, particles after the direct synthesis of hydrogen peroxide or storage over time, sharper XRD peaks, lower surface atomic ratio from XPS and lower CO chemisorption on the basis of metal loading were achieved compared with corresponding fresh samples, indicating decrease of metal dispersion. In a meanwhile, both used and aged carbon supported catalysts demonstrated enhanced H_2O_2 productivity and suppressed hydrogenation productivity. Moreover, with the increase of Pd loading, a decrease of particle dispersion was noticed from XRD, XPS and CO chemisorption analysis and simultaneously a dropping of hydrogenation activity of H_2O_2 on the basis of metal loading. All of these points together infer a size dependent performance over metallic Pd particles.

Abate and co-workers[39] discovered that distinct from rough and disordered surface, large ordered crystallites on the surface showed a higher reaction rate of H_2O_2 synthesis and a lower decomposition rate. F. Menegazzo's experiments demonstrated that for Pd monometallic catalysts, the catalysts with particles smaller than 2 nm showed lower activity and selectivity to H_2O_2 compared with the samples with relatively larger particles.[40,41] The comparison of experimental results for peroxide synthesis over Pd@SiO_2 with distinct Pd particle size-3.4, 3.7 and 4.2 nm, the catalyst with relatively large particles demonstrated higher H_2 conversion and H_2O_2 selectivity after fixed reaction time and also enhanced H_2O_2 production rate in the comparison with small particle samples.[42] All the results in these publications are consistent with each other and the results in this chapter.

It is well known that the surface structure of metal determines the dissociation of absorbed molecules for instance O_2.[43,44] Deguchi and Iwamoto performed a density functional theory (DFT) study of direct hydrogen peroxide synthesis on a Pd surface, and claimed that unsaturated sites such as a corner or an edge were responsible for high adsorption and dissociation ability of H_2, O_2 and H_2O_2.[45] Integrated with the results and publications mentioned above, it indicates that very well-dispersed Pd particles are detrimental for the direct synthesis of hydrogen peroxide, because more energetic sites (defects, edges, corners, etc.) will dissociatively chemisorb O_2 or re-adsorb produced H_2O_2, which is able to react with chemisorbed hydrogen and lead to the formation of water. On the other hand, O_2 chemisorbs on large, non-defective (and hence less energetic) Pd particles without dissociation which is a crucial step for forming the desired product H_2O_2.[41]

(1)	$H_2 + 2^* \rightarrow 2H^*$	(6)	$O_2 + 2^* \rightarrow 2O^*$
(2)	$O_2 + ^* \rightarrow O_2^*$	(7)	$O^* + H^* \rightarrow OH^* + ^*$
(3)	$H^* + O_2^* \rightarrow OOH^* + ^*$	(8)	$OH^* + H^* \rightarrow H_2O^* + ^*$
(4)	$OOH^* + H^* \rightarrow H_2O_2^* + ^*$	(9)	$H_2O^* \rightarrow H_2O + ^*$
(5)	$H_2O_2^* \rightarrow H_2O_2 + ^*$	(10)	$H_2O_2^* + ^* \rightarrow H_2O^* + O^*$

Scheme 3-1: Plausible mechanism for the direct synthesis of hydrogen peroxide and side reactions (* denotes a vacant surface site).[48]

The possible pathway has been shown as Scheme 3-1 for the formation of hydrogen peroxide, and Equation (2) and (3) demonstrate a well-accepted mechanism that HO_2 is formed as surface intermediate[46] during hydrogen peroxide synthesis. It is necessary to supplement that all the assumption sated here based on this reaction pathway for the formation of hydrogen peroxide. In addition, including the mechanism shown in Scheme 3-1, Lunsford used $^{16}O_2$ mixed with isotope-$^{18}O_2$ as one of the reactants for the direct synthesis of hydrogen peroxide and gained product including $H_2^{18}O_2$ and $H_2^{16}O_2$ without the evidence of $H_2^{18}O^{16}O$. This again indicates the activation of O_2 without dissociation is the actual pathway for the peroxide synthesis.[47] Moreover, this conclusion assists the

comprehension of the detrimental effect originated from high energy Pd sites which tend to dissociatively chemisorb O_2.

Hence, in conclusion, well dispersed metallic Pd is detrimental for the direct synthesis of hydrogen peroxide because more energetic sites can chemisorb O_2 and H_2O_2 with dissociation which is benefit for the H_2O formation rather than H_2O_2. As a consequence, corresponding catalyst demonstrated suppressed H_2O_2 selectivity and relatively low production rate. Since the chemisorption of O_2 without dissociation is a crucial pathway for the peroxide synthesis, low energetic sites on large, non-defective Pd particles are the active and selective species for the direct synthesis of hydrogen peroxide.
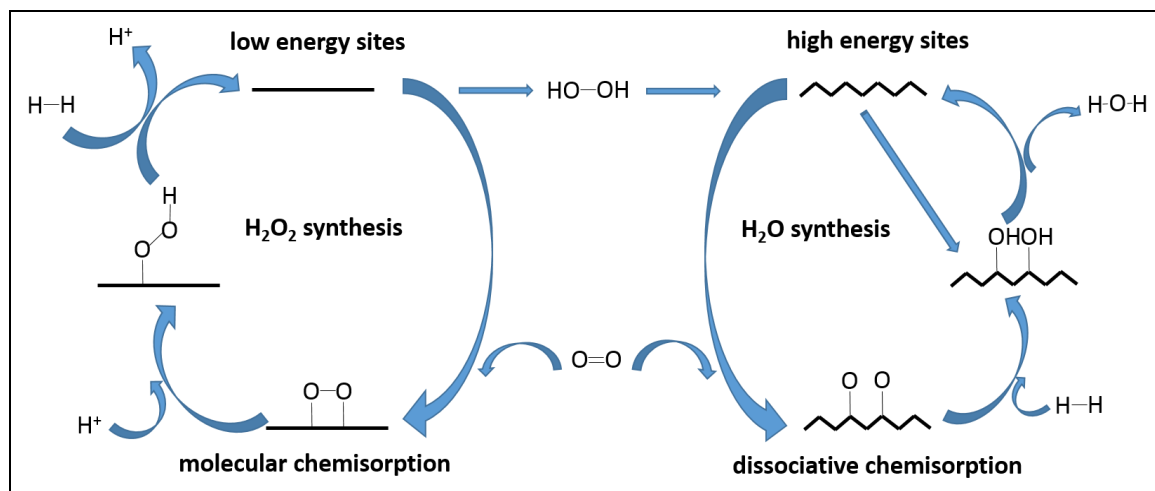
Scheme 3-2: Possible pathway for the direct synthesis of H_2O_2 on monometallic Pd surface.[40]

A paradox of size-dependant activity over Pd only and Ni-Pd bimetallic catalysts seems to be addressed in this chapter. However, the addition of a secondary metal to Pd is able to alter the nature of the sites through changing either geometric or electronic environment, which was suggested to be crucial for selective hydrogenation of O_2 towards H_2O_2.[1] According to the results in this chapter, particle size or the energy of the surface is of vital importance over Pd only catalysts for the direct synthesis of hydrogen peroxide. While for bimetallic catalyst, the individuality of Pd atoms and charge transfer were shown to be the possible factors responsible for the variation of catalytic performance. This was also in agreement with previous research.[49]

3.7 Conclusions

The addition of Ni in Pd catalysts improved catalytic performance for the direct synthesis of hydrogen peroxide, with bimetallic catalysts showing greater activity and lower hydrogenation productivity than Pd monometallic catalysts. Improved Pd dispersion with addition of a second metal was observed through XRD analysis in the comparison with monometallic samples. All the characterisation methods carried out including MP-AES, XRD, TPR and XPS suggested a possible morphology of the particles in the bimetallic catalyst, namely metallic Pd sitting on the top of Ni oxides, with some dissolution of Ni in Pd. Moreover, electron transfer from Ni to Pd was probably occurred.

The reason for the increase in activity of the catalysts after hydrogen peroxide synthesis, and after 12-month storage can be explained by the disappearance of well-dispersed Pd particles. Those particles were washed off during reactions or sintered into larger particles during the storage which are detrimental for peroxide synthesis as they are able to chemisorb O_2 and H_2O_2 with dissociation leading to water formation.

3.8 References

1.　 F. Gao and D. W. Goodman, *Chem. Soc. Rev.*, 2012, **41**, 8009–8020.

2.　 L. Guczi, Z. Schay, G. Stefler, L. F. Liotta, G. Deganello, and A. M. Venezia, *J. Catal.*, 1999, **182**, 456–462.

3.　 T. Inui, K. Kitagawa, T. Takeguchi, T. Hagiwara, and Y. Makino, *Appl. Catal. A Gen.*, 1993, **94**, 31–44.

4.　 J. Hermannsdörfer, M. Friedrich, N. Miyajima, R. Q. Albuquerque, S. Kümmel, and R. Kempe, *Angew. Chem. Int. Ed. Engl.*, 2012, **51**, 11473–11477.

5.　 G. Budroni, S. A. Kondrat, S. H. Taylor, D. J. Morgan, A. F. Carley, P. B. Williams, and G. J. Hutchings, *Catal. Sci. Technol.*, 2013, **3**, 2746-2754.

6.　 N. Toshima and Y. Wang, *Chem. Lett.*, 1993, **22**, 1611–1614.

7.　 M. Armbrüster, G. Wowsnick, M. Friedrich, M. Heggen, and R. Cardoso-Gil, *J. Am. Chem. Soc.*, 2011, **133**, 9112–9118.

8. A. L. Bonivardi, D. L. Chiavassa, C. A. Querini, and M. A. Baltanás, in *12th International Congress on Catalysis Proceedings of the 12th ICC*, Elsevier, 2000, **130**, 3747–3752.

9. K. Kovnir, M. Armbrüster, D. Teschner, T. V Venkov, F. C. Jentoft, A. Knop-Gericke, Y. Grin, and R. Schlögl, *Sci. Technol. Adv. Mater.*, 2007, **8**, 420–427.

10. Y. Nakagawa and K. Tomishige, *Catal. Commun.*, 2010, **12**, 154–156.

11. P. Lu, T. Teranishi, K. Asakura, M. Miyake, and N. Toshima, *J. Phys. Chem. B*, 1999, **103**, 9673–9682.

12. Y. Mats, A. Johan, and G. Wolfgang, *US Pat. 6210651 B1*, 2001.

13. M. Sankar, Q. He, M. Morad, J. Pritchard, S. J. Freakley, J. K. Edwards, S. H. Taylor, D. J. Morgan, A. F. Carley, D. W. Knight, C. J. Kiely, and G. J. Hutchings, *ACS Nano*, 2012, **6**, 6600–6613.

14. J. K. Edwards, A. F. Carley, A. A. Herzing, C. J. Kiely, and G. J. Hutchings, *Faraday Discuss.*, 2008, **138**, 225-239.

15. J. K. Edwards, A. Thomas, A. F. Carley, A. A. Herzing, C. J. Kiely, and G. J. Hutchings, *Green Chem.*, 2008, **10**, 388-394.

16. J. K. Edwards, B. Solsona, P. Landon, A. F. Carley, A. A. Herzing, C. J. Kiely, and G. J. Hutchings, *J. Catal.*, 2005, **236**, 69–79.

17. W. Brockner, C. Ehrhardt, and M. Gjikaj, *Thermochim. Acta*, 2007, **456**, 64–68.

18. Q. Lin, Y. Ji, Z. Jiang, and W. Xiao, *Ind. Eng. Chem. Res.*, 2007, 7950–7954.

19. D. A. Stevens and J. R. Dahn, *Carbon N. Y.*, 2005, **43**, 179–188.

20. Y. Han, D. Kumar, and C. Sivadinarayana, *Catal. Letters*, 2004, **94**, 131–134.

21. D. S. Sidhaye, T. Bala, S. Srinath, H. Srikanth, P. Poddar, M. Sastry, and B. L. V. Prasad, *J. Phys. Chem. C*, 2009, **113**, 3426–3429.

22. J. Richardson, R. Scates, and M. Twigg, *Appl. Catal. A Gen.*, 2003, **246**, 137–150.

23. Y. Li, S. Chen, J. Xu, and H. Zhang, *CLEAN–Soil, Air, Water*, 2013, **42**, 1140-1144.

24. A. P. Grosvenor, M. C. Biesinger, R. S. C. Smart, and N. S. McIntyre, *Surf. Sci.*, 2006, **600**, 1771–1779.

25.   F. Hillebrecht, J. Fuggle, and P. Bennett, *Phys. Rev. B*, 1983, **27**, 2179-2193.

26.   J. Laine, A. Calafat, and M. Labady, *Carbon N. Y.*, 1989, **27**, 191–195.

27.   C. Mims and J. Krajewski, *J. Catal.*, 1986, **102**, 140–150.

28.   C. Mims and J. Pabst, *J. Catal.*, 1987, **107**, 209–220.

29.   S. Pavlova, L. Kapokova, R. Bunina, G. Alikina, N. Sazonova, T. Krieger, A. Ishchenko, V. Rogov, R. Gulyaev, V. Sadykov, and C. Mirodatos, *Catal. Sci. Technol.*, 2012, **2**, 2099-2108.

30.   M. Bonarowska, J. Pielaszek, W. Juszczyk, and Z. Karpinski, *J. Catal.*, 2000, **195**, 304–315.

31.   B. J. Joice, J. J. Rooney, P. B. Wells, and G. R. Wilson, *Discuss. Faraday Soc.*, 1966, **41**, 223.

32.   H. Noh, T. B. Flanagan, R. Balasubramaniam, and J. A. Eastman, *Scr. Mater.*, 1996, **34**, 863–868.

33.   A. Bonivardi and M. Baltanás, *J. Catal.*, 1992, **517**, 500–517.

34.   G. Fagherazzi, *Catal. Letters*, 1995, **32**, 293-303.

35.   F. Pinna, M. Signoretto, and G. Strukul, *React. Kinet. Catal. Lett*, 1997, **60**, 9–13.

36.   B. E. Solsona, J. K. Edwards, P. Landon, A. F. Carley, A. Herzing, C. J. Kiely, and G. J. Hutchings, *Chem. Mater.*, 2006, **18**, 2689–2695.

37.   C. Park and M. A. Keane, *J. Catal.*, 2004, **221**, 386–399.

38.   P. W. Voorhees, *J. Stat. Phys.*, 1985, **38**, 231–252.

39.   S. Abate, G. Centi, S. Melada, S. Perathoner, F. Pinna, and G. Strukul, *Catal. Today*, 2005, **104**, 323–328.

40.   F. Menegazzo, P. Burti, M. Signoretto, M. Manzoli, S. Vankova, F. Boccuzzi, F. Pinna, and G. Strukul, *J. Catal.*, 2008, **257**, 369–381.

41.   F. Menegazzo, M. Signoretto, G. Frison, F. Pinna, G. Strukul, M. Manzoli, and F. Boccuzzi, *J. Catal.*, 2012, **290**, 143–150.

42.   S. Kim, D.-W. Lee, K.-Y. Lee, and E. A. Cho, *Catal. Letters*, 2014, **144**, 905-911.

43.   T. Matsushima, *Surf. Sci.*, 1989, **217**, 155–166.

44.   A. Rar and T. Matsushima, *Surf. Sci.*, 1994, **318**, 89–96.

45.   T. Deguchi, H. Yamano, and M. Iwamoto, *J. Catal.*, 2012, **287**, 55–61.

46.   T. A. Posepelova, *Russ. J. Phys. Chem.*, 1961.

47.   J. Lunsford, *J. Catal.*, 2003, **216**, 455–460.

48.   M. Piccinini, E. Ntainjua, J. K. Edwards, A. F. Carley, J. A. Moulijn, and G. J. Hutchings, *Phys. Chem. Chem. Phys.*, 2010, **12**, 2488–2492.

49   L. Ouyang, G. Da, P. Tian, T. Chen, G. Liang, J. Xu and Y, Han, *J. Catal.*, 2014, **311**, 129-136

Chapter 4

TiO$_2$ supported Ni-Pd catalysts for the direct synthesis of hydrogen peroxide

4.1 Introduction

Following the results reported in Chapter 3, active carbon with special properties including low iso-electric point[1] and high surface area has been proved to be an outstanding support for the peroxide synthesis[2]. Nevertheless, its porous structure makes active carbon able to easily absorb impurities. Moreover, active carbon (G60) manufactured from different sources demonstrates distinct properties, and as a result makes it difficult to control the experimental consistency. TiO$_2$ (P-25) supported Au-Pd bimetallic particles demonstrated outstanding catalytic performance than other metal oxides including SiO$_2$, Al$_2$O$_3$ and MgO for the direct synthesis of hydrogen peroxide.[1]

Strong metal strong interaction from TiO_2 is expected to be benefit for the stability of the Pd based catalysts. Hence, a series of TiO_2 (P-25) supported Ni/Pd catalysts (including Ni monometallic, Pd monometallic and Ni-Pd bimetallic catalysts) were prepared in this chapter in order to further investigate the effect of Ni to Pd for the direct synthesis of hydrogen peroxide. $NiCl_2$ was used as Ni precursor for catalysts prepared on TiO_2 by a standard impregnation method as the bimetallic catalyst made from $NiCl_2$ demonstrated relatively higher activity than the one made from $Ni(NO_3)_2$ in Table A-1 Appendix. Hence, MP-AES, STEM, XPS, TPR and CO-DRIFTS were employed to evaluate catalyst morphology and structure for understanding the relation between catalyst structure and catalytic performance.

4.2 The direct synthesis of hydrogen peroxide

4.2.1 Ni/Pd mono- and bi-metallic catalysts

Table 4-1: Results summary for Ni-Pd monometallic and bimetallic catalysts* for the direct synthesis of hydrogen peroxide

Catalyst	Productivity ($mol_{H2O2}\,kg_{cat.}^{-1}\,h^{-1}$)
2.5 wt% Ni/TiO₂	1
2.5 wt% Pd/TiO₂	13
5 wt% Ni/TiO₂	3
5 wt% Pd/TiO₂	20
2.5 wt% Ni 2.5 wt% Pd /TiO₂	103

* Heat treatment: 20 °C/min, 400 °C, 3 h, static air

Table 4-1 shows the production rates of TiO_2 supported Ni/Pd monometallic and bimetallic catalysts for the direct synthesis of hydrogen peroxide. All the catalysts were prepared by impregnation followed by 400 °C calcination under static air. Pd monometallic catalysts were active for H_2O_2 synthesis, yet when pure Ni catalysts were tested only trace amounts of H_2O_2 were detected. With the addition of Ni to Pd, 2.5 wt%

Ni-2.5 wt% Pd catalyst demonstrated a H$_2$O$_2$ productivity of 103 mol kg^{-1} h^{-1} which was shown to be significantly more active than either pure Pd or Ni catalysts. Nevertheless, this active catalyst was not stable after use as shown in Table 4-2. Its production rate for H$_2$O$_2$ synthesis decreased 30% after one use, and the rate for side reaction-hydrogenation was doubled from 225 mol kg^{-1} h^{-1} to 425 mol kg^{-1} h^{-1}.

Table 4-2: Catalyst reusability for the direct synthesis of hydrogen peroxide

Catalyst	Productivity (mol$_{H2O2}$ kg$_{cat.}^{-1}$ h^{-1})	Hydrogenation (mol$_{H2O2}$ kg$_{cat.}^{-1}$ h^{-1})
2.5 wt% Ni-2.5 wt% Pd/TiO$_2$ fresh	103	225
2.5 wt% Ni-2.5 wt% Pd/TiO$_2$ used×1	77	425

4.2.2 Optimum calcination temperature for H$_2$O$_2$ synthesis

In order to try and stabilize Ni-Pd bimetallic catalysts to multiple reaction cycles, higher calcination temperatures were investigated. In Figure 4-1, reusability of the catalysts for hydrogen peroxide synthesis is demonstrated. With the increase of calcination temperature from 400 °C to 600 °C, catalytic activity was drastically suppressed from 103 mol kg^{-1} h^{-1} to 2 mol kg^{-1} h^{-1}. Simultaneously, catalyst stability was substantially enhanced, when comparing the activity difference between fresh and used catalysts changed from a 26 mol kg^{-1} h^{-1} drop at 400 °C calcination to a 5 mol kg^{-1} h^{-1} at 600 °C. It is known that high temperature heat treatment is very efficient for the enhancement of particle-particle and particle-support interaction; however it can also promote particle agglomeration that compromises the number of active surface sites available and therefore catalytic performance. Similar phenomena were also observed in our previous work on Au-Pd catalysts for the direct synthesis of hydrogen peroxide.[3,4] Hence, according to the results shown in Figure 4-1, the catalyst treated at 475 °C gave the best compromise of catalytic activity and stability that was therefore chosen for the preparation of the following catalysts.
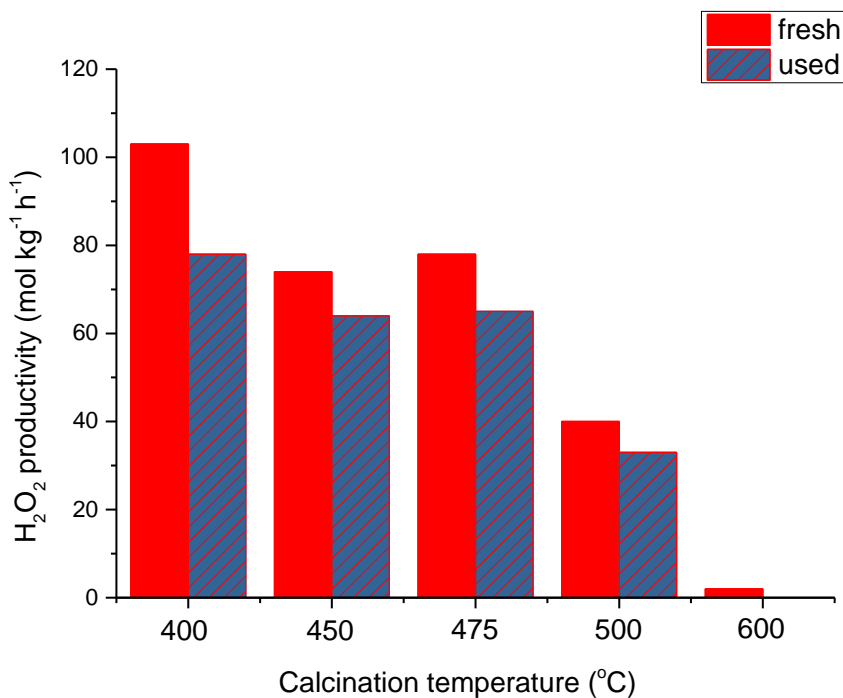
Figure 4-1: The reusability of the catalysts calcined at different temperatures

4.2.3 The effect of Ni/Pd ratio for H_2O_2 synthesis

The effect of Ni/Pd ratio was also investigated for the direct synthesis of hydrogen peroxide in order to achieve the best catalytic performance. A group of 5 wt% catalysts with various Ni/Pd molar ratios were prepared and evaluated for both activity and stability for direct hydrogen peroxide synthesis. The results are shown in Figure 4-2. It can be noticed that the variation of Ni/Pd ratio results in a volcano plot with the peak value observed at 1:1 Ni/Pd ratio with a productivity of 80 mol kg^{-1} h^{-1}. Ni-Pd (2:1) catalyst demonstrated a second highest productivity-78 mol kg^{-1} h^{-1}. All the bimetallic catalysts demonstrated enhanced activity than either Ni or Pd monometallic catalyst which indicates the synergistic effect of Ni and Pd. Moreover, for catalyst stability, the sample with 1:2 Ni/Pd ratio was stable, and Ni-Pd (2:1) catalyst is more reusable than Ni-Pd (1:1) catalyst with a productivity difference of 15 mol kg^{-1} h^{-1} between fresh and used catalysts. Hence, it can be noticed that the catalyst with 2:1 Ni/Pd molar ratio demonstrated the best compromise of H_2O_2 productivity and reusability. It is necessary

93

to stress that 2:1 Ni/Pd catalyst stated here is equivalent to 1:1 weight ratio which was mentioned previously as 2.5 wt% Ni-2.5 wt% Pd.
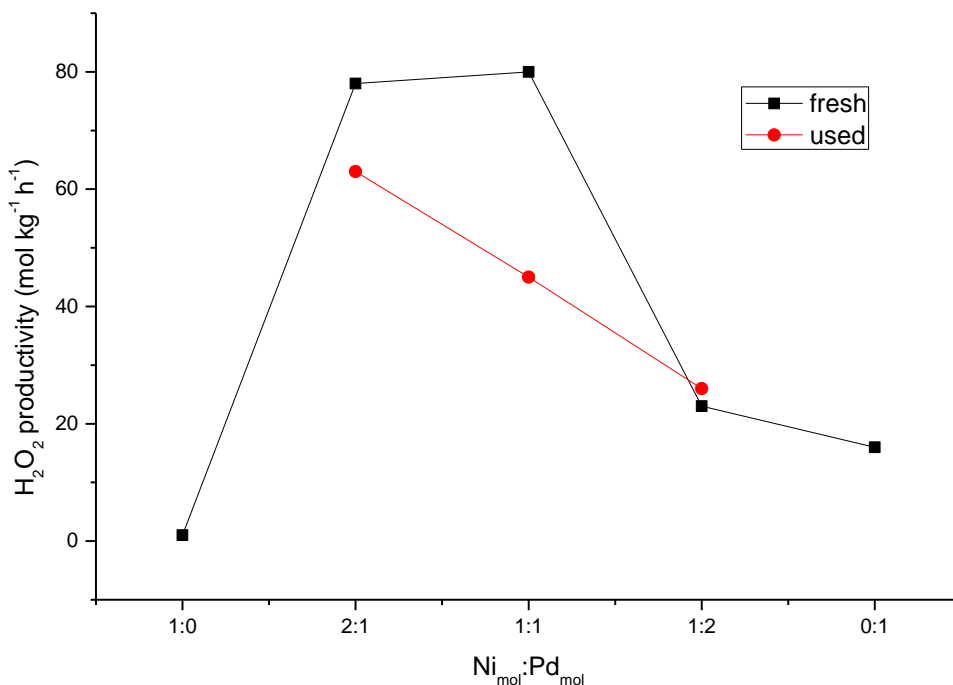

Figure 4-2: The reusability test for 5wt%Ni-Pd/TiO₂ catalysts with different Ni/Pd molar ratios after 475 °C calcination.

4.2.4 The investigation of H₂ conversion, H₂O₂ selectivity and H₂O₂ production rate over Ni/Pd mono- and bi-metallic catalysts

Figure 4-3 shows the curves of time-on-line H₂ conversion over bimetallic catalysts (Ni/Pd molar ratio = 2:1 and 1:1) and Ni/Pd monometallic catalysts which was used to demonstrate the activity for activating H₂. Activated hydrogen was then able to react with activated ·O₂ and ·O radicals or H₂O₂ resulted in products including H₂O₂ and H₂O. Hence, time-on-line H₂ conversion is able to indicate the overall activity for H₂ activation during hydrogen peroxide direct synthesis. As seen in Figure 4-3, the curves of bimetallic catalysts demonstrate much steeper slopes than that of Pd only sample indicating the higher activity of bimetallic catalysts for activating H₂. Without showing any H₂ conversion even after 12 h reaction elucidates that Ni only catalyst prepared through stated method was not active for H₂ activation under these reaction conditions.
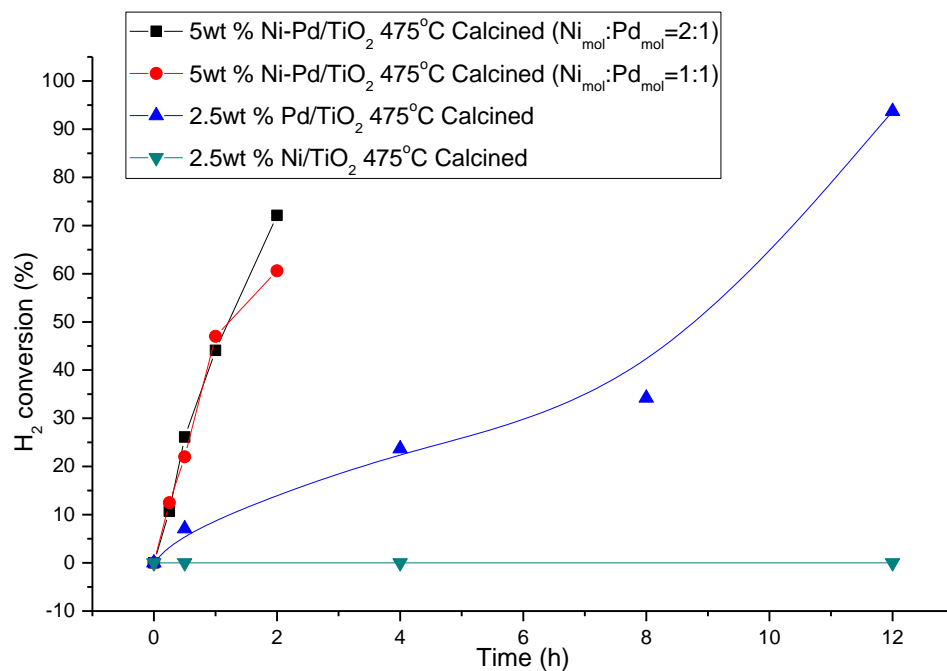
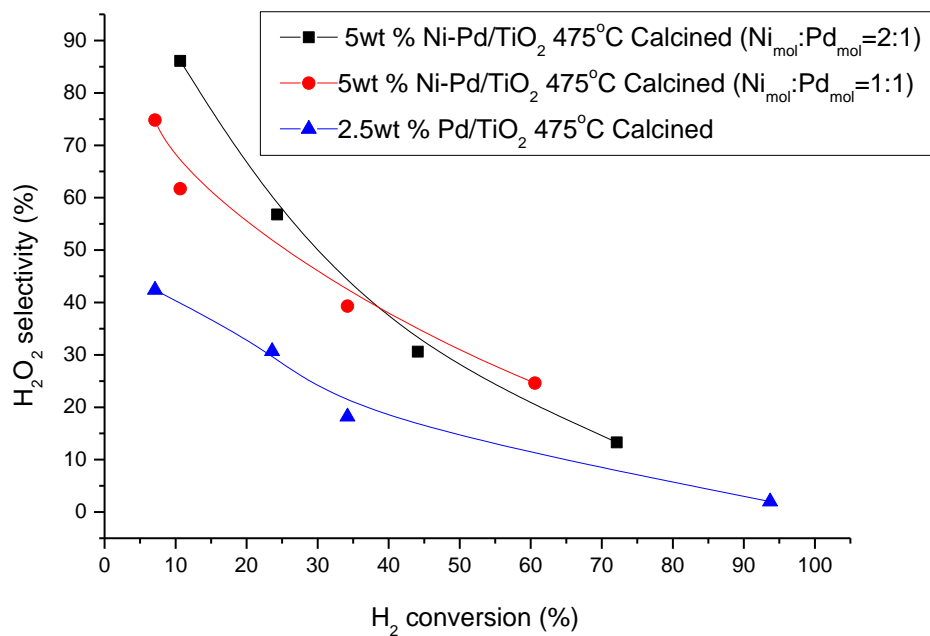**Figure 4-3:** Time-on-line H_2 conversion over Ni-Pd/TiO₂ and Pd/TiO₂ catalysts

Figure 4-4: The relation of H_2 conversion and H_2O_2 selectivity over Ni-Pd/TiO₂ and Pd/TiO₂ catalysts

The curves of H_2 conversion and H_2O_2 selectivity relation over Ni-Pd bimetallic (molar ratio=2:1 and 1:1) and Pd only catalysts are demonstrated in Figure 4-4. It can be noticed that the bimetallic catalysts demonstrate higher selectivity towards H_2O_2 than that of Pd only sample. This indicates that the addition of Ni to Pd enhanced catalytic selectivity towards H_2O_2 during the reaction of H_2 and O_2.

Time-on-line molar production of H_2O_2 for bimetallic and monometallic catalysts was also determined and is shown in Figure 4-5. Separate experiments were conducted for each reaction time and so the data present the amount of H_2O_2 formed over the reaction period. The slope of the curve between two points reflects an average H_2O_2 production rate over the reaction time between two points. As seen in Figure 4-5, at the very beginning of each curve, the steepest slopes appeared indicating the highest rate of hydrogen peroxide for short time reaction indicating the fast reaction of H_2O_2 direct formation. With the accumulation of hydrogen peroxide over time, the rate of side reactions increased simultaneously until a balance of target reaction and side reactions, thereby, peak concentrations of hydrogen peroxide appeared at maximum points. After the maximum point which can be observed in the figure, the rate of consuming H_2O_2 was higher than that of H_2O_2 production, thereby resulted in a decrease of the product. According to the results in Figure 4-5, the peak values of bimetallic catalysts appeared much higher and earlier than that of pure Pd catalyst indicating a higher production rate towards H_2O_2 over bimetallic catalysts relative to Pd monometallic catalyst.
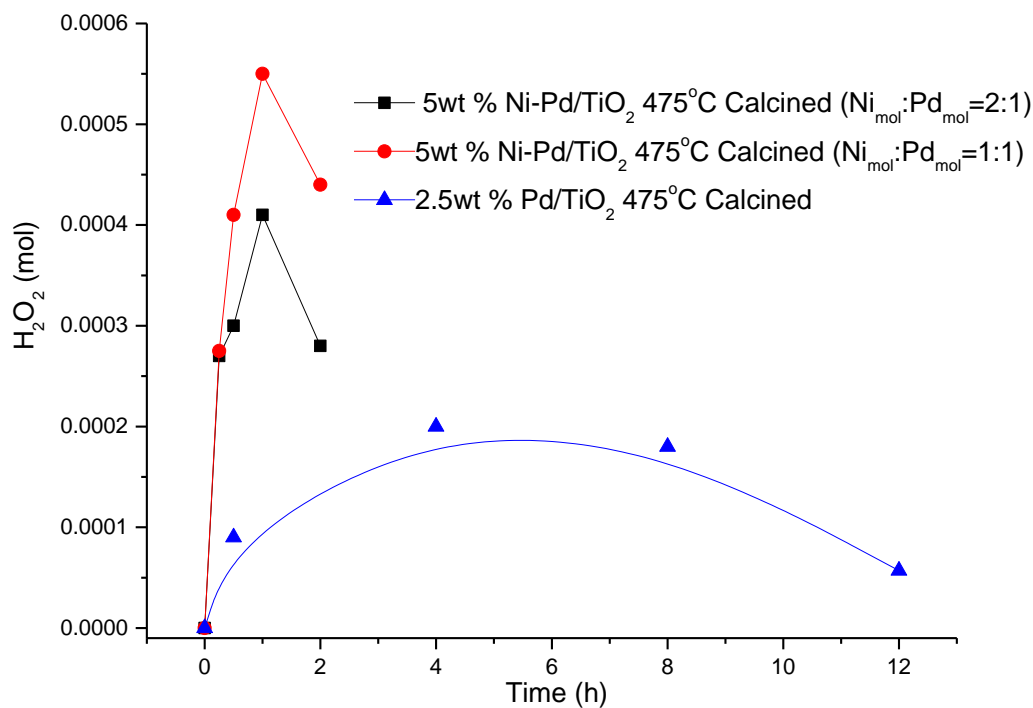
Figure 4-5: The production of H₂O₂ over time using Ni-Pd/TiO₂ and Pd/TiO₂ catalysts

4.3 Characterization

4.3.1 Microwave Plasma-Atomic Emission Spectrometer (MP-AES)

MP-AES analysis was used for the investigation of the actual loading on TiO₂ which is an essential reference for the investigation of catalytic performance and catalyst characterizations. The summarized results are listed in Table 4-3. For Pd in both bimetallic and monometallic catalysts, approximately 40 wt% was lost in the preparation indicating some of Pd stayed in the containers during the impregnation. Moreover, Pd contents were similar in bi- and mono-metallic samples inferring the enhanced activity was originated from the addition of Ni rather than the variation of Pd loading. In the comparison between fresh and used 2.5 wt% Ni-2.5 wt% Pd/TiO₂ catalysts, it can be noticed that c.a. 24 wt% Ni and 9 wt% Pd leached into the medium after one standard reaction. This was possibly responsible for the suppressed activity for hydrogen peroxide synthesis over the used Ni-Pd catalyst.

Table 4-3: The summary of metal loading in catalysts according to the analysis of MP-AES

Catalyst	Target metal loading (wt%)		Actual metal loading (wt%)		Leaching (%)	
	Ni	Pd	Ni	Pd	Ni	Pd
Ni-Pd/TiO$_2$ (2:1) fresh	2.5	2.5	2.51	1.54	-	-
Ni-Pd/TiO$_2$ (2:1) used	-	-	1.92	1.40	23.8	8.9
Pd/TiO$_2$	-	2.5	-	1.36	-	-
Ni/TiO$_2$	2.5	-		-	-	-
Ni-Pd/TiO$_2$ (1:1)	1.7	3.3	1.69	1.71	-	-
Ni-Pd/TiO$_2$ (1:2)	1.0	4.0	1.02	2.35	-	-

4.3.2 Scanning Transmission Electron Microscopy (STEM)

Detailed STEM analysis combined with XEDS was carried out to compare the morphologies of 2.5 wt% Ni-2.5 wt% Pd/TiO$_2$ and 2.5 wt% Pd/TiO$_2$ catalysts to understand the effect of Ni. Representative HAADF-STEM images are shown in Figure 4-6 for comparative particle size analysis of bimetallic and monometallic catalysts. It was observed that the bimetallic catalyst demonstrated highly dispersed particles and tight particle size distribution centred around 1-2 nm with a few isolated particles ranged from 2-4 nm. The Pd only catalyst demonstrated relatively larger particles with a much wider particle size range of 1-14 nm including a number of much larger particles over 14 nm, and as a consequence, relatively limited amount of particles could be observed from the corresponding images. Scanning electron microscopy was also used attempting to find grains which were possibly neglected by HAADF-STEM. It turned out that large particles could not be observed in either of the samples. The phenomenon of the better dispersion in Ni-Pd bimetallic catalyst relative to monometallic Pd is consistent with the

results of XRD in Chapter 3 that the addition of Ni to Pd reduced the particle size. Moreover, the 2.5 wt% Ni-2.5 wt% Pd/TiO$_2$ catalyst demonstrated outstanding metal dispersion which was superior than TiO$_2$ supported Au-Pd catalyst prepared through the same method.[5] The attained activity from 2.5 %Ni-2.5 %Pd catalyst was also higher than Au analogue for the direct formation of H$_2$O$_2$.

The approximated particle size distributions for the bimetallic and Pd only catalysts are presented in Figure 4-7 which are able to provide a statistical information of the metal dispersion of these two catalysts. The reason of emphasizing "approximated" is that (i) particles in the bimetallic catalyst demonstrated rather low contrast and poorly defined edges, hence, making it difficult for measuring the accurate particle size; moreover (ii) because of the low dispersion of the particles in the Pd only sample that insufficient particles could be found from the images for the particle size distribution analysis. Hence, the approximated results in Figure 4-7 were originated from 150 and 50 particles in the bi- and mono-metallic samples respectively, and the calculated mean size of the particles in these two catalysts were 1.3 and 7.1 nm.
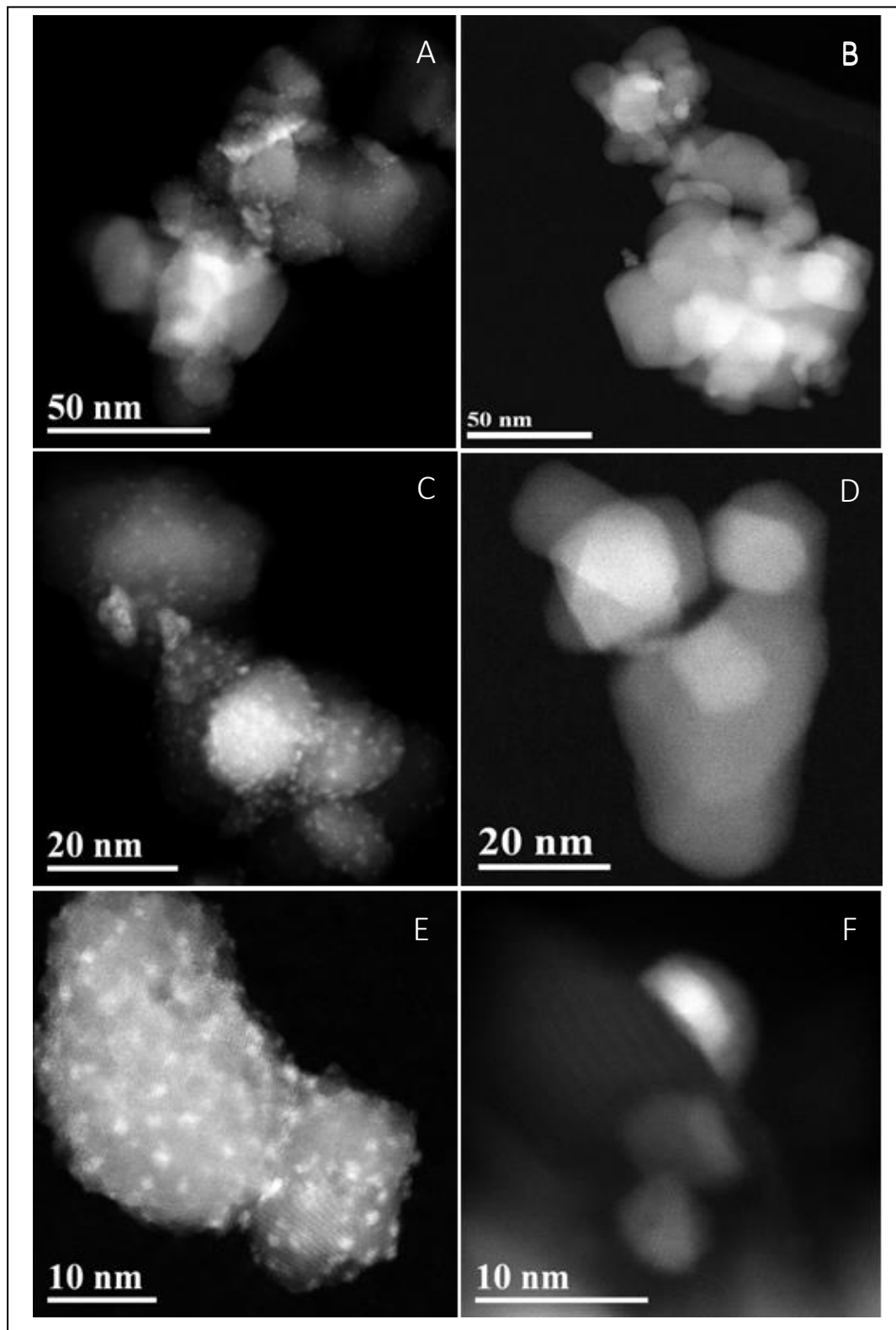
Figure 4-6: HAADF-STEM images of Ni-Pd/TiO₂ and Pd/TiO₂ catalysts. (A, C, E) = 2.5 wt%Ni-2.5 wt%Pd/TiO₂; (B, D, F) = 2.5 wt%Pd/TiO₂
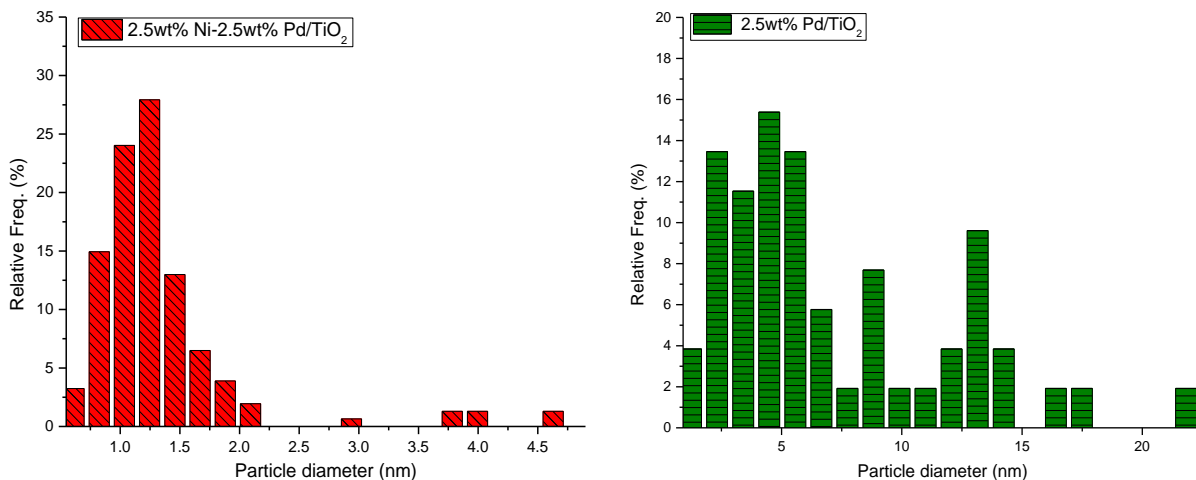
Figure 4-7: Particle size distributions for 2.5 wt% Ni-2.5 wt% Pd/TiO$_2$ (left) and 2.5 wt% Pd/TiO$_2$ catalysts (right).

Compositional information from individual particles was also investigated by STEM-XEDS for both samples. The attained results revealed that in the 2.5 wt% Ni-2.5 wt% Pd/TiO$_2$ catalyst, most of the smaller (1-2 nm) particles were relatively Pd rich with relatively lower amount of Ni, and in contrast, all the lager particles (3-4 nm) were Ni-Pd mixtures. Figure 4-8 demonstrates XEDS line scans for the particles with two sizes in the bimetallic catalyst whose results proved the stated observation. As we can see, Ni and Pd co-existed in the particles shown Figure 4-8 (A, B) with the size of 4 nm, while relatively lower intensity of Ni were demonstrated in the particle with the size of 2 nm (Figure 4-8 (C, D)).
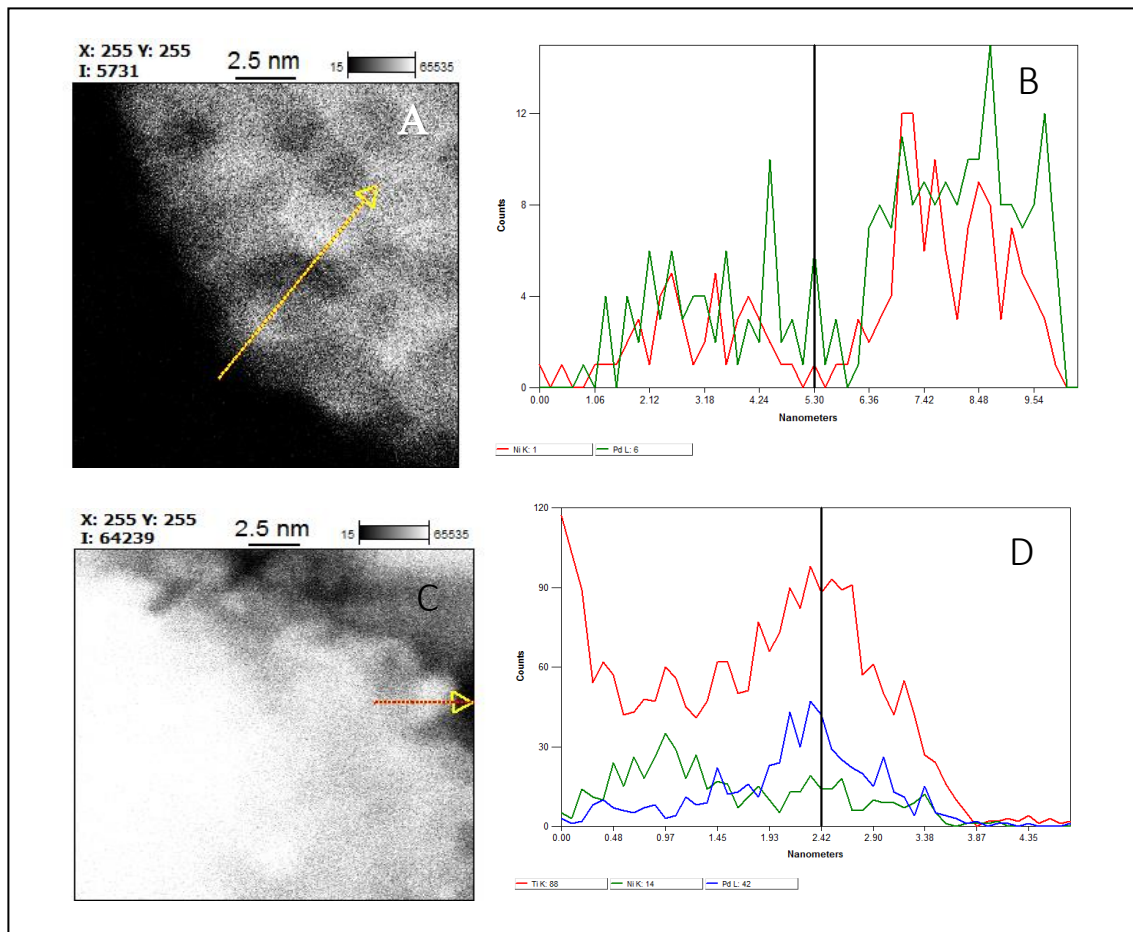
Figure 4-8: High magnification STEM-HAADF image and corresponding XEDS spectrum from individual particles in the 2.5wt%Ni-2.5wt%Pd/TiO₂ catalyst. Image A and B: XEDS line scan over two 4 nm particles, red line-Ni K, green line-Pd L; Image C and D: XEDS line scan over one 2 nm particle, green line-Ni K, blue line-Pd L

XEDS maps of the particles in the Ni-Pd catalyst show a definite discrepancy between the spatial extent of the Pd and Ni signals. Representative images are shown in Figure 4-9, that Pd L and Ni K were chosen and marked as purple and green respectively. It can be noticed that both Ni and Pd were noticeable in particles which however did not demonstrate a regular morphology of Ni and Pd in the particles (e.g. core-shell structure).
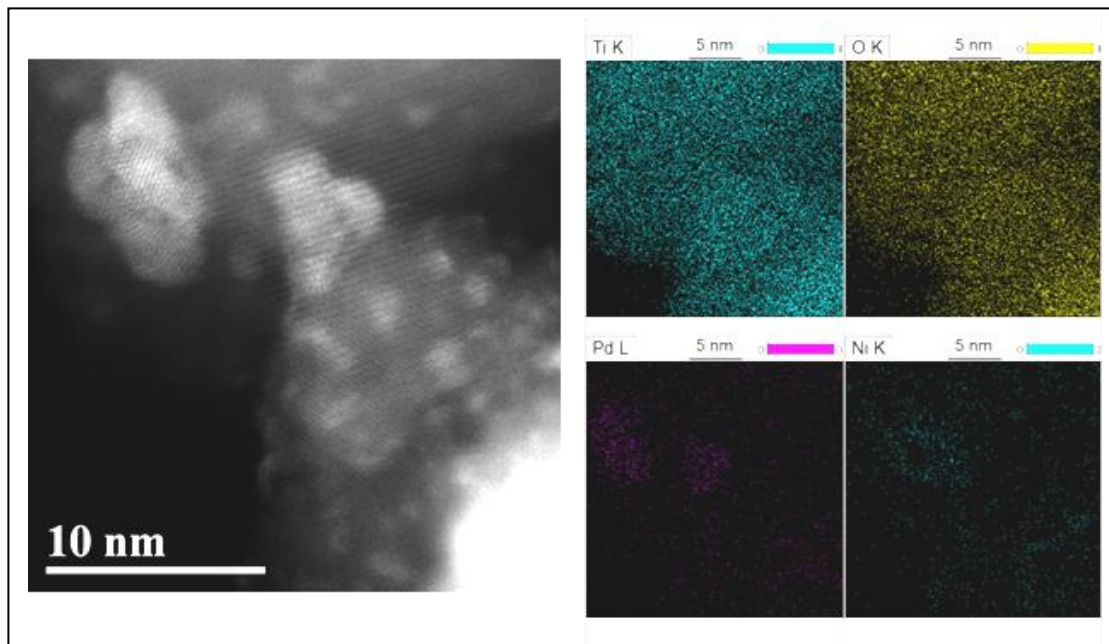
Figure 4-9: HAADF-STEM image (left) and corresponding XEDS maps (right) of Ti (top left), O (top right, Pd (bottom left) and Ni (bottom right) for the 2.5wt%Ni-2.5wt%Pd/TiO$_2$ catalyst
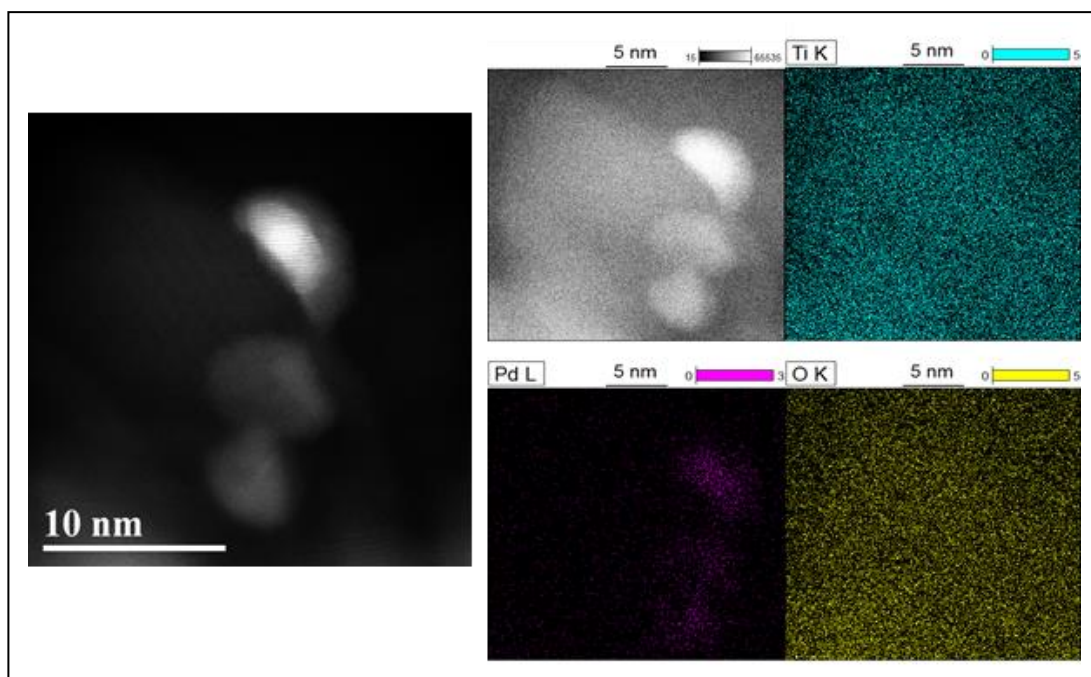

Figure 4-10: HAADF-STEM image (left) and corresponding XEDS maps (right) of Ti (top right), Pd (bottom left) and O (bottom right) for the 2.5wt%Pd/TiO$_2$ catalyst

HAADF-STEM analysis combined with XEDS maps were also carried out for individual particles in the Pd only catalyst. The representative images in Figure 4-10 demonstrated that the shell of the Pd particle were poorly defined that represents Pd oxides, nevertheless, well defined crystallite lattice could be observed in the core of the particles representing metallic Pd. Hence, conclusion can be made that the structure of Pd particles in Pd only catalyst were Pd oxide shell and Pd(0) core.

4.3.3 X-ray Photoelectron Spectroscopy (XPS)

XPS analysis was used to detect the oxidation states and atomic ratio of the elements on the catalyst surface. Fresh and used samples were first analysed in order to investigate the effect of reaction conditions during hydrogen peroxide synthesis on the surface structure of the catalysts. Moreover, Ni-Pd bimetallic catalysts calcined at different temperature were also tested for understanding the influence of calcination temperature. The attained spectra and summarized results are demonstrated in Figure 4-11, Figure 4-12, Table 4-4 and Table 4-5 respectively. As we can see in Figure 4-11, the Ni 2p spectra of all these four samples show a complex structure content with main peaks and adjacent shake up peaks which were attribute to multi-electron excitation.[7] This is in agreement with the explanation in Chapter 3. The binding energies around 855.7 eV in all the spectra are corresponding to Ni $2p_{3/2}$ of Ni^{2+} indicating that Ni species were dominant by Ni oxides on the surface of the catalysts.[8]
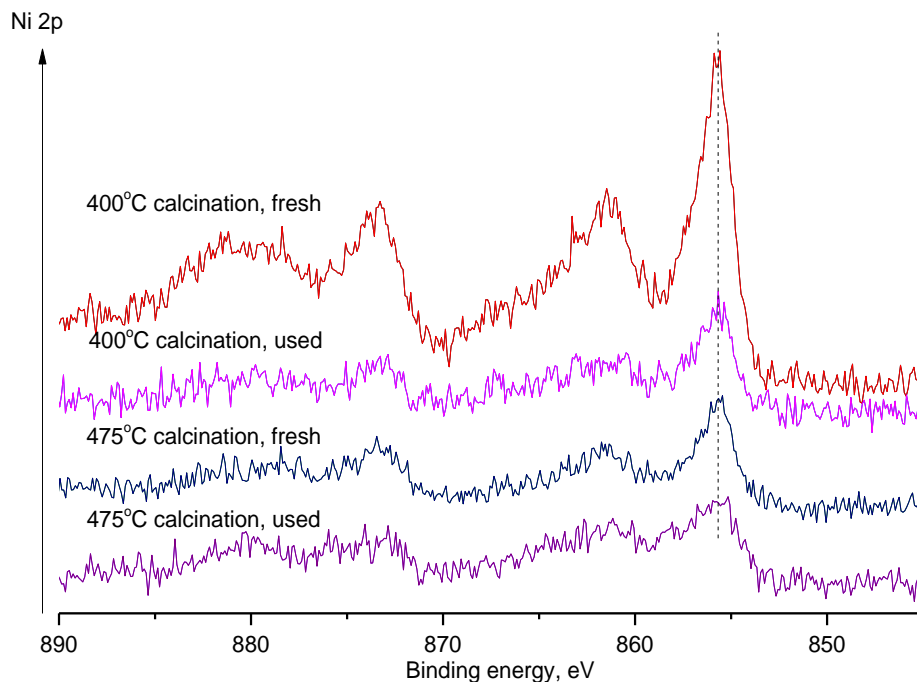
Figure 4-11: XPS spectra of Ni 2p in 2.5%Ni-2.5%Pd/TiO₂ catalysts

It has been demonstrated by XPS results of single crystal metallic Pd and PdO surface that the binding energy for Pd^0 $3d_{5/2}$ and $3d_{3/2}$ corresponding to 335.0 and 340.1 eV, respectively, while the binding energy at 337.2 and 342.2 eV was assigned to $3d_{5/2}$ and $3d_{3/2}$ of Pd^{2+}.[9] In each Pd 3d spectrum of Ni-Pd catalysts, two main peaks with shoulders showed up inferring the coexistence of Pd^0 and Pd^{2+} (Figure 4-12). It can be noticed that the ratio of Pd^0/Pd^{2+} increased after reactions of peroxide synthesis relative to both fresh samples, indicated by $Area_{Pd,\ 3d}/Area_{PdO,\ 3d}$ (Table 4-5). It has been proved that the composition of H_2/O_2 can strongly influence the time-on-line behaviour of the oxidation state of Pd in the catalysts.[10] Similar as the observation of Melada *et al.*[11], fresh Ni-Pd catalyst with yellow colour turned into dark grey after the direct synthesis of hydrogen peroxide. Hence, the adopted reaction conditions with the $H_2:O_2$ ratio of 1:2 provided a reducing environment for Pd during hydrogen peroxide synthesis. This observation can provide a possible interpretation of the increased hydrogenation rate of the used catalyst (Table 4-2) as Pd^0 is active but not selective for the H_2O_2 formation.[12,13]
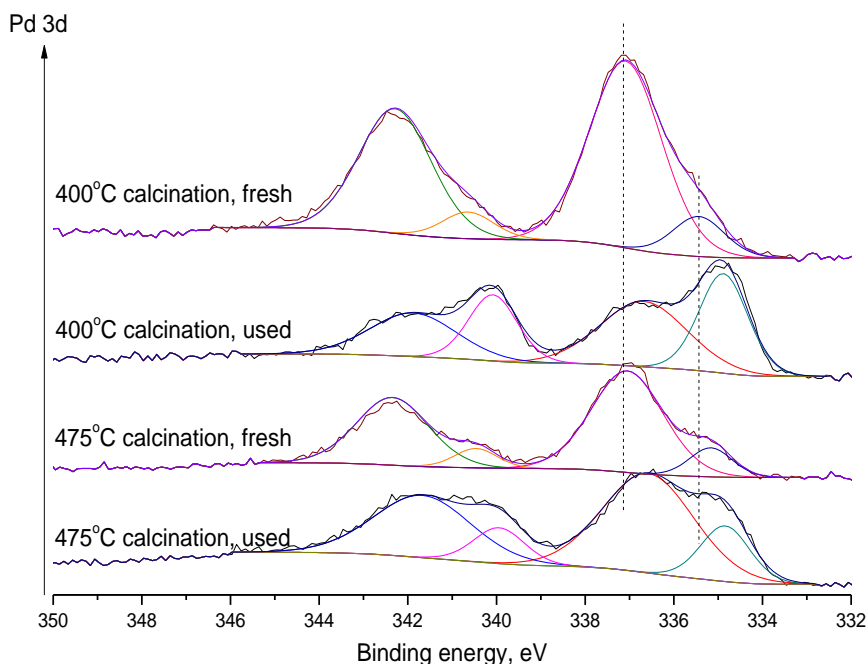
Figure 4-12: XPS spectra of Pd 3d in 2.5%Ni-2.5%Pd/TiO₂ catalysts

Table 4-4: The summary of the binding energies assigned to Pd $3d_{5/2}$ and Ni $2p_{3/2}$

Catalyst	Productivity (mol kg^{-1} h^{-1})	B.E. /eV		Ni(2p)
		Pd(3d)		
		Pd(II)	Pd(0)	
2.5%Ni2.5%Pd/TiO₂ 400 °C cal. fresh	103	337.1	335.4	855.7
2.5%Ni2.5%Pd/TiO₂ 400 °C cal. used	77	336.7	334.8	855.7
2.5%Ni2.5%Pd/TiO₂ 475 °C cal. fresh	78	337.2	335.2	855.8
2.5%Ni2.5%Pd/TiO₂ 475 °C cal. used	63	336.6	334.8	855.7

According to Figure 4-12 and Table 4-5, both used catalysts demonstrated lower Ni and Pd atomic ratio on the surface in the comparison with the fresh samples that may be caused by metal leaching during reaction. This is in agreement with the observations

106

from MP-AES (Table 4-3). Moreover, the sample treated by 475 $^{\circ}$C calcination demonstrated lower Ni and Pd atomic ratios relative to the 400 $^{\circ}$C treated analogue suggesting the lower metal dispersion originated from the higher temperature heat treatment. This provided an explanation for the relatively low activity of the sample treated at high temperature (Figure 4-1), which may possess relatively lower number of active sites. In addition, the surface ratio of Ni/Pd is lower than that of bulk indicating a Pd rich surface. This can be understood by STEM-XEDS results that a number of small size Pd rich particles were observed.

Table 4-5: Results summary of Ni/Pd ratio and oxidation states according to XPS and MP-AES

5 wt% Ni-Pd/TiO₂ (Ni:Pd=2:1)	Pd(II):Pd(0)	Ni at%	Pd at%	Ni$_{at}$/Ti$_{at}$ (surface)	Pd$_{at}$/Ti$_{at}$ (surface)	Ni$_{at}$/Pd$_{at}$ (surface)	Ni$_{at}$/Pd$_{at}$ (bulk)*	Cl at%
400°C cal. fresh	87:13	4.84	1.90	0.19	0.073	2.55	3.23	3.30
400°C cal. used	54:36	1.93	1.40	-	-	-	-	0.64
475°C cal. fresh	88:12	2.30	1.48	0.079	0.051	1.55	3.23	1.08
475°C cal. used	77:23	1.22	1.16	-	-	-	-	0.57

*Determined by MP-AES

5 wt% metal loading samples with distinct Ni/Pd ratios were also investigated through XPS analysis, and patterns including results summary are shown in Figure 4-13, Figure 4-14 and Table 4-6 respectively. As seen in Figure 4-13, similar spectra of Ni 2p were attained whose binding energies around 855.8 eV were all assigned to Ni 2p$_{3/2}$ of Ni^{2+} suggesting Ni oxides dominant on the surface. According to Figure 4-14, in the Pd 3d$_{5/2}$ spectrum of the monometallic sample, peaks were fitted into one component and binding energy centred at 336.3 eV was ascribed to Pd(II). With the addition of Ni, an obvious shoulder adjacent to the Pd(II) peak appeared which was corresponding to Pd (0), indicating additive Ni to Pd enhanced the stability of surface metallic Pd.
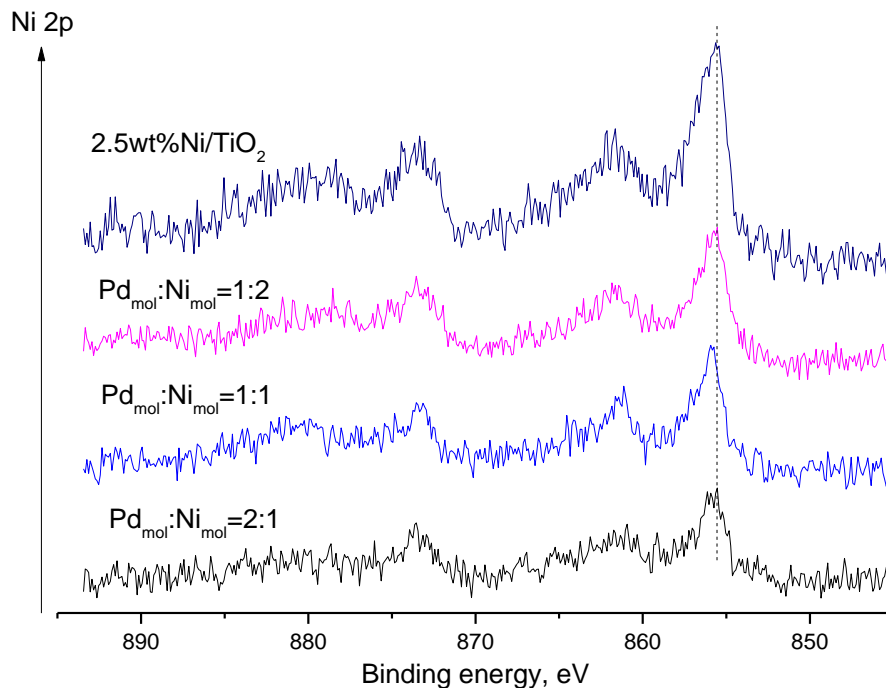
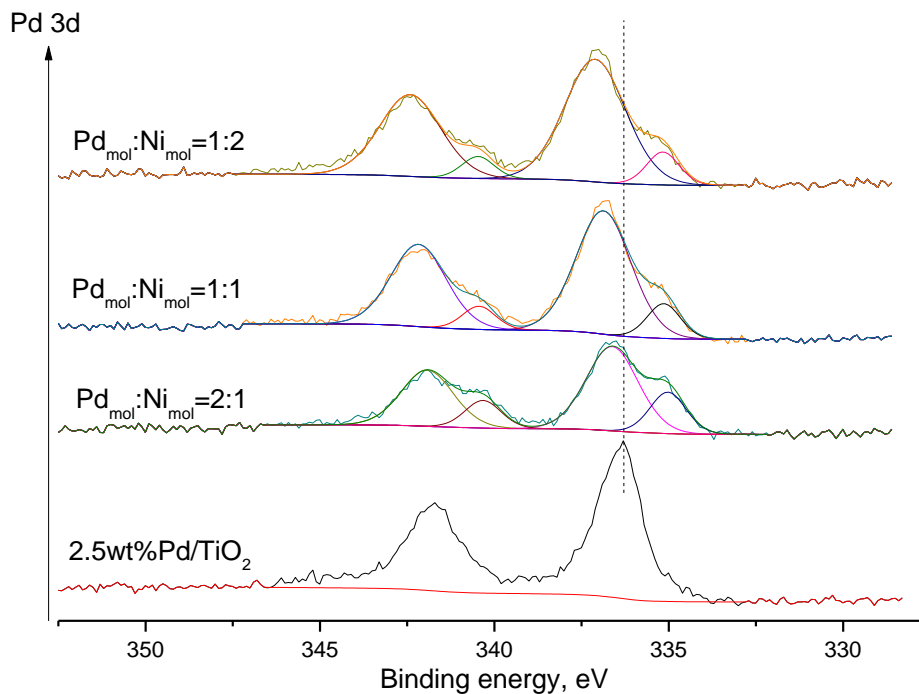**Figure 4-13:** The Ni 2p spectra of Ni, Pd monometallic and bimetallic catalysts

Figure 4-14: The Pd 3d spectra of Ni, Pd monometallic and bimetallic catalysts

According to the quantified results in Table 4-6, Ni-Pd bimetallic catalysts demonstrate higher surface atomic ratio of Pd than that of the Pd only catalyst. Moreover, with the

increase of Ni loading in 5 wt% Ni-Pd catalysts, the corresponding atomic ratio of Pd increased on the surface simultaneously. As shown, surface composition of Pd increases from 0.79% for 5%Ni-Pd/TiO₂ (Ni:Pd=1:2) to 1.48% in 5%Ni-Pd/TiO₂ (Ni:Pd=2:1). This is in agreement with HAADF-STEM results as much better dispersed particles in Ni-Pd bimetallic catalyst than Pd only catalyst.

Table 4-6: Summary of surface atom concentration and oxidation states for Ni/Pd catalysts

Catalyst		Ni at%	Pd at%	Pd(II):Pd(0)	$Ni_{at}:Pd_{at}$ (surface)	$Ni_{at}:Pd_{at}$ (bulk)*	$(Ni+Pd)_{at}/Ti_{at}$ (surface)	$(Ni+Pd)_{at}/Ti_{at}$ (bulk)
2.5 wt% Ni/TiO₂		2.48	-	-	-	-	0.086	0.072
5 wt% Ni-Pd/TiO₂ (Ni:Pd)	**2:1**	2.30	1.48	88:12	1.55	3.23	0.132	0.056
	1:1	1.77	1.18	86:14	1.50	-	0.103	0.051
	1:2	1.16	0.79	75:25	1.47	-	0.066	0.046
2.5 wt% Pd/TiO₂		-	0.72	100:0	-	-	0.023	0.040

*Determined by MP-AES

It can be noticed that the binding energy of Pd $3d_{5/2}$ assigned to Pd^{2+} over bimetallic samples was at around 336.5-337 eV, to some extent higher than the measured binding energy of Pd $3d_{5/2}$ assigned to PdO in the range 336.0±0.2 eV and also the binding energy of Pd $3d_{5/2}$ over the 2.5 wt% Pd/TiO₂ catalyst. STEM and XPS analysis together suggests this energy to be indicative of two possibilities: (i) particle size effects, wherein the Pd core-hole screening during photoemission results in a higher binding energy for small particles[14] or (ii) $Pd^{\delta+}$ formation through charge transfer with Cl[15] adsoprtion on either Pd itself or neighbouring sites. The latter point is supported by the XPS results of used sample that the binding of Pd^{2+} shifted back to 336 eV (Table 4-4) and metal leaching occurred during reaction, which indicates $PdCl_x$ could be washed off the surface after reaction. Shen and co-workers' work[16] also supported the second inference

as Pd has a more positive valence than the corresponding halide-free system, consequently demonstrating relatively higher binding energies.

In conclusion, during the direct synthesis of hydrogen peroxide, reaction medium provided a reducing environment that increased the ratio of Pd (0) on the catalyst surface and simultaneously, unstable metal particles leached into the reaction solvent, possibly caused an decrease of both Ni and Pd on the surface of the used samples. In addition, high temperature heat treatment led to an agglomeration of particles, as a consequence, resulted in a lower metal atomic ratio on the surface and also a lower reaction rate. Moreover, the addition of Ni in Pd stabilized surface Pd (0) and a higher atomic ratio of Pd on the surface. The latter was consistent with the observations from STEM that higher dispersion of particles in the bimetallic catalyst compared with Pd only sample. Besides, relative atomic ratio of Pd was higher than that of bulk indicating a Pd rich surface on Ni-Pd bimetallic catalyst. This is to some extent in agreement with one of the observations from STEM-XEDS that small size Pd rich particles were observed.

4.3.4 Temperature Programmed Reduction (TPR)

TPR was used for the investigation of the reducibility of the species over TiO$_2$ supported catalysts and the attained profiles are shown in Figure 4-15. For 2.5 wt% Ni/TiO$_2$ sample, a single positive peak with a maximum at 380 ℃ is observed, which could be assigned to the reduction of NiO. The profile of 2.5 wt% Ni-2.5 wt% Pd/TiO$_2$ demonstrated a single reduction peak centred at 282 ℃ which negatively shifted by 98 ℃ compared to the reduction temperature of NiO in Ni only catalyst. The substantial decrease indicates that Pd assisted the formation of metallic Ni possibly by H$_2$ spillover effect.[17] A mixture of Ni and Pd in individual particles shown by STEM-XEDS may support this inference.

Although XPS and STEM suggested the existence of PdO on the top of Pd monometallic catalyst, no bulk reduction signal of PdO could observed in the profile of 2.5 wt% Pd/TiO$_2$ catalyst except a small positive peak centred at 227 ℃. It was reported that PdO is exclusively reducible that majority of Pd oxides can be reduced even below

room temperature under H_2 with a reduction peak of the bulk ranging from 182 to 250 ºC.[17] Hence, PdO could be reduced at room temperature during the stabilization of TCD signal. It also can be noticed that a strong single negative peak centred at 86 ºC assigned to the decomposition of β-PdH$_x$. Herein, β-PdH$_x$ is defined as a crystallographic phase of Pd caused by the absorption of hydrogen into Pd metal, whose peculiar property can be used to characterize supported Pd catalysts.[18–21] For the profile of 2.5 wt% Ni-2.5 wt% Pd/TiO₂ catalyst, the negative peak representing β-PdH$_x$ negatively shifted from 80 ºC to 60 ºC by adding Ni to Pd, whose intensity was also substantially suppressed. The integrated results of β-PdH$_x$ are shown in Table 4-7. Both changes possibly caused by a few indicative possibilities: (i) the addition of Ni enhanced the dispersion of Pd particles as well-dispersed Pd has been proved to absorb relatively low amount of H_2[22,23] compared to bulk Pd; and (ii) the interaction of Ni and Pd (e.g. Ni-Pd alloys) caused a lower stability of β-PdH$_x$ which consequently decomposed at lower temperature;[24,25] (iii) moreover, the additive Ni possibly blocked Pd surface sites that inhibited the formation of β-PdH$_x$. In fact, the first two inferences are consistent with the observations from STEM in 4.3.2 as a better particle dispersion over the bimetallic catalyst and the possible formation of Ni-Pd random alloys were noticed.
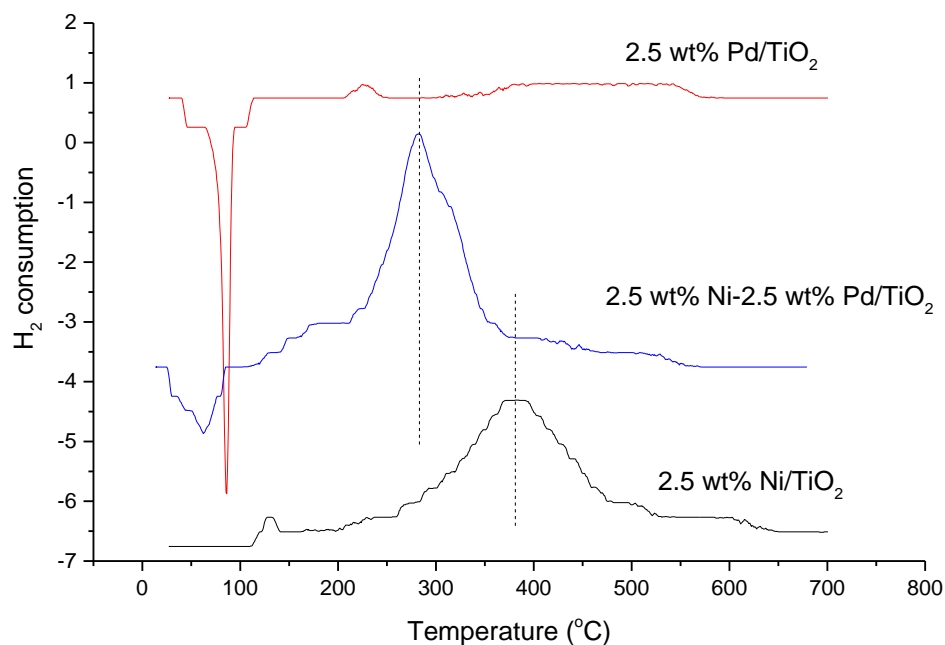

Figure 4-15: TPR analysis for Ni/Pd monometallic and bimetallic catalysts after 475 ºC calcination

Table 4-7: Integrated information of β-PdH$_x$ through TPR over Ni/Pd bimetallic and Pd only catalysts

Catalyst	Catalyst mass (mg)	Peak area (β-PdH$_x$)
2.5wt%Pd/TiO$_2$	50	-87.61
2.5wt%Ni-2.5wt%Pd/TiO$_2$	50	-39.49

In summary, TPR analysis demonstrated a substantial decrease of Ni reduction temperature with the addition of Pd to Ni. The reduction of Pd however was not noticeable since PdO species in both catalysts may already be reduced at room temperature. Moreover, the substantial decrease of both decomposition temperature and TCD intensity of Pd hydrides can be explained by HAADF-STEM observations in 4.3.2 as a better dispersion of Pd and the formation of Ni-Pd mixture in individual particles.

4.3.5 *In situ* Diffuse Reflectance Infrared Fourier Transform Spectroscopy (DRIFTS) with CO adsorption and desorption

In situ DRIFTS were recorded with the adsorption and desorption of CO on 2.5 wt% Ni-2.5 wt% Pd/TiO$_2$ and 2.5 wt% Pd/TiO$_2$ catalysts after 475 ℃ calcination for 3 h in order to investigate the surface property of these two catalysts. Both samples were pre-treated under N$_2$ with a flow rate of 12 ml/min at 110 ℃ for 1 h in order to dehydrate the catalysts, followed by an additional CO flow with a rate of 3 ml/min at room temperature. Infrared scan was conducted every 60 seconds until the surface was saturated with CO that spectra did not demonstrate any change. CO was then switched off followed by a continuous flow of 15 ml/min N$_2$, and infrared spectra were also recorded every 60 seconds. Selected spectra are presented in Figure 4-16, 4-17, 4-18 and 4-19. According to previous research, the wavenumbers of CO bonds at 2096, 1977, 1910 and 1851 cm^{-1} were assigned to the adsorption of CO on metallic Pd with distinct bonds.[26] The wavenumbers at 2096 cm^{-1} represents the linear bond of CO at the Pd with a low coordination. The bonds in the range of 1750-2000 cm^{-1} correspond to bridge or multi-bonded CO on Pd ensembles which consist two or more continuous Pd atoms on

the surface.[27] The obtained spectra of adding CO to 2.5 wt% Pd/TiO_2 sample are demonstrated in Figure 4-16. Previous XPS analysis (Figure 4-14) demonstrated that the Pd species was PdO on the surface of 2.5 wt% Pd/TiO_2 catalyst, and STEM (Figure 4-10) proved the PdO shell and metallic Pd core structure for the particles in Pd only catalyst. Nevertheless, the peak assigned to linear CO bond with limited intensity can be observed indicating that a number of Pd atoms were pulled out to the surface because of the strong interaction of Pd and CO.[28] As Haire *et al.* stated, on thermodynamic aspect, the surface composition can be adjusted to enrich in the element which interacts strongly with the adsorbate.[29]
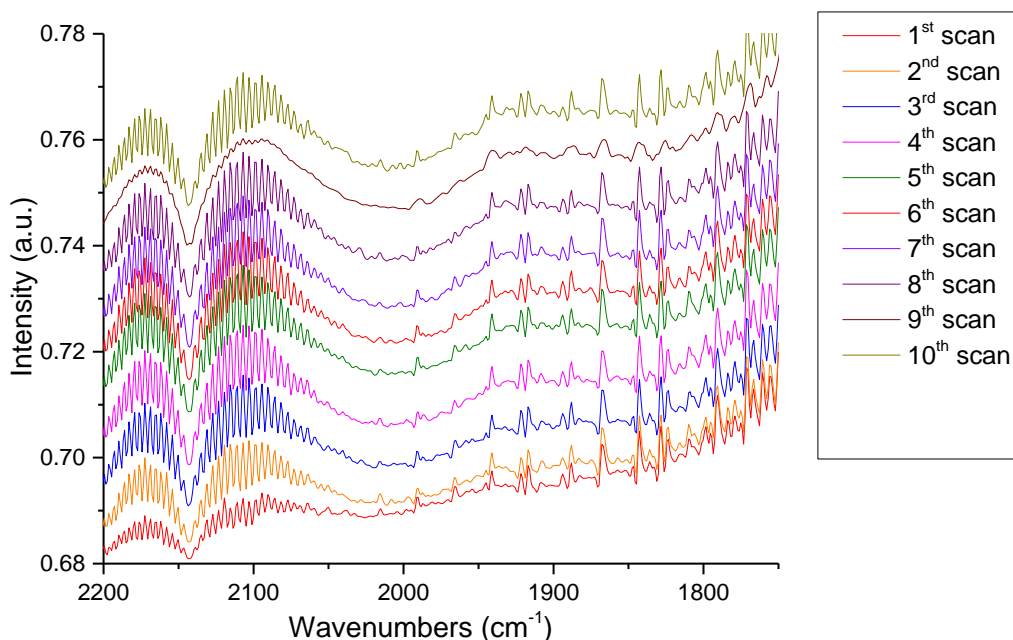
Figure 4-16: In situ DRIFTS of CO adsorption over 2.5 wt% Pd/TiO_2 catalyst

The comparison spectra of CO adsorption over 2.5 wt% Ni-2.5 wt% Pd/TiO_2 and 2.5 wt% Pd/TiO_2 catalysts are shown in Figure 4-17 in order to comprehend the effect of Ni on the surface chemisorption behaviour of Pd. The spectrum of the calcined 2.5 wt% Ni-2.5 wt% Pd/TiO_2 catalyst demonstrates a sharp peak at 2095 cm^{-1} representing the linear bonds of CO and a broad peak from 1973-1875 cm^{-1} assigned to bridge and multi-bonded CO on continuous Pd sites. The total peak area of both linear and multi-bond CO is substantially larger than that of 2.5 wt% Pd/TiO_2 indicating the existence of

metallic Pd on the surface induced by the addition of the secondary metal-Ni. This result is consistent with the observation of XPS (Table 4-6). Furthermore, it can be noticed that the linear bond of CO red shifted from 2017 cm^{-1} to 2095 cm^{-1} on the alloying with Ni. A similar phenomenon was also observed from CO-DRIFTS for Au-Pd catalysts in the comparison with Pd only sample, which was explained as the electron transfer from Au to Pd.[27] As Pd is more electronegative than Ni, the shift probably resulted from an enhancement in d orbital electron because of electron transfer from Ni to Pd that led to a stronger electronic back donation to $2\pi^*$ molecular orbitals of CO.[30]
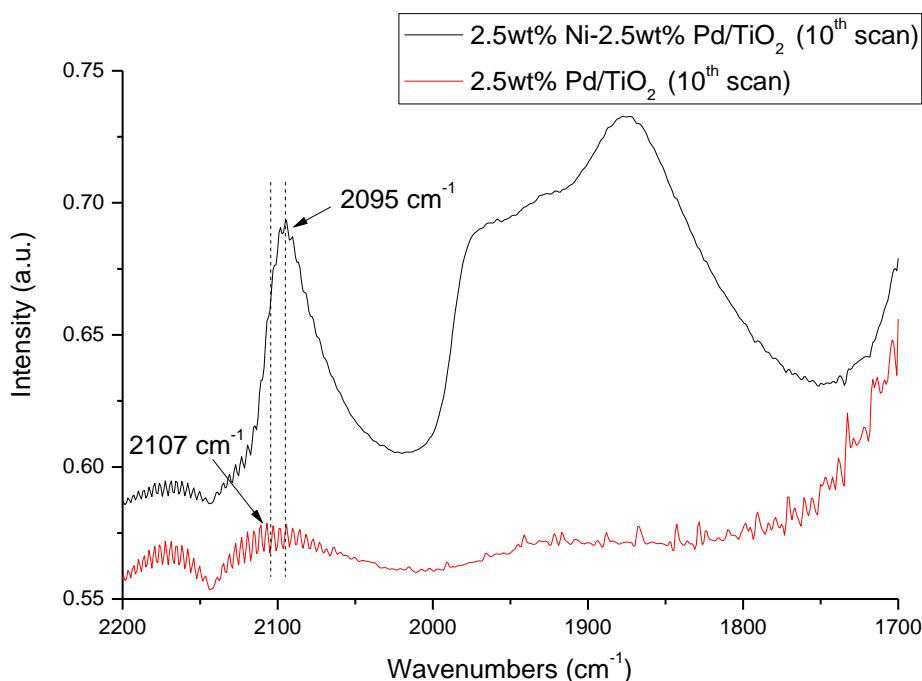
Figure 4-17: Comparison spectra of In situ DRIFTS with CO adsorption over 2.5 wt% Ni-2.5 wt% Pd/TiO₂ and 2.5 wt% Pd/TiO₂ catalysts

Figure 4-18 demonstrates in situ IR spectra with CO adsorption over 2.5 wt% Ni-2.5 wt% Pd/TiO₂ catalyst. As soon as the catalyst was exposed to CO under stated conditions, isolated Pd sites were saturated with linear bond CO that peak intensity did not obviously change after 10 scans. Whereas, the high coordinated Pd sites did not get saturated with multi-bond CO until the 9th scan after ca. 9 min. Moreover, with the increase of exposure time of CO over the bimetallic catalyst surface, bridge bond of CO

gradually appeared which was centred at 1971 cm^{-1} in the end. This probably resulted from the competitive adsorption of CO with the increase of CO in the atmosphere that three-fold or even more bond CO switched into bridge bonds.
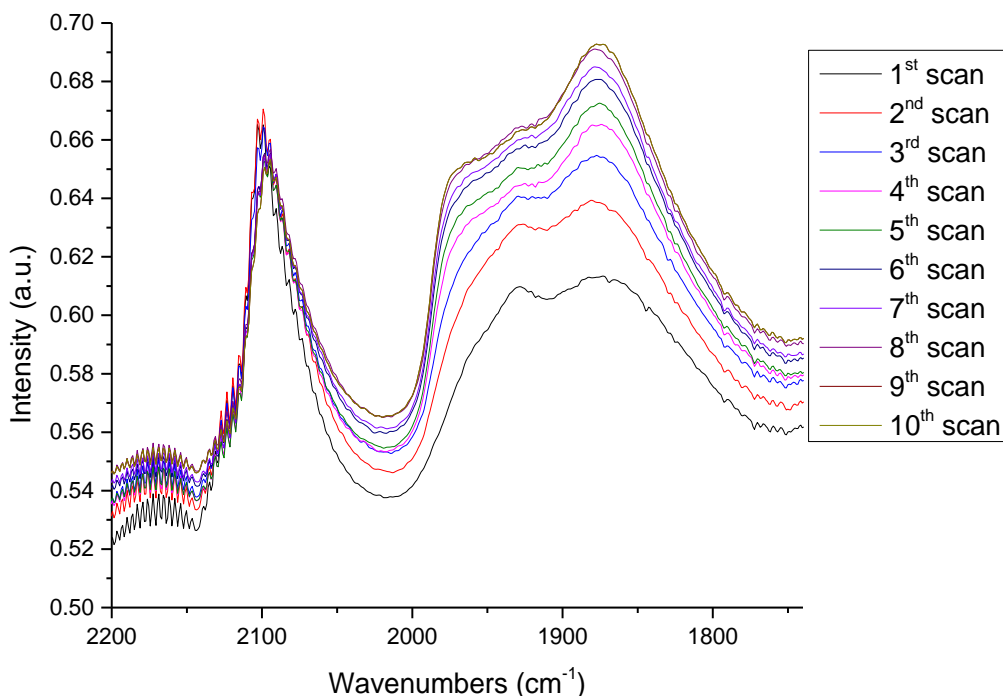
Figure 4-18: In situ DRIFTS with CO adsorption over 2.5 wt% Ni-2.5 wt% Pd/TiO$_2$ catalyst

Furthermore, after switching off CO with a continuous flow of N$_2$, CO on isolated Pd sites - linear-bonded CO was desorbed more efficiently than that on continuous Pd, hence as a result, the peak intensity assigned to individual Pd sites decreased faster than that of continuous Pd which is shown in Figure 4-19. This claims that isolated Pd sites adsorbed and desorbed much more efficiently relative to continuous Pd sites. As a result, individual Pd sites are probably beneficial for the direct synthesis of hydrogen peroxide through the quicker and weaker interaction of reactant and product without dissociation.[31,32]
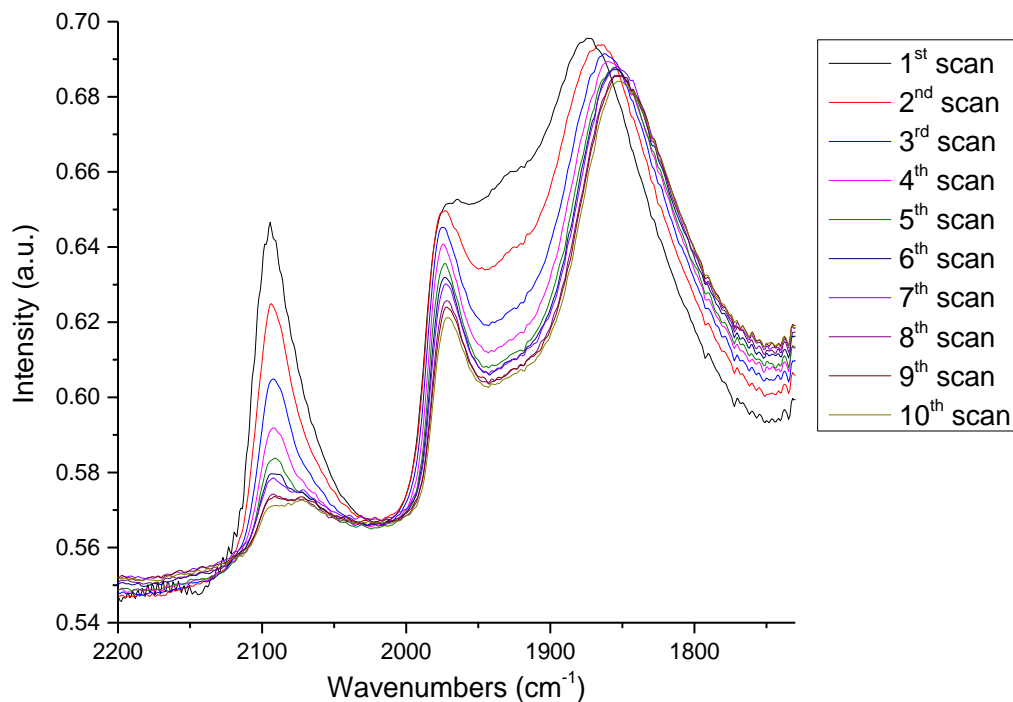
Figure 4-19: In situ DRIFTS with CO desorption over 2.5 wt% Ni-2.5 wt% Pd/TiO$_2$ catalyst

4.4 Discussion

4.4.1 The overall activity, H$_2$O$_2$ selectivity and H$_2$O$_2$ production rate for the direct synthesis of hydrogen peroxide

First of all, it is necessary to understand the concepts of the overall activity, H$_2$O$_2$ selectivity and H$_2$O$_2$ production rate for the direct synthesis of hydrogen peroxide and the relation between them. Scheme 4-1 demonstrates the target reaction (Route A) and side reactions (Route B, C and D) during the hydrogen peroxide synthesis which is helpful for the comprehension of the results in Figure 4-3, 4-4 and 4-5. According to Route A and B, the atoms of activated hydrogen are able to react with activated oxygen molecules and atoms, and subsequently produce H$_2$O$_2$ and H$_2$O. Produced H$_2$O$_2$ can be possibly further hydrogenated or decomposed into water by Route C and D. Hence, H$_2$O$_2$ in fact acts as an intermediate of Route A+C and Route A+D that both overall reaction equations can be written as Equation 4-1 which is the same as H$_2$ combustion (Route B). Therefore, the consumption rate of hydrogen shown in Figure 4-3 is a sum

116

rate of Equation 4-1 and 4-2, namely the overall reaction rate. The attained results shown that the bimetallic catalysts demonstrated much enhanced overall reaction rate relative to Pd only catalyst.
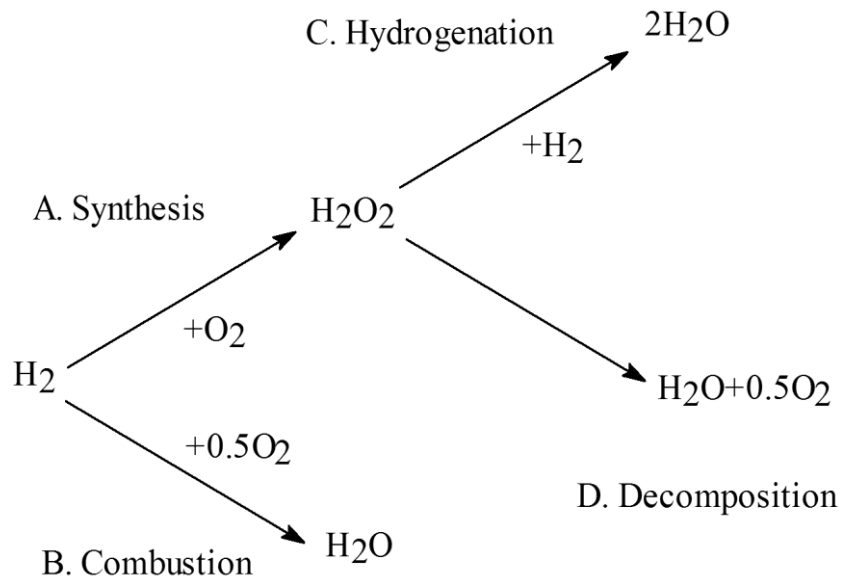
Scheme 4-1: Reaction routes during the direct synthesis of hydrogen peroxide.

$$H_2 + 0.5O_2 \rightarrow H_2O \qquad \text{(Equation 4-1)}$$

$$H_2 + O_2 \rightarrow H_2O_2 \qquad \text{(Equation 4-2)}$$

Furthermore, including the higher overall reaction rate for hydrogen peroxide synthesis, the bimetallic catalysts also demonstrated superior selectivity than that of the pure Pd catalyst (Figure 4-4). According to Equation 4-3, if one catalyst exhibits an outstanding performance in both H_2O_2 selectivity and overall H_2 consumption rate, it has to demonstrate a high observed production rate of H_2O_2. Equation 4-4 explains that the observed H_2O_2 is the remained product after the consumption of parallel hydrogenation and decomposition. The results of time-on-line observed H_2O_2 over Ni-Pd and Pd only catalysts (Figure 4-5) supported this deduction as Ni-Pd bimetallic catalyst not only demonstrated higher H_2 conversion rate and superior H_2O_2 selectivity, but also showed enhanced H_2O_2 productivity relative to those of Pd only catalyst.

$$H_2O_2 \text{ selectivity } (\%) = \frac{H_{2}O_{2 \text{ observed}} \text{ (mol)}}{\text{overall } H_2 \text{ consumption (Route A + B + C)(mol)}} \times 100\%$$

(**Equation 4-3**)

$H_2O_2 \text{ productivity}_{observed} = H_2O_2 \text{ productivity} - \text{Hydrogenation rate} - \text{Decomposition rate}$

(**Equation 4-4**)

### 4.4.2 The relation between catalyst structure and catalytic performance

Pd is well known as an active catalyst for hydrogenation reactions[33] which demonstrates superior performance for activating H_2 than that of Ni.[34,35] In this work, the addition of Ni to Pd did not compromise the activity for activating H_2, on the contrary, it improved the time-on-line H_2 consumption as shown in Figure 4-3. A direct evidence from STEM analysis (Figure 4-6 and 4-7) proved a superior particle dispersion of 2.5%Ni-2.5%Pd/TiO₂ catalyst with a mean size of 1.3 nm whereas 7.1 nm for 2.5%Pd/TiO₂. Moreover, XPS results also demonstrated a higher atomic ratio of Pd on the surface of the bimetallic catalyst relative to that of Pd only catalyst (Table 4-7). Hence, the higher H_2 consumption rate over bimetallic catalysts compared with Pd monometallic catalyst possibly attributed to the increased particle dispersion of Ni-Pd catalysts than Pd only catalyst.

In addition, if the additive Ni merely dispersed Pd without forming strong interaction with Pd (e.g. Ni-Pd alloys), the H_2O_2 selectivity originated from the bimetallic catalysts should be similar to or even lower than that of Pd only catalyst according to the observations in Chapter 3. Hence, the nature of the Pd sites were apparently altered by Ni that resulted in both higher overall reaction rate and H_2O_2 selectivity. TPR results in Figure 4-15 imply the strong interaction of Ni and Pd as the reduction temperature of Ni oxides was substantially decreased by nearly 100 °C in the bimetallic catalysts compared with that of the Ni only catalyst. Moreover, the decomposition temperature and peak intensity assigned to β-PdHₓ were also both remarkably decreased. STEM analysis combined with XEDS presented a mixture of Ni and Pd in individual particles. In addition, *in situ* CO-DRIFTS hinted a possible electron transfer from Ni to Pd. Hence,

the addition of Ni to Pd not only decreased the particle size but also may alter the nature of Pd sites by ensemble effect and also probably ligand effect.

It has to be realized that the direct synthesis of hydrogen peroxide is actually a hydrogenation reaction of O_2 rather than a reaction of oxidizing H_2.[28] This is understood by the fact that activating H_2 with H-H bond breaks and remaining O_2 without dissociation are the actual reaction routes.[36] Therefore, Pd only catalysts are not able to achieve high selectivity towards H_2O_2 as to be excellent catalysts for both hydrogenation (H_2O_2 hydrogenation) and oxidation reactions (O_2 dissociation). The outstanding ability for O_2 dissociation however can merely perform over continuous Pd sites rather than isolated Pd sites. Through the reaction of CO oxidation, F. Gao *et al.* proved the critical role of continuous Pd sites for O_2 dissociation.[31,37] A well-annealed Au-Pd (100) surface without continuous Pd never demonstrated CO_2 formation in any reaction conditions. In contrast, for a fresh ion sputtered Au-Pd surface with continuous Pd, CO_2 formation was detectable. Moreover, it was also revealed from CO-DRIFTS (Figure 4-17) that relative to continuous Pd, isolated Pd sites less strongly interacted with adsorbate which easily desorbed product without dissociation.[28,32]

Including preventing O_2 and H_2O_2 from dissociation, isolated Pd sites are still able to activate H_2.[38,39] Hence, taking advantage of the ensemble effect through adding an appropriate secondary metal to Pd is a good strategy for improving H_2O_2 activity and selectivity. This inference has already proved by a large number of experimental results that for instance the addition of Au to Pd dramatically improved H_2O_2 selectivity.[2,40,41] The results from G. Hutchings' group revealed that homogeneous Au-Pd alloys in Au-Pd/C catalyst were more selective than TiO_2 or Al_2O_3 supported Au-Pd core-shell particles[4,42,43] that supports the vital effect of individual Pd sites. In this chapter, similar as the effect of Au to Pd, the additive Ni isolated Pd through the formation of Ni-Pd alloys that improved H_2O_2 selectivity. Scheme 4-2 demonstrates the different pathways during H_2O_2 synthesis over continuous Pd sites and individual Pd sites isolated by Ni.
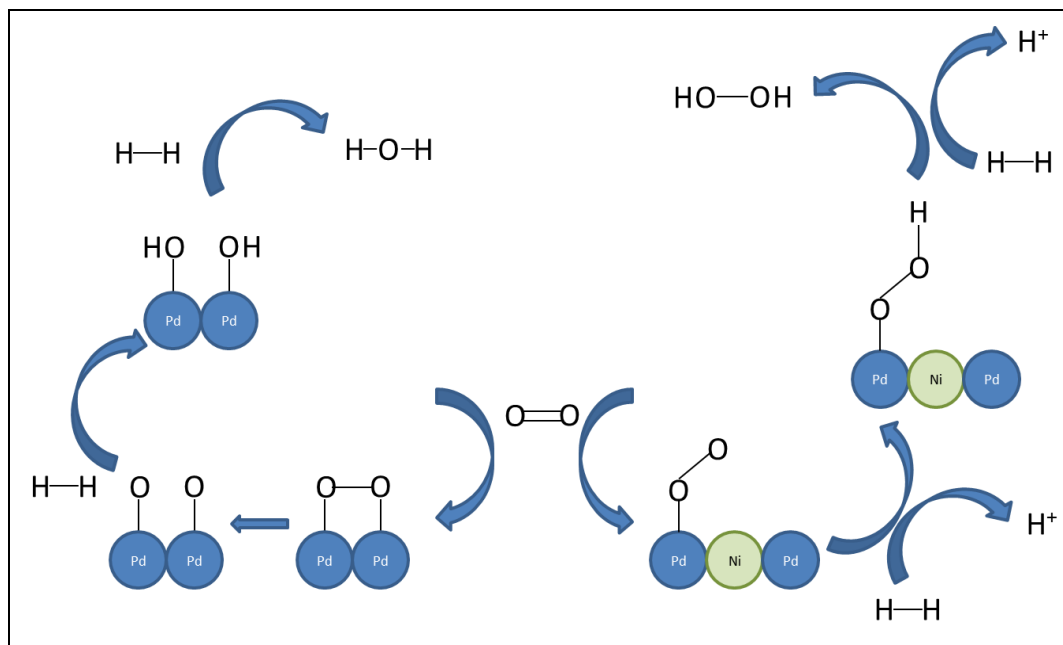
Scheme 4-2: The H_2 and O_2 reactions happen over continuous and individual Pd sites.

Including ensemble effect which can benefit selective reactions, ligand effect is also crucial in alloys.[28] For Pd catalysts, the secondary metal perturbs Pd electronic environment that makes the Pd d band to be more filled, moving the d band centre away from the Fermi level.[28] Pd becomes more atomic like therefore binding reactant and product more weekly improved selectivity. C. Baddeley and co-workers explained the possible reason of the effective Au-Pd alloys for acetylene trimerization to benzene relative to a pure Pd catalyst that through electronic perturbation of Pd, it desorbed benzene more easily without dissociation.[32] For the direct synthesis of hydrogen peroxide, Au-Pd core-shell particles demonstrated enhanced catalytic performance in the comparison with Pd only particles indicating the electron provider-Au improve the activity of Pd located on the top of the particles.[42] In this chapter, CO-DRIFTS demonstrated red shift of linear bond CO on isolated Pd sites which was possibly resulted from electron transfer from Ni to Pd. The d band of Pd was then to be more filled and led to a stronger electronic back donation to $2\pi^*$ molecular orbitals of CO.[30] Moreover, the fact of the higher electronegativity of Pd relative to Ni provides one more theoretical support to this inference.[44] Hence, Ni may also act as electron provider to Pd

that improved catalyst performance for the direct formation of hydrogen peroxide synthesis.

4.5 Conclusions

At the beginning of the work, calcination temperature and Ni/Pd ratio were investigated for achieving the best catalytic performance for hydrogen peroxide synthesis. It was revealed that with the increase of calcination temperature, the reusability of the catalyst was enhanced with a compromise of the activity for H_2O_2 formation. Moreover, Ni/Pd monometallic and bimetallic catalysts treated at both 400 ºC and 475 ºC demonstrated a Ni-Pd synergistic effect for the direct synthesis of H_2O_2. Through tuning Ni/Pd of 5wt% metal loading catalyst, catalysts with 2:1 and 1:1 Ni/Pd molar ratio demonstrated similarly high H_2O_2 productivity which were selected for the further investigation on hydrogen peroxide synthesis. In addition, all the bimetallic catalysts showed superior H_2O_2 productivities relative to Ni/Pd monometallic catalysts.

The investigation of fresh and used Ni-Pd bimetallic catalysts demonstrated the effect of the reactions for hydrogen peroxide synthesis on the catalyst under stated reaction conditions, 2:1 O_2/H_2 ratio in fact provided a reducing environment for the catalyst that more Pd oxides were reduced into Pd metal. As a result, the used catalysts demonstrated higher hydrogenation rates as metallic Pd was the species giving a high activity and low selectivity towards H_2O_2 compared to Pd oxide.

Moreover, Ni-Pd bimetallic and Pd only catalysts were tested for time-on-line H_2 conversion, H_2O_2 selectivity and time-on-line H_2O_2 production rate. Results showed that bimetallic catalysts demonstrated a superior catalytic performance in all the three aspects. STEM and XPS analysis showed a better particle dispersion in the bimetallic catalyst indicating an explanation of the higher H_2 conversion rate-the overall activity over Ni-Pd bimetallic catalyst.

The negative shift of NiO_x reduction temperature and the substantial decrease of PdH_x decomposition temperature and peak area over Ni-Pd bimetallic catalyst inferred both a higher particle dispersion and a strong interaction of Ni and Pd. This is consistent with

the observations from STEM. STEM combined with XEDS revealed a mixture of Ni-Pd in individual particle. As it was proved that isolated Pd was the actual selective active site for the direct synthesis of H_2O_2. Hence, adding Ni to Pd diluted surface Pd into isolated Pd sites through the formation of Ni-Pd alloys, thereby resulted in an enhanced H_2O_2 selectivity. According to Equation 4-3, it is understandable that with a high H_2 conversion rate and H_2O_2 selectivity, a catalyst will inevitably demonstrate an enhanced H_2O_2 productivity.

Ligand effect is also essential for the catalytic performance in alloys. In situ DRIFTS with CO adsorption demonstrated a red shift of linear bond CO over the bimetallic catalyst indicating a possible electron transfer from Ni to Pd. This provided one more possible explanation for the superior catalytic performance of Ni-Pd catalyst as with more filled d band, Pd was more atomic like therefore binding with reactant and product more weakly without dissociation.

4.6 Reference

1. E. N. Ntainjua, J. K. Edwards, A. F. Carley, J. A. Lopez-Sanchez, J. A. Moulijn, A. A. Herzing, C. J. Kiely, and G. J. Hutchings, *Green Chem.*, 2008, **10**, 1162-1169.

2. J. K. Edwards, B. Solsona, E. N. Ntainjua, A. F. Carley, A. A. Herzing, C. J. Kiely, and G. J. Hutchings, *Science*, 2009, **323**, 1037–1041.

3. J. K. Edwards, A. F. Carley, A. A. Herzing, C. J. Kiely, and G. J. Hutchings, *Faraday Discuss.*, 2008, **138**, 225-239.

4. J. K. Edwards, A. Thomas, A. F. Carley, A. A. Herzing, C. J. Kiely, and G. J. Hutchings, *Green Chem.*, 2008, **10**, 388-394.

5. J. Edwards, B. Solsona, P. Landon, A. F. Carley, A. A. Herzing, C. J. Kiely, and G. Hutchings, *J. Catal.*, 2005, **236**, 69–79.

6. M. Sankar, Q. He, M. Morad, J. Pritchard, S. J. Freakley, J. K. Edwards, S. H. Taylor, D. J. Morgan, A. F. Carley, D. W. Knight, C. J. Kiely, and G. J. Hutchings, *ACS Nano*, 2012, **6**, 6600–6613.

7. Y. Li, S. Chen, J. Xu, and H. Zhang, *CLEAN–Soil, Air, Water*, 2013, **42**, 1140-1144.

8.   D. Briggs and M. P. Steah, in *Pratical surface analysis*, John Wiley & Sons, Secon edit., 1993.

9.   M. Brun, A. Berthet, and J. Bertolini, *J. Electron Spectrosc.*, 1999, **104**, 55–60.

10.   C. Samanta, *Appl. Catal. A Gen.*, 2008, **350**, 133–149.

11.   S. Melada, R. Rioda, F. Menegazzo, F. Pinna, and G. Strukul, *J. Catal.*, 2006, **239**, 422–430.

12.   V. R. Choudhary, C. Samanta, and T. V. Choudhary, *Catal. Commun.*, 2007, **8**, 1310–1316.

13.   C. Samanta and V. R. Choudhary, *Chem. Eng. J.*, 2008, **136**, 126–132.

14.   W. E. Jr and G. Tibbetts, *Phys. Rev. B*, 1979, **19**.

15.   H.-F. Wang, H. Ariga, R. Dowler, M. Sterrer, and H.-J. Freund, *J. Catal.*, 2012, **286**, 1–5.

16.   Y. Shen, S. Wang, and K. Huang, *Appl. Catal.*, 1990, **57**, 55–70.

17.   V. Sandoval and C. Gigola, *Appl. Catal. A Gen.*, 1996, **148**, 81-96.

18.   A. Renouprez, J. Faudon, and J. Massardier, *J. Catal.*, 1997, **190**, 181–190.

19.   P. C. Aben, *J. Catal.*, 1968, **10**, 224.

20.   H. Noh, T. B. Flanagan, R. Balasubramaniam, and J. A. Eastman, *Scr. Mater.*, 1996, **34**, 863–868.

21.   G. Fagherazzi, *Catal. Letters*, 1995, **32**, 293-303.

22.   M. Boudart and H. Hwang, *J. Catal.*, 1975, **39**, 44-52.

23.   P. Newbatt, P. Sermon, and M. Luengo, *Zeitshrift fur Physikdische Chemie Neue Folge*, 1986, **147**, 105-114.

24.   M. Skotak, Z. Karpinski, W. Juszczyk, J. Pielaszek, L. Kepinski, D. Kazachkin, V. Kovalchuk, and J. Ditri, *J. Catal.*, 2004, **227**, 11–25.

25.   Y. Sakamoto, K. Ohira, N. Ishimaru, F. L. Chen, M. Kokubu, and T. B. Flanagan, *J. Alloys Compd.*, 1995, **217**, 226–234.

26.   C. W. Yi, K. Luo, T. Wei, and D. W. Goodman, *J. Phys. Chem. B*, 2005, **109**, 18535–1850.

27. L. Ouyang, G. Da, P. Tian, T. Chen, G. Liang, J. Xu, and Y. F. Han, *J. Catal.*, 2014, **311**, 129–136.

28. F. Gao and D. W. Goodman, *Chem. Soc. Rev.*, 2012, **41**, 8009–8020.

29. A. R. Haire, J. Gustafson, A. G. Trant, T. E. Jones, T. C. Q. Noakes, P. Bailey, and C. J. Baddeley, *Surf. Sci.*, 2011, **605**, 214–219.

30. P. Hu, D. King, M. Lee, and M. Payne, *Chem. Phys. Lett.*, 1995, 18–23.

31. F. Gao, Y. Wang, and D. W. Goodman, *J. Am. Chem. Soc.*, 2009, **131**, 5734–5735.

32. C. Baddeley, *J. Phys. Chem.*, 1995, 5146–5151.

33. L. ĈERVENÝ, *Chem. Eng. Commun.*, 1989, **83**, 31–63.

34. P. Lu, T. Teranishi, K. Asakura, M. Miyake, and N. Toshima, *J. Phys. Chem. B*, 1999, **103**, 9673–9682.

35. Y. Li, L. Zhu, K. Yan, J. Zheng, B. H. Chen, and W. Wang, *Chem. Eng. J.*, 2013, **226**, 166-170.

36. J. Lunsford, *J. Catal.*, 2003, **216**, 455–460.

37. F. Gao, Y. Wang, and D. W. Goodman, *J. Phys. Chem. C*, 2009, **113**, 14993–15000.

38. V. Ponec and G. C. Bond, *Catalysis by metals and alloys*, Elsevier, Amsterdam, 1995.

39. V. Ponec, *Appl. Catal. A Gen.*, 2001, **222**, 31–45.

40. P. Landon, P. J. Collier, A. F. Carley, D. Chadwick, A. J. Papworth, A. Burrows, C. J. Kiely, and G. J. Hutchings, *Phys. Chem. Chem. Phys.*, 2003, **5**, 1917–1923.

41. J. Xu, L. Ouyang, G. J. Da, Q. Q. Song, X. J. Yang, and Y. F. Han, *J. Catal.*, 2012, **285**, 74–82.

42. J. K. Edwards, B. E. Solsona, P. Landon, A. F. Carley, A. A. Herzing, C. J. Kiely, and G. J. Hutchings, *J. Catal.*, 2005, **236**, 69–79.

43. B. E. Solsona, J. K. Edwards, P. Landon, A. F. Carley, A. A. Herzing, C. J. Kiely, and G. J. Hutchings, *Chem. Mater.*, 2006, **18**, 2689–2695.

44. F. Hillebrecht, J. Fuggle, and P. Bennett, *Phys. Rev. B*, 1983, **27**, 2179-2193.

Chapter 5

A modified impregnation method for the direct synthesis of hydrogen peroxide

5.1 Introduction

As a kind of the circulated currencies, gold was considered as an inactive material whose catalytic activity was once explained by impurities in the gold.[1] However, when the size is reduced from bulk to nanoscale, Au particles become catalytically active for numerous reactions including environmental catalysis[2–5], energy processing[6,7] and chemical synthesis[8–12]. It has been reported that the addition of Pd to Au is able to drastically enhance corresponding catalytic performance such as for aerobic oxidation of alcohols[13,14] and the direct synthesis of hydrogen peroxide[15–17]. Moreover, the catalytic

activity for both Au and Au-Pd nanoparticles follow a size dependent trend *i.e.* activity increases with decreasing particle size.[18] Thereby, the preparation of these materials is crucial. Until now, a number of preparation methods have been developed in order to achieve effective catalytic performance which include wet impregnation[15], incipient wetness[19], deposition precipitation[20], sol-immobilization[21] and physical grinding[22]. All the methods have their own advantages and disadvantages; for instance, conventional wet impregnation (C_{Im}) is the simplest method, but also suffers several disadvantages. For example, catalysts prepared through C_{Im} demonstrate a wide range of particles from sub-nm clusters up to over 100 nm particles that consequently show a moderate activity for reactions. Another problem of C_{Im} method is the size dependent composition as large particles are gold rich and small particles are Pd rich.[17] Sol-immobilization (S_{Im}) is a convenient method for controlling the average particle size and size distribution.[21] However, the preparation of S_{Im} nanoparticles adopts reducing agent and stabilizer ligands both of which possibly block active sites of such catalysts. Moreover, on the contrary with C_{Im} method, S_{Im} method demonstrates the size dependent composition as small particles are gold rich and large particles are Pd rich. Hence, a simple and convenient catalyst preparation method to control particle size and its components is of vital importance.

Further work on a modified impregnation method[23] will be reported here. This new method is as simple as that of C_{Im} however it also allows convenient control of the Au-Pd nanoparticles size distribution as S_{Im}. But above all, bimetallic catalysts prepared through M_{Im} demonstrate a homogeneous composition in particles which are beneficial for the direct synthesis of hydrogen peroxide.[23] The key of M_{Im} is using an excess anion in the impregnation procedure followed by H_2 reduction. The attained Au-Pd nanoparticles showed a fine dispersion and outstanding catalytic performance for the direct synthesis of hydrogen peroxide and benzyl alcohol oxidation compared with conventional impregnation (C_{Im}) and sol-immobilization (S_{Im}) analogues (Figure 5-1). In addition, with an appropriate amount of additive HCl in the preparation, M_{Im} Au-Pd material is highly reusable relative to S_{Im} Au-Pd catalysts. In a previous study, detailed STEM analysis combined with EDS revealed that excess anion increased Au content in

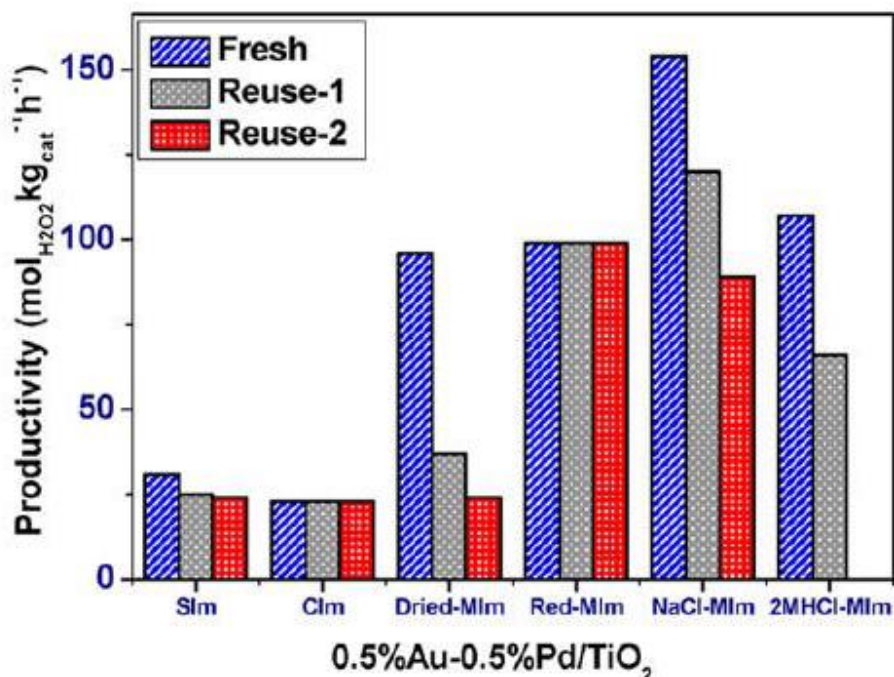individual particles. This may therefore represent a method to tune the composition of the nanoparticles.[23]

Figure 5-1: Result comparison of H_2O_2 productivity and reusability over 0.5wt%Au-0.5wt%Pd/TiO$_2$ samples prepared through different methods. (Cat-1: S_{Im}; Cat-2: C_{Im}; Cat-3-6: M_{Im}, and Cat-3: dried only, Cat-4: standard M_{Im}, Cat-5: M_{Im} prepared by NaCl excess and Cat-6: M_{Im} prepared by 2M HCl) [23]

Herein, 1 wt% Au-Pd and Pd only catalysts with different Pd ratios were prepared through both M_{Im} and C_{Im}, in order to investigate: (i) the effect of additive Cl$^-$ and the advantages of M_{Im} for the direct peroxide synthesis relative to C_{Im}, and (ii) the role of Au addition to Pd for the H_2O_2 direct formation. The comparison of TiO$_2$ and MgO supported catalysts will reveal the effect of support for hydrogen peroxide synthesis. Testing a range of Au/Pd ratios, a volcano trend of production rate is able to hint at the active sites required for the direct synthesis of hydrogen peroxide.

Three kinds of Au-Pd catalysts will be discussed in this chapter-M_{Im} (varying Cl$^-$), M_{Im} (constant Cl$^-$) and C_{Im}. The only difference between these groups of catalysts was the quantitative variation of additive Cl$^-$. For M_{Im} (varying [Cl$^-$]) catalysts, Pd^{2+} in 0.58 M

HCl was adopted as the Pd precursor. Hence, with the increase of Pd ratio for 1 wt% Au-Pd catalyst, the amount of Cl^- introduced in the preparation correspondingly increased until a maximum for the 1 wt% Pd catalyst. In order to study the effect of Au/Pd ratio independently without the effect of Cl^- variation, a fixed amount of Cl^- was used in the preparation whose resultant catalysts were named as M_{Im} (constant $[Cl^-]$). For the preparation procedure of C_{Im} described in Chapter 2, $PdCl_2$ salt was used and dissolved in the gold precursor-$HAuCl_4$ with additional deionized water. Figure 5-2 demonstrates the amount of Cl^- introduced in the preparation by the different methods.
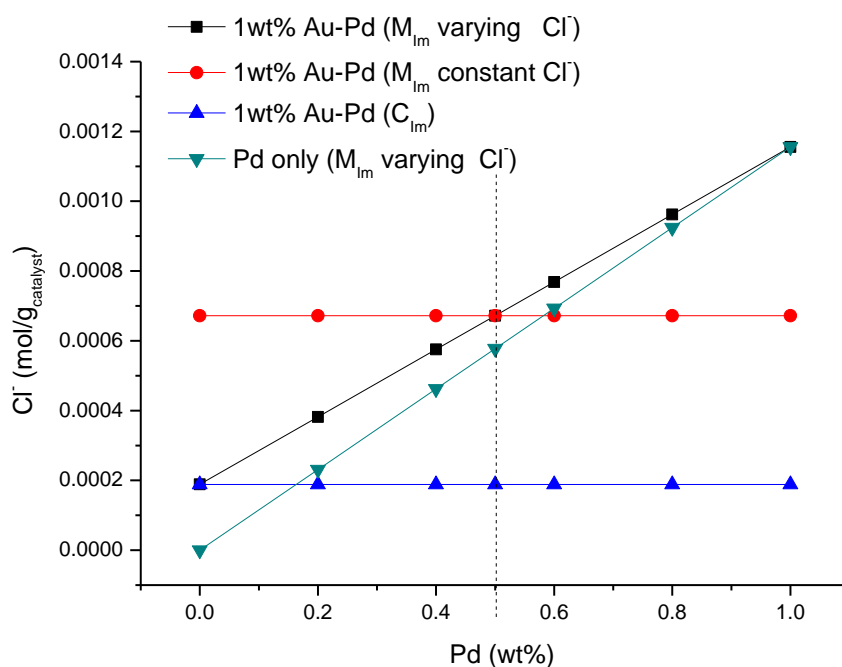

Figure 5-2: The amount of Cl per gram catalyst introduced in the preparation system for different material preparations. (1 wt% Au-Pd M_{Im} (varying Cl^-), **Black** square; 1 wt% Au-Pd M_{Im} (constant Cl^-), **Red** circle; 1 wt% Au-Pd C_{Im}, **Blue** upper triangle and Pd only M_{Im} (varying Cl^-), **Green** lower triangle)

5.2 Au-Pd catalysts for the direct synthesis of hydrogen peroxide
5.2.1 The direct synthesis of hydrogen peroxide

1 wt% Au-Pd and Pd only catalysts prepared through M_{Im} with different Pd ratios were tested for the direct synthesis of hydrogen peroxide. The results are shown in Figure 5-3. For the Pd only samples, with increasing metal loading, productivity increased such that

0.8 wt% and 1.0 wt% Pd/TiO$_2$ demonstrated similarly high activities - 68 mol kg^{-1} h^{-1} and 64 mol kg^{-1} h^{-1}, respectively. Bimetallic 1 wt% Au-Pd catalysts were tested three times in order to get relatively accurate results and data trends. The averaged results with standard deviation are demonstrated in Figure 5-3 which presented a general "volcano" shape as the productivity increased from 1 wt% Pd (64 mol kg^{-1} h^{-1}) to the maximum at 0.5 wt% Au-0.5 wt% Pd (116 mol kg^{-1} h^{-1}) and then a decrease on increasing Au ratio.

Moreover, as we can see in Figure 5-3, the Au monometallic sample demonstrated very limited activities for peroxide formation which was consistent with the results of the previous work,[15,21,24] claiming low activity of Au for the direct synthesis of hydrogen peroxide. However, the addition of Au to Pd increased H$_2$O$_2$ productivity significantly, and comparison of the bimetallic and monometallic catalysts with 0.2, 0.5 and 0.8 wt% Pd loading confirms the synergistic effect of Au and Pd.[25–27]
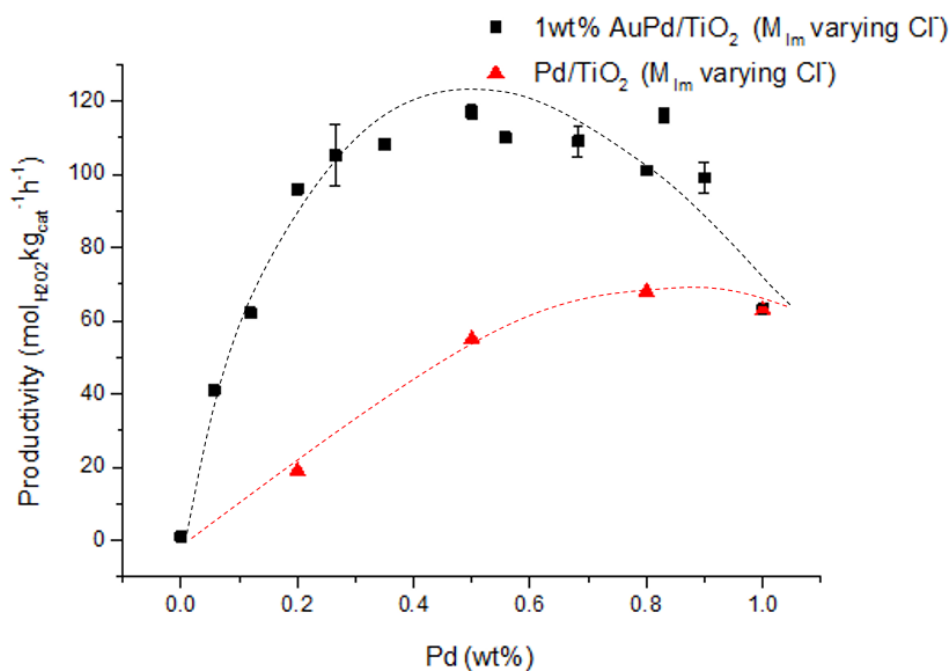
Figure 5-3: Results comparison of 1 wt% AuPd/TiO$_2$ (M$_{Im}$ varying Cl$^-$) (**Black** square) and Pd/TiO$_2$ (M$_{Im}$ varying Cl$^-$) (**Red** triangle) catalysts for the direct synthesis of H$_2$O$_2$. Dashed lines demonstrate plausible trends of the activities in this chapter.

1 wt% Au-Pd and Pd only M_{Im} catalysts with different Pd content were also evaluated for the hydrogenation of hydrogen peroxide. The attained results are shown in Figure 5-4. It can be noticed that for Au-Pd bimetallic catalysts, the hydrogenation rate of H_2O_2 followed a positive correlation with increasing Pd ratio. This is consistent with previous results that high Pd content catalysts demonstrate higher hydrogenation rates throughout a whole range of Au/Pd ratios.[21] In addition, Pd monometallic catalysts showed lower H_2O_2 hydrogenation activities relative to those of the corresponding Au-Pd bimetallic catalysts. This indicates that the addition of Au to Pd increased not only H_2O_2 synthesis but also H_2O_2 hydrogenation activity. Scatter results of bimetallic samples were ascribed to an integrated effect of Au/Pd ratio and the distinct amount of Cl⁻ introduced in the preparation procedure.

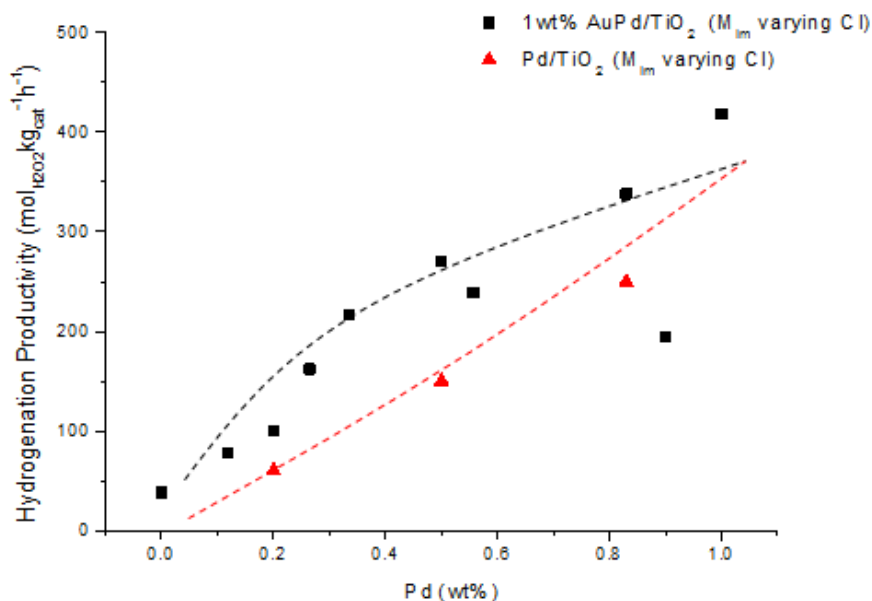**Figure 5-4:** H_2O_2 hydrogenation reaction rates of 1 wt% Au-Pd/TiO$_2$ (M_{Im} varying Cl⁻) (**Black** square) and Pd/TiO$_2$ (M_{Im} varying Cl⁻) (**Red** triangle) catalysts.

TiO$_2$-supported 1 wt% Au-Pd and Pd only catalysts with varying Pd content were also prepared through C_{Im} followed by H_2 reduction. Comparison results of Au/Pd bimetallic and Pd only catalysts for the direct synthesis of hydrogen peroxide were plotted in Figure 5-5. It is revealed that H_2O_2 productivities of both bimetallic and Pd only catalyst increased with the increase of Pd content from 1 mol_{H2O2} kg_{cat}^{-1} h^{-1} for the 1 wt% Au/TiO$_2$ catalyst to 72 mol_{H2O2} kg_{cat}^{-1} h^{-1} for 1 wt% Pd/TiO$_2$. Moreover, bimetallic

catalysts also demonstrated relatively higher activities than corresponding Pd monometallic catalysts and this was assigned to the synergistic effect between Au and Pd.
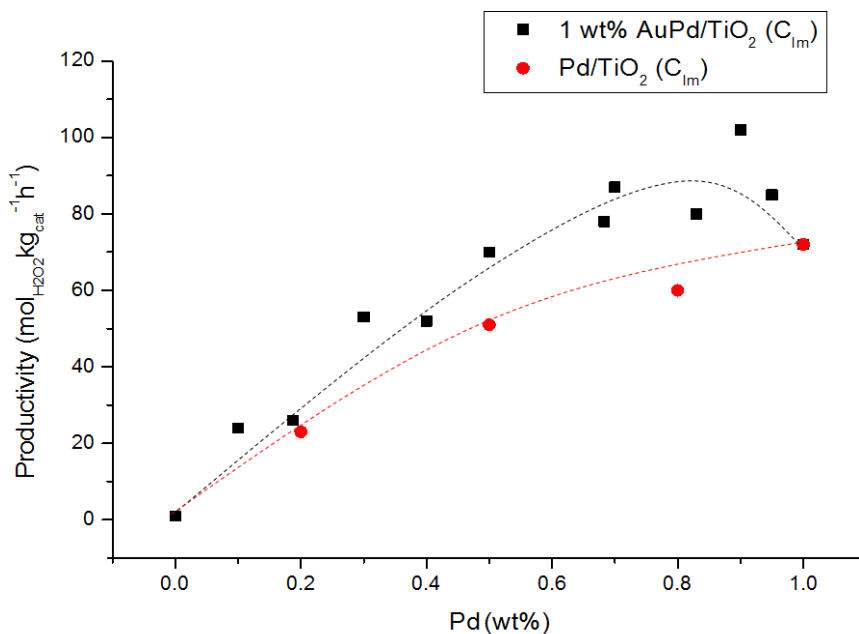

Figure 5-5: Productivity comparison of 1 wt% Au-Pd (**Black** square) and corresponding Pd only (**Red** circle) catalysts for the direct synthesis of H_2O_2 prepared through C_{Im}.

In order to investigate the difference between M_{Im} and C_{Im} for H_2O_2 direct formation, comparison between Au-Pd and Pd only catalysts prepared through both methods were plotted in Figure 5-6. It can be noticed that: (i) Pd only catalysts prepared through both methods demonstrated very similar activities for H_2O_2 synthesis; (ii) bimetallic samples prepared through M_{Im} showed much more enhanced activity than those by C_{Im} indicating the superiority of the modified method; (iii) moreover, the synergistic effect between Au and Pd was demonstrated more significantly for the bimetallic samples in M_{Im}, given that the addition of Au in Pd enhanced the production rate much more drastically relative to that of C_{Im}; and (iv) the activity enhancement from additive Au was demonstrated more significantly on increasing the Au content within M_{Im} catalysts.
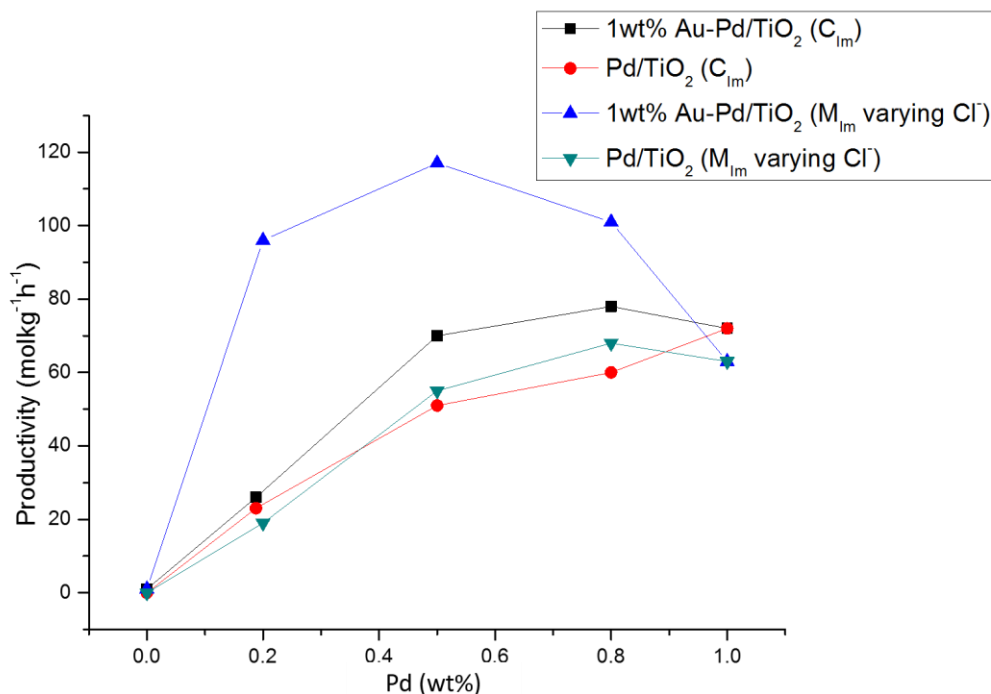
Figure 5-6: Activity comparison of the catalysts prepared through M_{Im} and C_{Im} with different Au/Pd ratios for the direct synthesis of hydrogen peroxide

(1-x) wt% Au-x wt% Pd/TiO$_2$ C$_{Im}$ (**Black** square), x wt% Pd/TiO$_2$ C$_{Im}$ (**Red** circle), (1-x) wt% Au-x wt% Pd/TiO$_2$ M$_{Im}$ varying Cl$^-$ (**Blue** triangle) and x wt% Pd/TiO$_2$ M$_{Im}$ varying Cl$^-$ (**Green** diamond) Reaction conditions: 5% H$_2$/CO$_2$ and 25% O$_2$/CO$_2$, 50% H$_2$/O$_2$ at 3.7 MPa, MeOH (5.6 g), H$_2$O (2.9 g), catalyst (0.01 g), 2°C, 1200 rpm, 30 min.

MgO-supported 1 wt% Au-Pd bimetallic catalysts prepared by the M$_{Im}$ (varying Cl$^-$) were evaluated for the production rate of hydrogen peroxide (Figure 5-7). In the comparison with the TiO$_2$-supported M$_{Im}$ catalysts, MgO-supported catalysts demonstrated a very similar trend on changing the Au/Pd ratio, whose activities, however, were distinctly suppressed. In order to investigate the origin of the lower productivity of the MgO catalysts, the hydrogenation activity of H$_2$O$_2$ over a 0.5 wt% Au-0.5 wt% Pd catalyst was tested and compared with the corresponding TiO$_2$ sample in Table 5-1. It can be noticed that including the higher H$_2$O$_2$ productivity of TiO$_2$-supported catalyst relative to MgO supported catalyst, the hydrogenation rate of TiO$_2$ M$_{Im}$ catalyst (270 mol$_{H2O2}$ kg$_{cat.}^{-1}$ h^{-1}) was nearly one fourth of that of MgO M$_{Im}$ sample

(1049 mol_{H2O2} $kg_{cat.}^{-1}$ h^{-1}). The attained results were consistent with previous observations that MgO samples demonstrated lower activity and selectivity for H_2O_2 formation compared with TiO_2.[23,28] The basicity and particularly the isoelectronic point of the support, is a major factor in controlling the stability of hydrogen peroxide under reaction conditions,[29] which means that basic/high isoelectronic point supports lead to the catalysis of the non-desired sequential hydrogenation and decomposition of hydrogen peroxide. Moreover, there is an inverse correlation between H_2O_2 formation and side reaction activity, hence relatively lower production rates were achieved over the MgO samples.
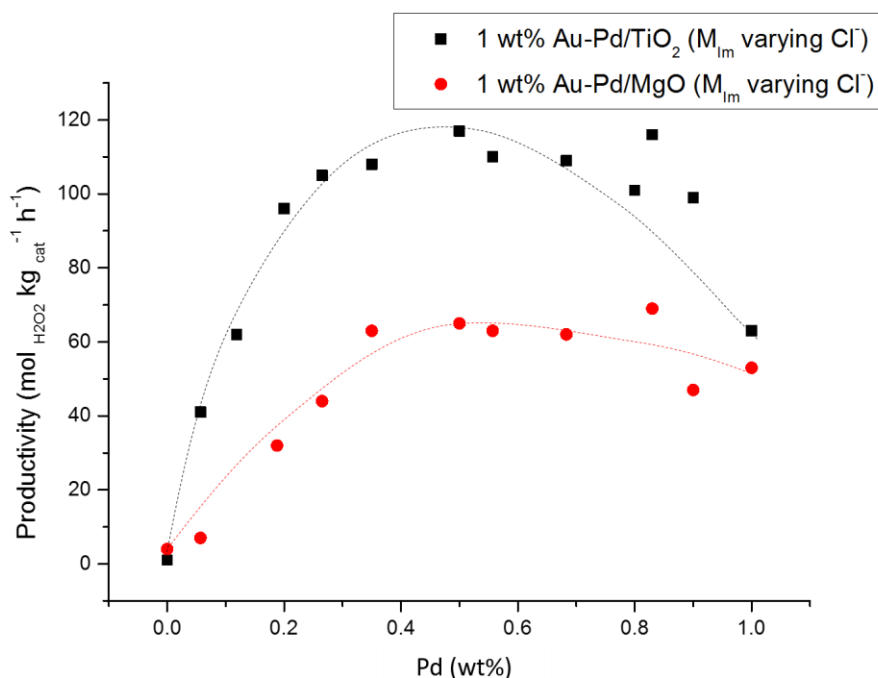
Figure 5-7: Results comparison of 1 wt% Au-Pd/TiO_2 (M_{Im} varying Cl⁻) (Black squares) and 1 wt% Au-Pd/MgO (M_{Im} varying Cl⁻) (Red circles) catalysts for the direct synthesis of H_2O.

As seen in Figure 5-7, both TiO_2 and MgO supported catalysts showed a volcano-shaped plot for hydrogen peroxide synthesis with the change of Au/Pd ratio. It follows a universal trend for peroxide formation that is independent of the utilized support. In order to investigate the effect of Au/Pd more thoroughly, a fixed amount of Cl⁻ was

introduced in the preparation, and the resultant catalysts were named modified impregnation constant Cl⁻ (M_{Im} constant Cl⁻). The attained results are shown in Fig 5-8.

Table 5-1: Activity comparison of supported 1 wt% Au-Pd catalysts on TiO_2 and MgO supports for hydrogen peroxide synthesis and hydrogen peroxide hydrogenation.

Catalyst (M_{Im} varying Cl⁻)	Productivity (mol_{H2O2} $kg_{cat.}^{-1}$ h^{-1})	Hydrogenation productivity (mol_{H2O2} $kg_{cat.}^{-1}$ h^{-1})
0.5 wt% Au-0.5 wt% Pd/TiO_2	115	270
0.5 wt% Au-0.5 wt% Pd/MgO	69	1049

With the increase of Pd ratio, 1 wt% Au-Pd/TiO_2 (M_{Im} constant Cl⁻) samples again demonstrated a volcano plot for H_2O_2 production rate. 1 wt% Pd catalyst showed a productivity of 81 mol_{H2O2} $kg_{cat.}^{-1}$ h^{-1} which dropped gradually with the decrease in Pd/Au ratio after surpassing a maximum of 119 mol_{H2O2} $kg_{cat.}^{-1}$ h^{-1} for the 0.4 wt% Au-0.6 wt% Pd catalyst. The trend is consistent with previous observations[21,30] for Au-Pd alloy catalysts which were prepared through wet impregnation and sol-immobilization, respectively. This indicates that the volcano shape actually originates from the effect of the Au/Pd ratio in the alloys and is independent with respect to the preparation method.

A volcano-shaped trend was also observed for the hydrogenation rates of H_2O_2, as the hydrogenation activity increased from 10 mol_{H2O2} $kg_{cat.}^{-1}$ h^{-1} for 1 wt% Au/TiO_2 to a maximum of 270 mol_{H2O2} $kg_{cat.}^{-1}$ h^{-1} for the 0.5 wt% Au-0.5 wt% Pd/TiO_2 and then decreased to 187 mol_{H2O2} $kg_{cat.}^{-1}$ h^{-1} for 1 wt% Pd/TiO_2 (Figure 5-8 **Blue** triangles). Hence, in the comparison to the hydrogenation rate over 1 wt% Pd/TiO_2, it can be noticed that the addition of Au to Pd enhanced H_2O_2 hydrogenation for the maximum at 0.5 wt% Au-0.5 wt% Pd/TiO_2 to 0.2 wt% Au-0.8 wt% Pd/TiO_2. This is also consistent with the observation for Au-Pd alloys prepared through sol-immobilization.[21]
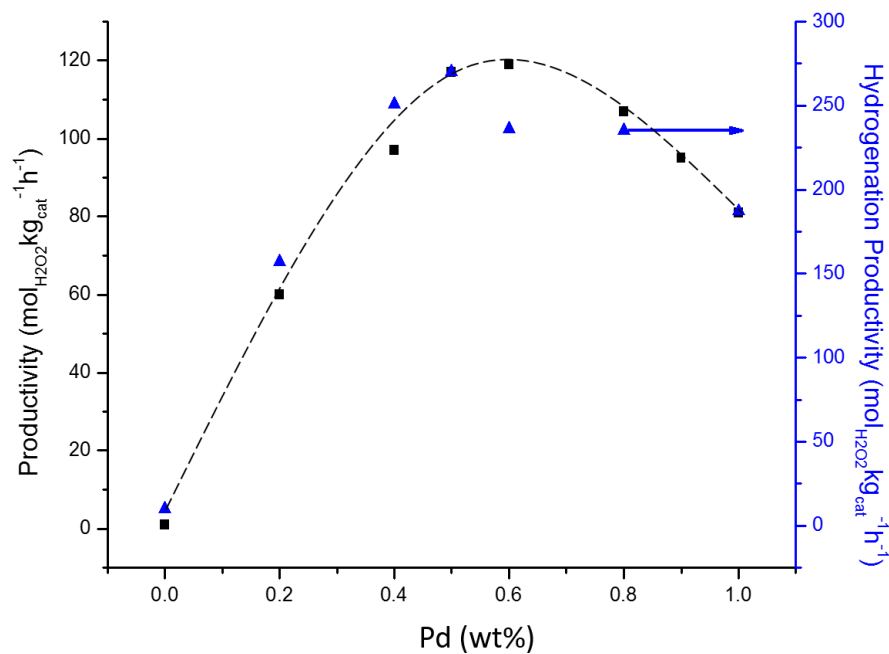
Figure 5-8: H_2O_2 synthesis (**Black** squares) and hydrogenation (**Blue** triangles) results of 1 wt% Au-Pd/TiO$_2$ (M$_{Im}$ constant Cl$^-$).
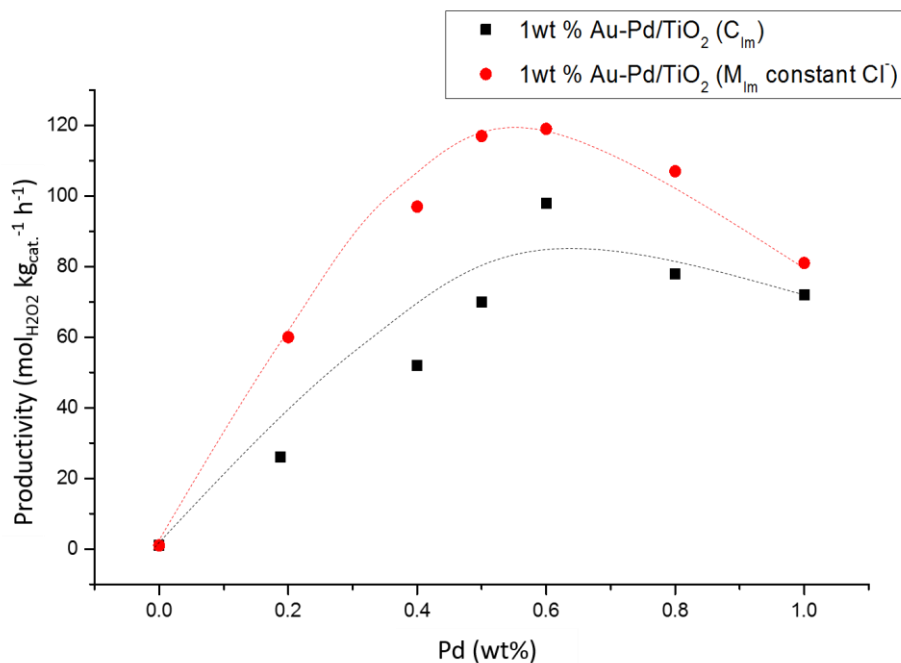

Figure 5-9: Results comparison of 1 wt% Au-Pd/TiO$_2$ (M$_{Im}$ constant Cl$^-$) (**Red** circle) and 1 wt% Au-Pd/TiO$_2$ (C$_{Im}$) (**Black** square) catalysts for the direct synthesis of H$_2$O$_2$.

Figure 5-9 demonstrates the comparison of two groups of catalysts made from C_{Im} and M_{Im} (constant Cl⁻) respectively. Consistent with previous results, catalysts prepared from M_{Im} showed superior production rates of H_2O_2 than those of C_{Im} catalysts.

5.3 Characterization

5.3.1 X-ray Diffraction (XRD)

XRD analysis was used for the crystallite structure analysis in the comparison of the catalysts with various Au/Pd ratios. Heat treated TiO_2 support under the same preparation conditions was also examined by X-ray diffraction. As seen in Figure 5-10, no distinct reflections attributed to Au or Pd could be observed which indicates particles on TiO_2 support were too small to be detectable through XRD. STEM analysis in the previous publication revealed that reduced Au-Pd particles prepared through both M_{Im} and C_{Im} were smaller than 5 nm[23] which exceeds the lower resolution of XRD. In Figure 5-10, an inconspicuous reflection assigned to crystallite Au can be vaguely noticed in the samples with a high Au content which also could originate from the noise of the signal. Hence, XRD analysis indirectly proved the formation of small Au-Pd nanoparticles by M_{Im} method.
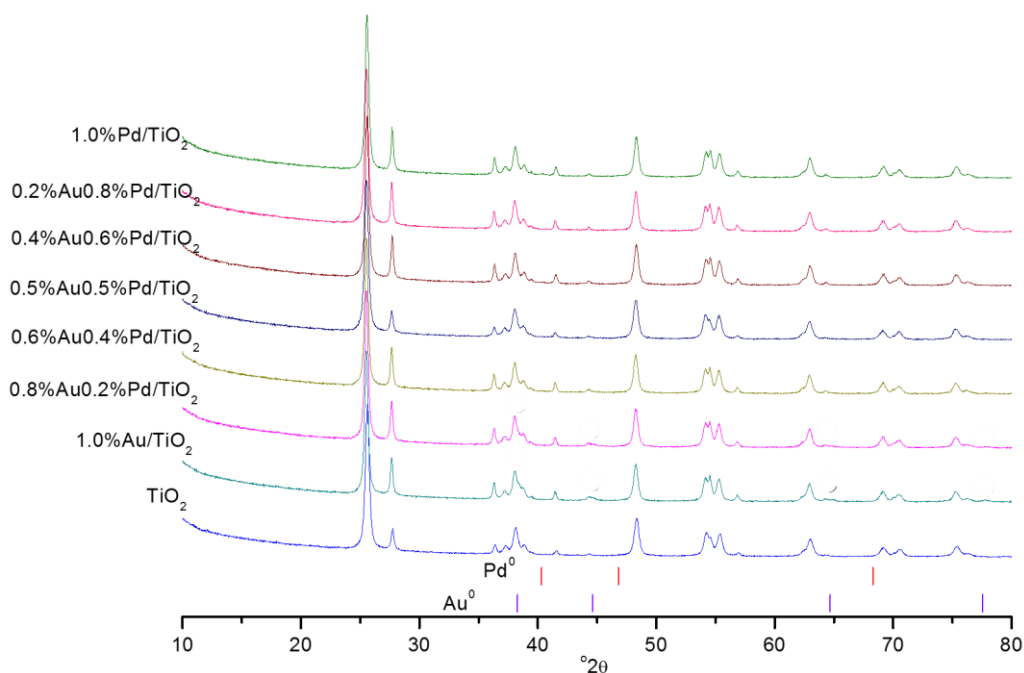

Figure 5-10: XRD patterns for 1 wt% Au-Pd/TiO_2 made from M_{Im} (varying Cl⁻) method and TiO_2 support

5.3.2 X-ray Photoelectron Spectroscopy (XPS)

XPS analysis was used to determine the oxidation state and atomic ratio of the elements on the surface. For Au-Pd bimetallic catalysts, it is more convenient to specify Pd $3d_{3/2}$ and Au $4f_{7/2}$ levels for the chemical states analysis because of the overlap of Pd and Au core levels, Au^0 $4d_{5/2}$ at 333.8 eV with Pd^0 $3d_{5/2}$ at 334.1 eV and Pd^0 4s at 88.2 eV with Au^0 $4f_{5/2}$ at 88.4 eV.[30,31] It has been demonstrated by the XPS results of single crystal metallic Pd and PdO surface that the binding energies for Pd^0 $3d_{5/2}$ and $3d_{3/2}$ correspond to 335.0 and 340.1 eV , while binding energies at 337.2 and 334.2 eV are assigned to Pd^{2+} $3d_{5/2}$ and $3d_{3/2}$ states ,respectively.[32] As shown in Figure 5-11, though all of the 1 wt% Au-Pd/TiO$_2$ (M$_{Im}$ varying Cl$^-$) catalysts with distinct Au/Pd ratios were reduced in H$_2$ at 673 K for 4 hours, Pd^0 and Pd^{2+} still coexisted on the surface of all the catalysts, and which can be obviously observed in high Pd content catalysts (e.g. 0.8% Pd-0.2% Au/TiO$_2$). For catalysts with a low concentration of Pd (e.g. 0.2% Pd-0.8% Au/TiO$_2$), the binding energy at 333.9 eV assigned to Pd^0 $3d_{5/2}$ was negatively shifted by 1.1 eV according to the value of single crystal metallic Pd. This is attributed to the overlap with Au^0 $4d_{5/2}$. Moreover, with the increase of additive Au in 1 wt% Au-Pd catalysts, the intensity of the peaks assigned to Pd 3d decreased, indicating that with the decrease of Pd content in the bulk, the atomic ratio of Pd on the surface was simultaneously reduced.

XPS spectra of the Au 4f region for 1 wt% Au-Pd/TiO$_2$ (M$_{Im}$ varying Cl$^-$) catalysts with different Pd ratios are demonstrated in Figure 5-12. The intensity of the peak corresponding to Au 4f increased with the increase of Au content, which also infers the positive correlation with the Au content present in bulk structure and on the surface. Quantified XPS results of surface Au ratio also proved the asending trend over bimetallic catalysts with the increase of Au in the bulk (Table 5-1). The binding energy of Au $4f_{7/2}$ at ca. 83.0 eV assigned to Au^0 which however was lower than that of bulk Au by ca. 1 eV. A number of plausible explanations were proposed for the negative shift of the binding energy: (i) the net charge flowing into s or p orbits of Au from Pd,[33,34] (ii) the quantum size effect, as nanosized Au particles with a decrease of coordination resulting in a shift of d-band energy to the Fermi level,[30,35] (iii) charge transfer between the support and metal,[36,37] and iv) an initial state effect resulting from H$_2$ pretreatment [38].
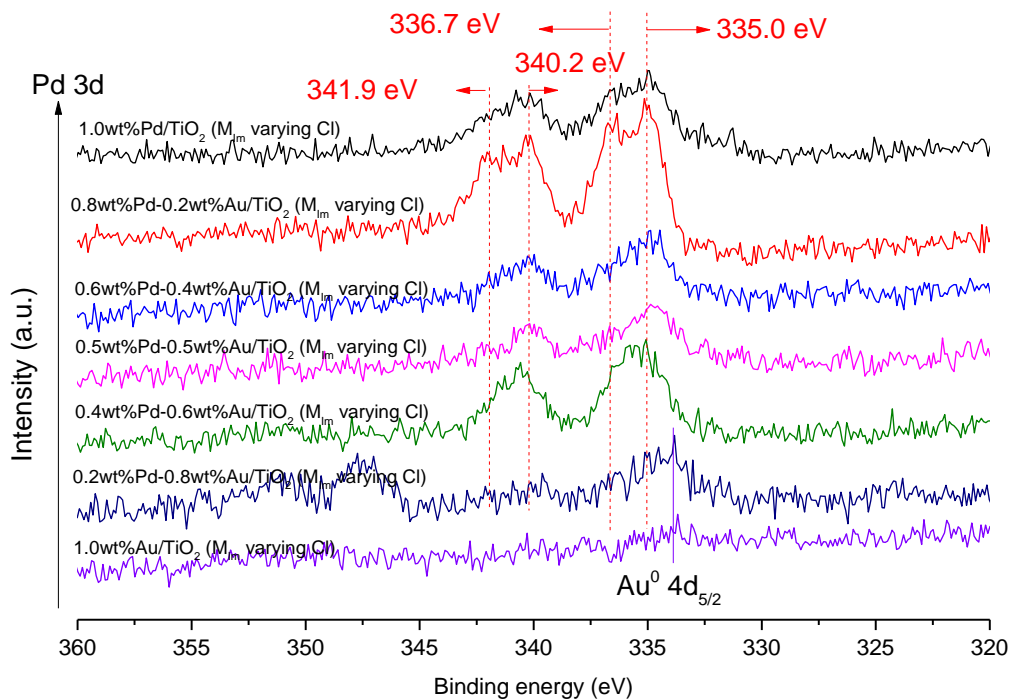
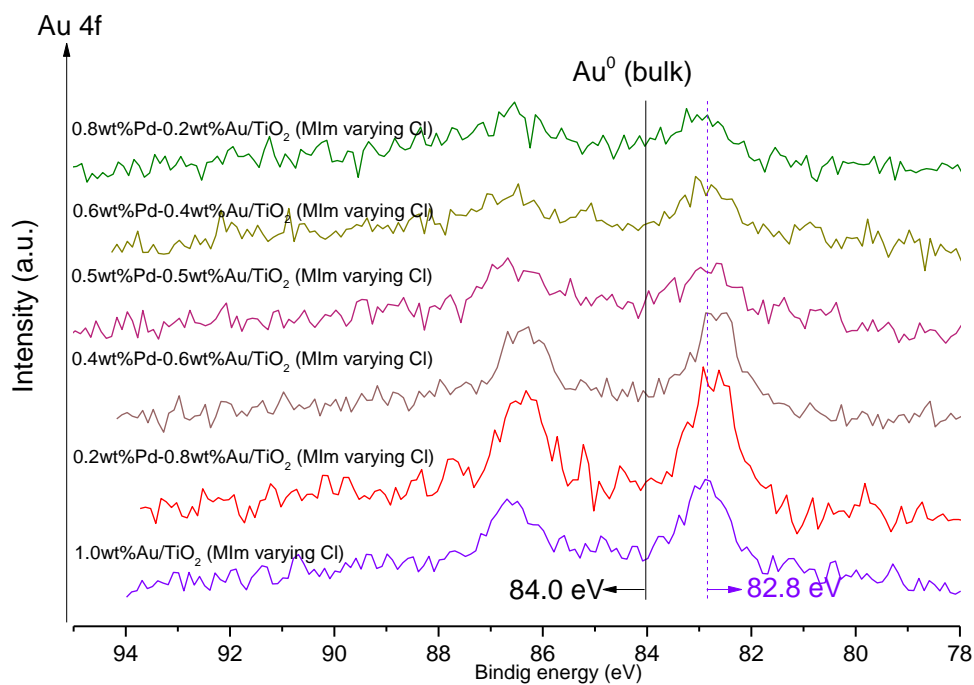**Figure 5-11:** XPS spectra for Pd 3d over M_{Im} catalysts with the change of Au/Pd ratios

Figure 5-12: XPS spectra for Au 4f over M_{Im} catalysts with different Au/Pd ratios

Table 5-1: Quantified XPS results for 1 wt% Au-Pd/TiO$_2$ samples prepared by M$_{Im}$. The elements compositions are mean values for the surface region sampled by XPS.

Atomic ratio	1 wt% Au-Pd/TiO$_2$ (M$_{Im}$ varying Cl$^-$) catalysts with various Pd ratio (wt%)						
	0	**0.2**	**0.4**	**0.5**	**0.6**	**0.8**	**1.0**
%Pd^a	-	0.19	0.38	0.26	0.25	0.58	0.38
%Au	0.11	0.17	0.12	0.08	0.08	0.07	-
Pd^a/Ti	-	0.0069	0.0134	0.0100	0.0096	0.0194	0.0125
Au/Ti	0.0040	0.0062	0.0042	0.0031	0.0031	0.0023	-
Pd/Au^b	-	0.62	2.7	2.8	2.6	7.8	-

^{a} calculated from the total apparent Pd(3d) intensity, which incorporates intensity from the Au(4d$_{5/2}$) component

^{b} ratio corrected for the overlap of the Pd(3d) doublet and the Au(4d$_{5/2}$) component

A substantial difference of H$_2$O$_2$ production rate was demonstrated over Au-rich bimetallic catalysts (e.g. 0.8% Au-0.2% Pd/TiO$_2$) prepared via M$_{Im}$ and C$_{Im}$ methods (Figure 5-6), samples of which were selected for XPS analysis in order to investigate the difference of surface properties between the catalysts. As shown in Figure 5-13, binding energies at 333.9 eV and 339.9 eV were assigned to Pd^0, suggesting that Pd species were present in the metallic form on the surface of such catalyst.[39] Nevertheless, the binding energy-333.9 eV attribute to Pd 3d$_{5/2}$ was lower than the reported value of single crystalite Pd^0 by 1.1 eV.[39] This was explained as the overlap of Pd 3d$_{5/2}$ and Au 4d$_{5/2}$[40] which however cannot be observed for the Pd spectrum or the peak assigned to Au 4d$_{5/2}$ in C$_{Im}$ sample. It infers that relatively higher Au dispersion on the surface that stronger peak corresponding to Au can be observed. Moreover, binding energies at 336.2 eV and 341.6 eV were attributed to Pd^{2+} on the surface of the C$_{Im}$ sample indicating the oxidized form of Pd on the surface.[40] It is very possible for the surface of Pd particles in C$_{Im}$ catalysts to be re-oxidized by air after the high temperature reduction treatment. One

the other hand, metallic Pd on M_{Im} catalyst suggests the strong interaction of Au and Pd that consequently protects Pd from being re-oxidized under the same operating environment.

The spectra of Au 4f originated from 0.8%Au-0.2%Pd/TiO_2 (C_{Im}) and 0.8%Au-0.2%Pd/TiO_2 (M_{Im} varying Cl$^-$) are deomstrated in Figure 5-14. It can be noticed that very similar binding energies at ca. 83 eV assigned to Au^0 for both samples indicating the presence of metallic Au on the surface of both catalysts.[41]
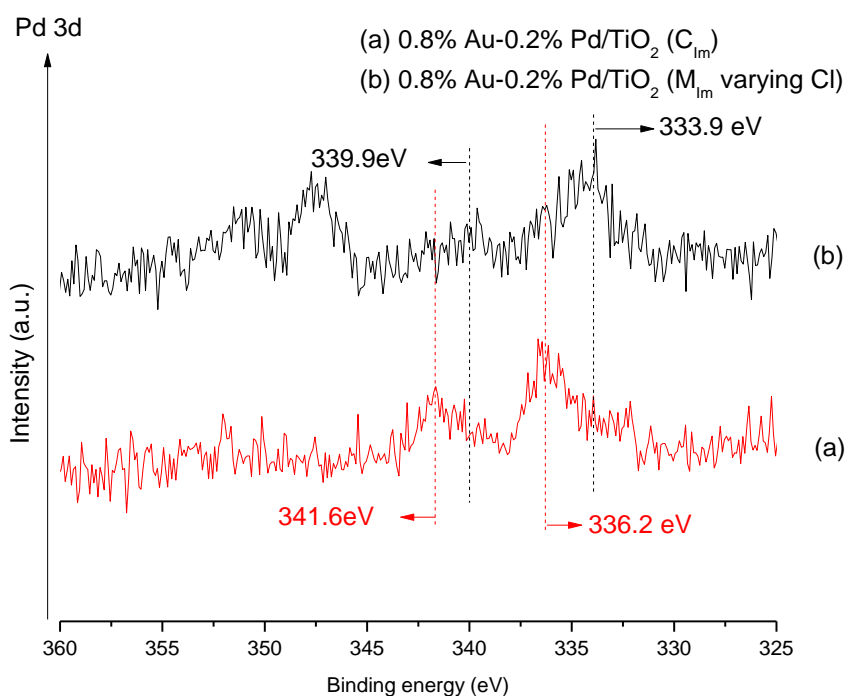
Figure 5-13: XPS spectra for Pd 3d over 0.2% Pd-0.8% Au catalysts prepared by M_{Im} and C_{Im}.

Quantified XPS results for 0.8%Au-0.2%Pd/TiO_2 (C_{Im}) and 0.8%Au-0.2%Pd/TiO_2 (M_{Im} varying Cl$^-$) catalysts can be seen in Table 5-2. It can be seen that Au atoms are relatively concentrated on the surface of the M_{Im} sample which demonstrates both higher Au atomic ratio among all the elements and the ratio of Au/Ti than those of the C_{Im} catalyst. This infers a better Au dispersion achieved through M_{Im}. Moreover, the ratio of Pd/Au in M_{Im} is less than half of that of C_{Im} moreover, and the former is closer to Pd/Au in bulk, suggesting a possible formation of a uniform Au/Pd mixture. This

adds further support to our previous observations regarding the formation of homogeneous Au-Pd alloys through the M_{Im} method.[23]
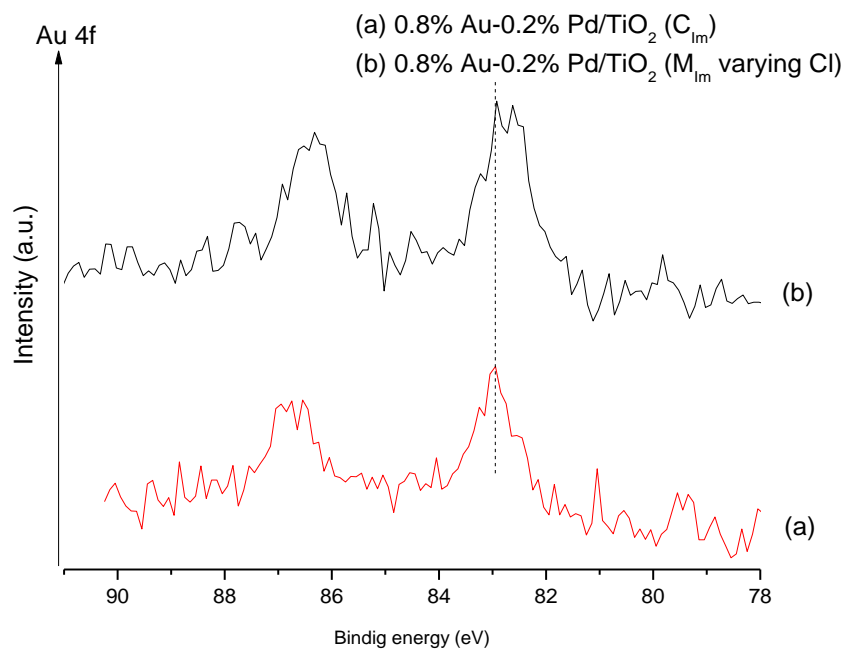
Figure 5-14: XPS spectra for Au 4f over 0.2% Pd-0.8% Au catalysts prepared by M_{Im} and C_{Im}.

Table 5-2: Quantified XPS results for TiO_2 supported 0.8% Au-0.2% Pd catalysts prepared by M_{Im} and C_{Im}. The elements compositions are mean values for the surface region sampled by XPS.

Catalyst	Atomic ratio					
	%Pd[a]	%Au	Pd[a]/Ti	Au/Ti	Pd/Au[b]	Pd/Au [c]
0.8%Au-0.2%Pd/TiO_2 (M_{Im} varying Cl⁻)	0.19	0.17	0.0069	0.0061	0.62	
						0.5
0.8%Au-0.2%Pd/TiO_2 (C_{Im})	0.24	0.12	0.0080	0.0040	1.5	

[a] calculated from the total apparent Pd(3d) intensity, which incorporates intensity from the Au($4d_{5/2}$) component

[b] ratio corrected for the overlap of the Pd(3d) doublet and the Au($4d_{5/2}$) component

[c] the ratio of Pd/Au in bulk

It was revealed that Pd monometallic catalysts prepared through M_{Im} and C_{Im} demonstrated very similar production rates of H_2O_2. Corresponding oxidation state of Pd and an estimate of Pd dispersion over 0.2% Pd/TiO_2 (C_{Im}), 0.2% Pd/TiO_2 (M_{Im} varying Cl^-), 0.5% Pd/TiO_2 (C_{Im}) and 0.5% Pd/TiO_2 (M_{Im} varying Cl^-) catalysts were investigated through XPS. The attained spectra of the catalysts are demonstrated in Figure 5-15. It can be noticed that binding energies centered at ca. 336.1 eV and 341.2 eV were attributed to PdO in all the samples. Thereby, oxidized Pd was predominant on the surface of all the Pd only catalysts prepared through both methods. Moreover, spectra are too noisy to determine the ratio of Pd^0 over all the catalysts.

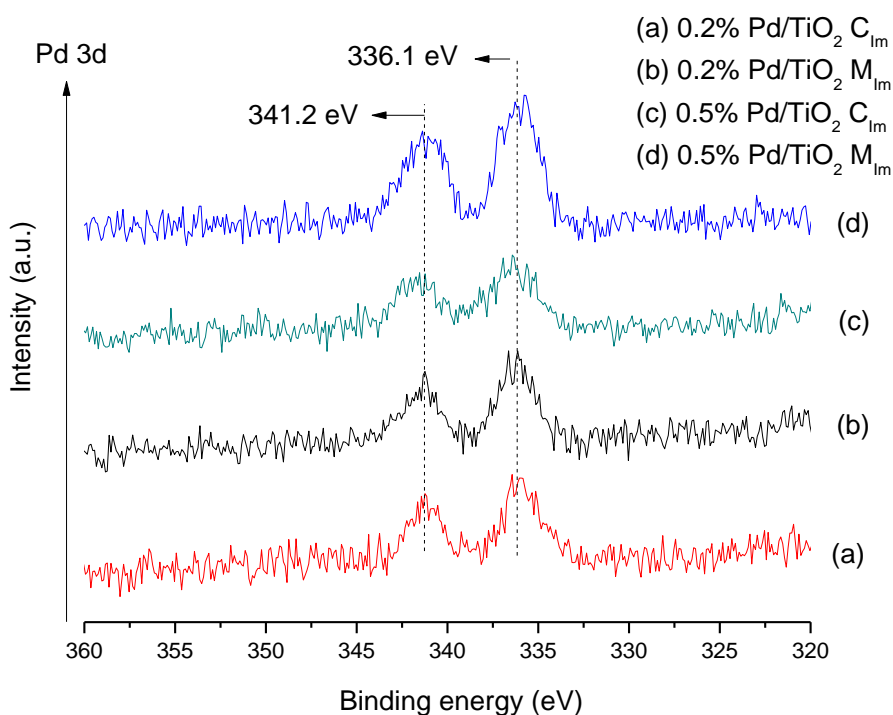**Figure 5-15:** XPS spectra for Pd 3d over Pd only catalysts prepared by M_{Im} and C_{Im}.

Table 5-3 demonstrates quantified XPS of elements compositions of these catalysts. It can be noticed a higher Pd ratio among the elements on the surface and the ratio of Pd/Ti over the M_{Im} samples relative to those of C_{Im} samples. This implies the possibility of a higher Pd dispersion achieved through the M_{Im} method.

Table 5-3: Quantified XPS results for TiO_2 supported Pd only samples prepared by M_{Im} and C_{Im}. The elements compositions are mean values for the surface region sampled by XPS.

Catalyst	Atomic ratio	
	% Pd[a]	Pd[a]/Ti
0.2%Pd/TiO$_2$ (M_{Im} varying Cl$^-$)	0.30	0.0105
0.2%Pd/TiO$_2$ (C_{Im})	0.16	0.0055
0.5%Pd/TiO$_2$ (M_{Im} varying Cl$^-$)	0.39	0.0130
0.5%Pd/TiO$_2$ (C_{Im})	0.23	0.0073

[a] calculated from the total apparent Pd(3d) intensity, which incorporates intensity from the Au(4d$_{5/2}$) component

[b] ratio corrected for the overlap of the Pd(3d) doublet and the Au(4d$_{5/2}$) component

[c] the ratio of Pd/Au in bulk

5.4   Discussion

5.4.1   Active sites in Au-Pd bimetallic catalysts for the direct synthesis of hydrogen peroxide

As demonstrated in Figure 5-7 and previous publications[21,30], a volcano plot of H_2O_2 productivities throughout the whole range of Au/Pd ratio in alloys is considered to be a universal trend which is independent with utilized support or preparation method. The volcano-shaped plot based on the mass of catalyst can also be transferred into a declining tendency of H_2O_2 productivities on the basis of Pd with the increase of Pd ratio which is demonstrated in Figure 5-16. In-situ diffuse reflectance infrared fourier transform spectroscopy with the adsorption of CO conducted by Ouyang *et al.*[30] demonstrated that the area ratio of the linear bonds/multi-bonded CO with Pd sites increased with the increase of Au/Pd ratio, indicating the higher ratio of isolated Pd sites in the catalysts with a high Au content. Our previous STEM-XEDS analysis of the Au-Pd sample prepared through M_{Im} sufficiently proved the formation of homogeneous Au-Pd nano-alloys.[23] Hence, it can be speculated that for the M_{Im} catalysts demonstrated in

Figure 5-15, upon alloying with Au, the ratio of individual Pd sites will increase with the increase of Au/Pd ratio. According to the well-accepted mechanism of the direct synthesis of hydrogen peroxide, the activation of O_2 without dissociation is one of the preconditions of H_2O_2 direct formation.[42] The H_2O_2 synthesis experiment adapted a mixture of $^{16}O_2/^{18}O_2$ as reactant proved that no $H_2^{16}O^{18}O$ could be produced.[43] High pressure reaction of CO oxidation conducted by Gao *et al.*[30,44] suggested that continuous Pd sites are responsible for O_2 dissociation which was able to demonstrate a production of CO_2. On the contrary, isolated Pd sites did not show any activity for the oxidation of CO. Hence, the ensemble effect of Au in Pd plays a crucial role for the direct synthesis of hydrogen peroxide which was demonstrated by the trend represented by the blue triangles in Figure 5-15, as the H_2O_2 production rate based on the weight of Pd was drastically enhanced with the increase of additive Au.

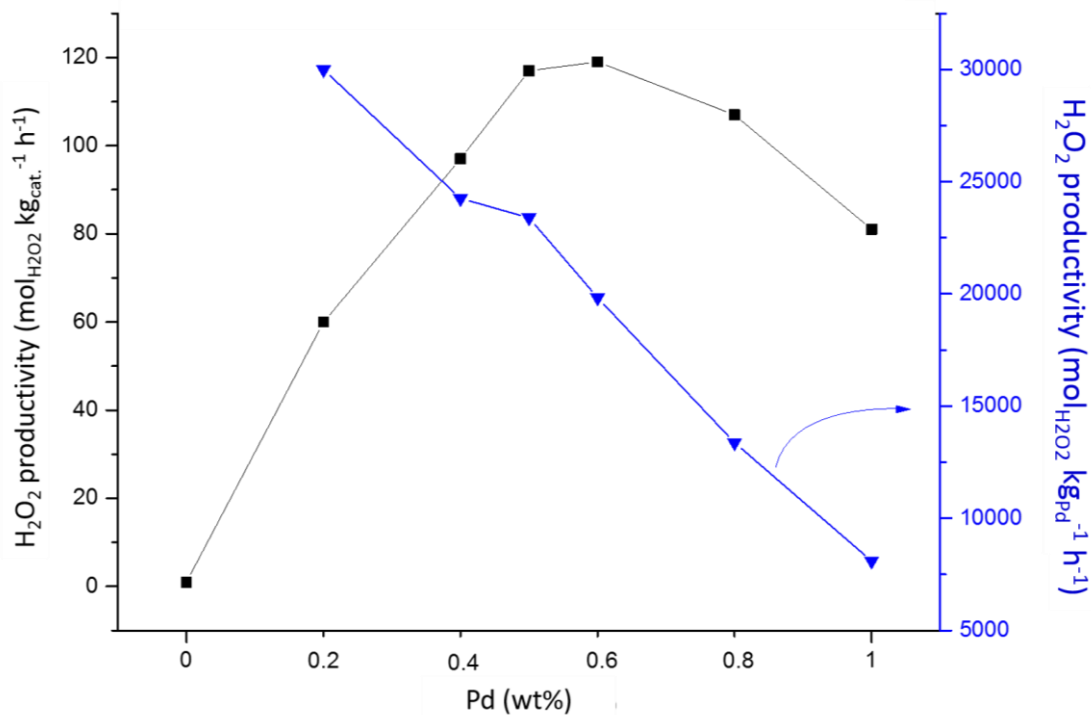**Figure 5-16:** Production rate for the direct synthesis of hydrogen peroxide calculated on the basis of the weight of the catalyst (black square, left axis) and Pd (blue triangle, right axis) over 1 wt % Au-Pd/TiO$_2$ M$_{Im}$ constant Cl$^-$. Reaction conditions: 5% H$_2$/CO$_2$ and 25% O$_2$/CO$_2$, 50% H$_2$/O$_2$ at 3.7 MPa, MeOH (5.6 g), H$_2$O (2.9 g), catalyst (0.01 g), 2 $^{\circ}$C, 1200 rpm, 30 min.

With the variation of Pd ratio in 1 wt% Au-Pd M_{Im} catalysts, a volcano plot of H_2O_2 hydrogenation activities was also observed, as shown in Figure 5-17Moreover, the lower Pd concentration demonstrated the higher hydrogenation production rates based on Pd which are shown as blue triangles also in Figure 5-17. It has been proved that dissociative chemisorption of O_2 was morphology sensitive whereas the activation of H_2 can be conducted on both individual and continuous sites of Pd.[34] Hence, enhanced dispersion of Pd through additive Au can prohibit the dissociation of O_2, yet provided more active sites based on the unit weight of Pd for the hydrogenation of H_2O_2.
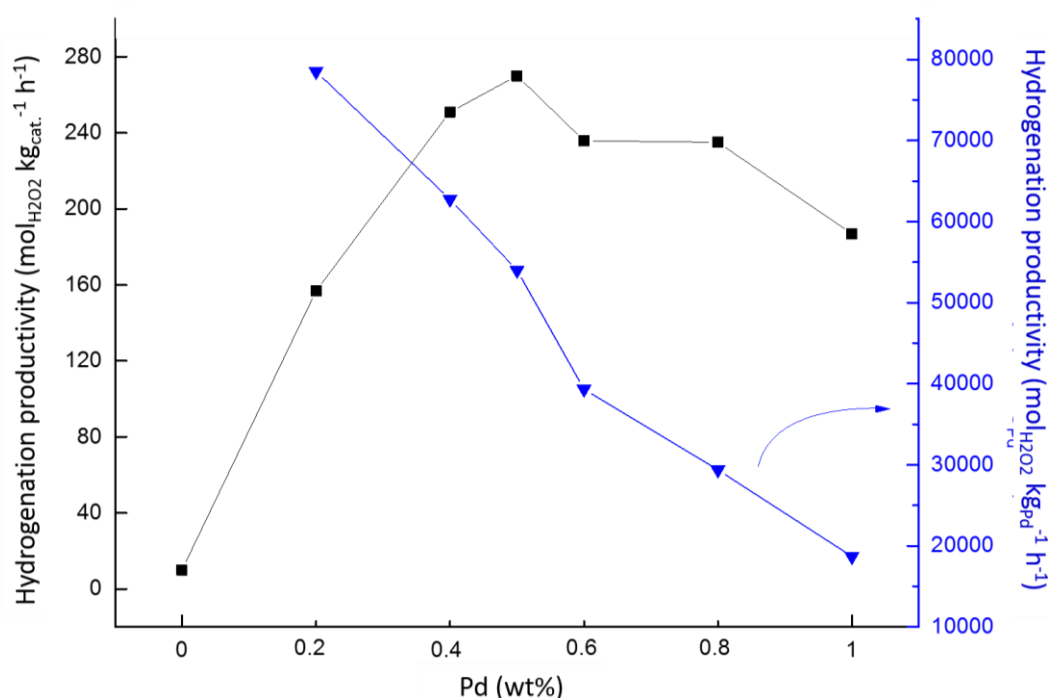
Figure 5-17: Production rate for the hydrogenation of hydrogen peroxide calculated on the basis of weight of the catalyst (black square, left axis) and Pd (blue triangle, right axis) over 1 wt % Au-Pd/TiO_2 M_{Im} constant Cl^-. Reaction conditions: 5% H_2/CO_2 at 2.8 MPa, MeOH (5.6 g), H_2O (2.22 g) and 50 wt% H_2O_2 (0.068 g), catalyst (0.01 g), 2 °C, 1200 rpm, 30 min.

In summary, the ensemble effect of Au in Pd is essential for the direct synthesis of hydrogen peroxide, as isolated Pd atoms are the actual active sites with high selectivity

of H_2O_2. Individual Pd sites are able to activate not only hydrogen but also O_2 molecules without dissociation, thereby benefit for hydrogen peroxide direct formation.

5.4.2 The effect of additive Cl⁻ in modified impregnation method

It is considered that the presence of Cl⁻ plays a crucial role in tuning the size and composition of Au-Pd nanoparticles.[18,23] In our previous study, the average size of Au-Pd nanoparticles were reduced from 4.7 nm to 2.6 nm with the increase of Cl⁻ concentration from 0 to 2 M.[23] Moreover, the Au-Pd catalyst prepared from Pd^{2+} in 0.58 M HCl demonstrated a substantially tighter particle size distribution than the C_{Im} analogue without using additional Cl⁻. The higher dispersion of particles provides one possible explanation of the superior H_2O_2 productivity of M_{Im} Au-Pd catalysts than C_{Im} catalysts as shown in Figure 5-6.

Moreover, previous detailed STEM-XEDS revealed that with the increase of additional Cl⁻ in the preparation, Au content in individual Au-Pd particles increased as a consequence which was identical with corresponding bulk ratio.[23] This result imply the formation of homogeneous Au-Pd alloy with the assistant of excess Cl⁻. In this chapter, XPS analysis of 0.8% Au-0.2% Pd/TiO_2 (M_{Im} varying Cl⁻) catalyst demonstrates that (i) a higher surface Au concentration relative to 0.8% Au-0.2% Pd/TiO_2 (C_{Im}) catalyst and (ii) a lower ratio of Pd/Au which was also close to that in bulk (Table 5-2). Both of the results are in agreement with the previous STEM observations. If additional Cl⁻ increased Au content in particles, with the increase of Au loading, Pd atoms are expected to be in a higher ratio of isolated Pd sites which are beneficial for H_2O_2 direct synthesis. This may help to explain the results in Figure 5-6 that M_{Im} Au-Pd bimetallic catalysts showed higher H_2O_2 activity than those of C_{Im} analogues. Furthermore, it is easier to understand that among all the bimetallic catalysts, the higher Au content in the catalyst the higher enhancement of activity relative to corresponding Pd monometallic catalyst. On the contrary, supported Au-Pd alloys prepared by C_{Im} demonstrate a size dependent composition variation as the prepared particles consist with large Au rich grains and Pd rich clusters, hence resulted in moderate activity for H_2O_2 direct synthesis.[45,46] Results in Figure 5-6 also suggested limited enhancements of H_2O_2

activity from the addition of Au to Pd through C_{Im} method because the secondary metal-Au could not strongly interact with Pd and as formed large individual Au particles.[23]

Pd only catalysts prepared through M_{Im} and C_{Im} showed very similar activities for the direct synthesis of H_2O_2 (Table 5-6). XPS analysis revealed that a relatively higher Pd atomic ratio on the surface of M_{Im} catalysts compared with the C_{Im} analogues. This can be explained as the limited solubility of $PdCl_2$ salt in water; less dispersed Pd particles therefore tend to be formed through C_{Im}. Moreover, PdO was predominant on the surface of both M_{Im} and C_{Im} Pd only catalysts, although it is difficult to determine the ratio of Pd^0 on the catalysts from the noisy spectra of Pd 3d. Hence, in order to clarify the effect of additional Cl^- on Pd only catalysts, techniques such as HR-TEM are necessary for the further analysis of the Pd morphology.

In conclusion, the additional Cl^- was proved to promote small Au-Pd nanoparticles and metal ion separation which can help to explain the superior performance of M_{Im} catalysts relative to C_{Im} analogues.[23] Detailed STEM analysis being conducted for firm conclusions.

5.5 Conclusions

Au-Pd bimetallic catalysts prepared through M_{Im} demonstrated superior production rate of H_2O_2 direct synthesis than those of C_{Im} throughout the whole range of Au/Pd ratio variation. Moreover, the synergistic effect of Au and Pd for H_2O_2 direct formation was observed over both C_{Im} and M_{Im} catalysts. Nevertheless, the latter showed a higher enhancement with the addition of Au to Pd. Both of the phenomena can be explained as the excess Cl^- in the preparation followed by high temperature reduction may allow the formation of well dispersed Au-Pd homogeneous alloys, which was proved by previous STEM analysis. As a result, stronger interaction of Au/Pd and higher ratio of isolated Pd sites were achieved through M_{Im}. By contrast, size-dependant composition variation was revealed in C_{Im} samples as both individual large Au rich particles and small Pd clusters were found.[15]

The enhancement from high concentration of Au in 1 wt% Au-Pd catalyst was demonstrated more significantly, and also with the increase of Au content, productivity based on Pd correspondingly increased over 1 wt% Au-Pd catalyst. Including ligand effect, the ensemble effect of Au to Pd is one of the explanations of the synergy of Au and Pd, as individual Pd atoms isolated by Au are in fact selective sites for the direct formation of H_2O_2. Hence, large amounts of additive Au to Pd increased catalyst productivity more significantly relative to the corresponding Pd only catalyst, and also more largely enhanced corresponding productivity of H_2O_2 on the basis of Pd mass.

In addition, TiO_2 supported Au-Pd catalysts show superior activities than the corresponding MgO supported catalysts throughout the whole range of Au/Pd ratio. MgO catalyst also demonstrated higher side reaction rate of H_2O_2 formation. This is consistent with our previous inference that supports with high isoelectronic point compromise the stability of H_2O_2 under reaction conditions.[28]

Pd monometallic catalysts prepared by M_{Im} demonstrated very similar production rate of H_2O_2 to the C_{Im} analogues. The effect of the modified method on Pd monometallic catalysts needs to be further investigated by more techniques such as HR-TEM for particle size distribution and Pd oxidation state analysis. STEM combined with XEDS will be helpful to prove Au-Pd particles are also homogeneous alloys in 1 wt% Au-Pd/TiO_2 (M_{Im}) catalysts with the variation of Au/Pd ratio.

5.6 References

1. J. K. Edwards, S. J. Freakley, A. F. Carley, C. J. Kiely, and G. J. Hutchings, *Acc. Chem. Res.*, 2013, **47**, 845-854.

2. M. Haruta, T. Kobayashi, H. Sano, and N. Yamada, *Chem. Lett.*, 1987, **2**, 405–408.

3. M. Haruta, N. Yamada, T. Kobayashi, and S. Iijima, *J. Catal.*, 1989, **115**, 301–309.

4. M. Haruta and M. Daté, *Appl. Catal. A Gen.*, 2001, **222**, 427–437.

5. T. Choudhary and D. Goodman, *Top. Catal.*, 2002, **21**, 25-34.

6. Q. Fu, H. Saltsburg, and M. Flytzani-Stephanopoulos, *Science*, 2003, **301**, 935–938.

7. P. Landon, J. Ferguson, B. E. Solsona, T. Garcia, A. F. Carley, A. A. Herzing, C. J. Kiely, S. E. Golunski, and G. J. Hutchings, *Chem. Commun. (Camb).*, 2005, **27**, 3385–3387.

8. G. J. Hutchings, *J. Catal.*, 1985, **96**, 292–295.

9. J. K. Edwards and G. J. Hutchings, *Angew. Chem. Int. Ed. Engl.*, 2008, **47**, 9192–9198.

10. A. Corma and P. Serna, *Science*, 2006, **313**, 332–334.

11. A. Corma and H. Garcia, *Chem. Soc. Rev.*, 2008, **37**, 2096–2126.

12. A. Corma, R. Juárez, M. Boronat, F. Sánchez, M. Iglesias, and H. García, *Chem. Commun. (Camb).*, 2011, **47**, 1446–1448.

13. D. I. Enache, J. K. Edwards, P. Landon, B. Solsona-Espriu, A. F. Carley, A. A Herzing, M. Watanabe, C. J. Kiely, D. W. Knight, and G. J. Hutchings, *Science*, 2006, **311**, 362–365.

14. A. Villa, N. Janjic, P. Spontoni, D. Wang, D. S. Su, and L. Prati, *Appl. Catal. A Gen.*, 2009, **364**, 221–228.

15. J. K. Edwards, B. E. Solsona, P. Landon, A. F. Carley, A. A. Herzing, C. J. Kiely, and G. J. Hutchings, *J. Catal.*, 2005, **236**, 69–79.

16. B. E. Solsona, J. K. Edwards, P. Landon, A. F. Carley, A. A. Herzing, C. J. Kiely, and G. J. Hutchings, *Chem. Mater.*, 2006, **18**, 2689–2695.

17. J. K. Edwards, A. F. Carley, A. A. Herzing, C. J. Kiely, and G. J. Hutchings, *Faraday Discuss.*, 2008, **138**, 225-239.

18. M. Morad, M. Sankar, E. Cao, E. Nowicka, T. E. Davies, P. J. Miedziak, D. J. Morgan, D. W. Knight, D. Bethell, A. Gavriilidis, and G. J. Hutchings, *Catal. Sci. Technol.*, 2014, **4**, 3120-3128.

19. C. Baatz and U. Pruse, *J. Catal.*, 2007, **249**, 34–40.

20. P. Miedziak, M. Sankar, N. Dimitratos, J. A. Lopez-Sanchez, A. F. Carley, D. W. Knight, S. H. Taylor, C. J. Kiely, and G. J. Hutchings, *Catal. Today*, 2011, **164**, 315–319.

21. J. Pritchard, L. Kesavan, M. Piccinini, Q. He, R. Tiruvalam, N. Dimitratos, J. A. Lopez-Sanchez, A. F. Carley, J. K. Edwards, C. J. Kiely, and G. J. Hutchings, *Langmuir*, 2010, **26**, 16568–16577.

22. S. Kondrat, G. Shaw, S. J. Freakley, Q. He, J. Hampton, J. K. Edwards, P. J. Miedziak, T. E. Davies, A. F. Carley, S. H. Taylor, C. J. Kiely, and G. J. Hutchings, *Chem. Sci.*, 2012, **3**, 2965-2971.

23. M. Sankar, Q. He, M. Morad, J. Pritchard, S. J. Freakley, J. K. Edwards, S. H. Taylor, D. J. Morgan, A. F. Carley, D. W. Knight, C. J. Kiely, and G. J. Hutchings, *ACS Nano*, 2012, **6**, 6600–6613.

24. J. K. Edwards, B. Solsona, E. N. Ntainjua, A. F. Carley, A. A. Herzing, C. J. Kiely, and G. J. Hutchings, *Science*, 2009, **323**, 1037–1041.

25. J. K. Edwards, B. Solsona, P. Landon, A. F. Carley, A. A. Herzing, C. Kiely, and G. J. Hutchings, *J. Catal.*, 2005, **236**, 69–79.

26. J. K. Edwards, A. Thomas, A. F. Carley, A. A. Herzing, C. J. Kiely, and G. J. Hutchings, *Green Chem.*, 2008, **10**, 388-394.

27. J. K. Edwards, A. F. Carley, A. A. Herzing, C. J. Kiely, and G. J. Hutchings, *Faraday Discuss.*, 2008, **138**, 225-239.

28. E. Ntainjua, M. Piccinini, J. Pritchard, Q. He, J. Edwards, A. Carley, J. Moulijn, C. Kiely, and G. Hutchings, *ChemCatChem*, 2009, **1**, 479–484.

29. E. Ntainjua N., J. K. Edwards, A. F. Carley, J. A. Lopez-Sanchez, J. A. Moulijn, A. A. Herzing, C. J. Kiely, and G. J. Hutchings, *Green Chem.*, 2008, **10**, 1162-1169.

30. L. Ouyang, G. Da, P. Tian, T. Chen, G. Liang, J. Xu, and Y.-F. Han, *J. Catal.*, 2014, **311**, 129–136.

31. A. Szytuła, D. Fus, B. Penc, and A. Jezierski, *J. Alloys Compd.*, 2001, **318**, 340–346.

32. M. Brun, A. Berthet, and J. Bertolini, *J. electron Spectrosc.*, 1999, **104**, 55–60.

33. J. Rodriguez, *Surf. Sci. Rep.*, 1996, **24**, 223–287.

34. F. Gao and D. W. Goodman, *Chem. Soc. Rev.*, 2012, **41**, 8009–8020.

35. R. Meyer, C. Lemire, S. Shaikhutdinov, and H. Freund, *Gold Bull.*, 2004, **37**, 72-124.

36. S. Arrii, F. Morfin, A. J. Renouprez, and J. L. Rousset, *J. Am. Chem. Soc.*, 2004, **126**, 1199–205.

37. A. Venezia, F. Liotta, G. Pantaleo, A Beck, A Horvath, O. Geszti, A. Kocsonya, and L. Guczi, *Appl. Catal. A Gen.*, 2006, **310**, 114–121.

38. J. Radnik, C. Mohr, and P. Claus, *Phys. Chem. Chem. Phys.*, 2003, **5**, 172–177.

39. H. F. Wang, H. Ariga, R. Dowler, M. Sterrer, and H. J. Freund, *J. Catal.*, 2012, **286**, 1–5.

40. D. Briggs and M. P. Steah, in *Pratical surface analysis*, John Wiley & Sons, Secon edit., 1993.

41. M. Bussell and P. Marcus, *Appl. Surf. Sci.*, 1992, **59**, 7–21.

42. T. A. Posepelova, *Russ. J. Phys. Chem.*, 1961.

43. J. Lunsford, *J. Catal.*, 2003, **216**, 455–460.

44. B. Zhou and L. Lee (Hydrocarbon Technologies USA Inc.), *US Pat. 6,168,775*, 2001, **1**.

45. G. J. Hutchings and C. J. Kiely, *Acc. Chem. Res.*, 2013, **46**, 1759-1772.

46. P. Paalanen, B. M. Weckhuysen, and M. Sankar, *Catal. Sci. Technol.*, 2013, **3**, 2869-2880.

Chapter 6

Further discussion, conclusions and future work

6.1 Further discussion and conclusions

As discussed in Chapter 1, the direct synthesis of hydrogen peroxide is a simple and straightforward alternative to currently the most widespread method - anthraquinone auto-oxidation, as the former can be more suitable for a small scale, on site and low concentration production of H_2O_2. Pd has been extensively utilized for the direct synthesis reaction; however, it is active for both hydrogenation and oxidation reactions and consequently cannot demonstrate satisfactory selectivity towards H_2O_2 in most cases. The addition of a secondary noble metal such as Au and Pt can remarkably enhance the catalytic selectivity; nevertheless, both of them are well-known to be expensive. Hence,

in order to decrease the cost of the utilized catalyst, using as small an amount of noble metal(s) as possible is one possible option. Moreover, through understanding the actual active sites for the direct formation of hydrogen peroxide, carefully designing the catalyst serves as a way to make an effective use of the noble materials. In this thesis, the selective sites for H_2O_2 synthesis over supported metallic Pd particles were first investigated. In Chapter 3, it was noticed that the reaction of H_2O_2 direct synthesis and storage under ambient conditions caused an increase in the productivity towards H_2O_2 and a decrease in the rate of hydrogenation of H_2O_2 over carbon supported metallic Pd catalysts. Moreover, on increasing the Pd loading in monometallic catalysts, particle dispersion was decreased, and also the hydrogenation activity of H_2O_2 on the basis of Pd was also suppressed. Integrated with previous publications on the relation between metallic Pd particle size and catalytic performance towards H_2O_2, both of these phenomena imply that active sites on large Pd particles or smooth surfaces are more selective for H_2O_2 than those-high energy sites on relatively small size particles or rough surfaces.

In Chapters 3 and 4, a base metal - Ni was then used as a substitute for Au in Pd catalysts for the direct synthesis of hydrogen peroxide, cost of which is less than one two-thousandth of that of Au.[1] In Chapter 3, active carbon (G60) supported Ni/Pd catalysts were prepared. The attained results demonstrated that Ni-Pd bimetallic catalyst showed greater H_2O_2 synthesis activity and lower hydrogenation activity than either Ni or Pd monometallic catalysts. Characterization techniques including XRD, XPS and TPR suggested that metallic Pd may sit on the top of Ni oxides with certain amount of dissolution of metallic Ni in Pd(0). Binding energy shifting of Pd 3d and Ni 2p were noticed by XPS indicating a possibility of electron transfer from Ni to Pd. Hence, both ensemble effect and ligand effect may be responsible for the superior activity of the bimetallic catalyst. TiO_2 (P-25) supported Ni/Pd catalysts were also prepared and investigated for H_2O_2 direct synthesis in Chapter 4 for a further understanding of the effect of Ni addition to Pd. Results demonstrated that the addition of Ni to Pd increased the conversion rate of H_2 (the overall activity of the H_2 and O_2 reactions), the selectivity towards H_2O_2, and H_2O_2 productivity. The Ni monometallic catalyst did not show any

activity even after a 12 hour reaction. The higher conversion rate of H_2 over Ni-Pd bimetallic catalysts was attributed to an improved dispersion of the particles which was demonstrated by STEM and XPS analysis. The enhanced selectivity towards H_2O_2 over Ni-Pd bimetallic catalysts was understood as the ensemble effect of Ni addition to Pd since it is known that isolated Pd sites are considered as the actual active sites for the direct synthesis of H_2O_2.[2] The formation of Ni-Pd alloys was also shown by STEM-XEDS, XPS and TPR analysis. In situ DRIFTS with CO adsorption also indicated the existence of a relatively large amount of isolated Pd sites on the bimetallic catalyst. Furthermore, a red shift of the linear-bonded CO with Pd could be observed indicating a possible electron transfer from Ni to Pd. It was claimed that Pd with more filled d-bands becomes more atomic like in nature leading to more weakly bound reactant and product states and thereby giving rise to H_2 selectivity.[2] Based on this information, ensemble and/or ligand effects can be used to explain the positive role of Ni addition to Pd. Ni as a substitute to Au demonstrated an outstanding catalytic performance for the direct synthesis of hydrogen peroxide and thereby has a great potential to replace gold as a cheaper alternative for the future use (Table 6-1).

Table 6-1: The comparison results of the direct synthesis of hydrogen peroxide over supported Ni-Pd catalyst and the Au-Pd analogue[3].

Catalyst	2.5 wt% Ni-2.5 wt% Pd/TiO$_2$	2.5 wt% Au-2.5 wt% Pd/TiO$_2$
H_2O_2 productivity (mol_{H2O2} $kg_{cat.}^{-1}$ h^{-1})	78	64
H_2 Conversion (%)	26	21
H_2O_2 Selectivity (%)	58	61
H_2O_2 yield (%)	15.1	12.8

Reaction conditions: Solvent (5.6 g CH$_3$OH + 2.9 g H$_2$O), 420 psi 5% H$_2$/CO$_2$ + 160 psi 25% O$_2$/CO$_2$,10 mg catalyst, 1200 rpm, 2ºC, 0.5 h

Another way of reducing the cost of the catalytic material is using a catalyst with a low metal loading prepared by a simple and effective preparation method. A modified impregnation method for 1 wt% Au-Pd catalyst was discussed in Chapter 5 which is able to control both particle size and Au/Pd composition in particles. The key of the new method is using an excess of Cl$^-$ ions in the preparation followed by high temperature reduction under dilute H$_2$ to remove the remaining Cl on the surface. The attained M$_{Im}$ catalyst demonstrated (i) higher dispersion of particles than those of C$_{Im}$ catalysts, (ii) homogeneous Au-Pd nanoparticles without size-dependant components and thereby (iii) a superior activity for H$_2$O$_2$ formation than the C$_{Im}$ analogue. It was also noticed that the synergistic effect of Au and Pd was demonstrated more remarkably over the 1 wt% Au-Pd M$_{Im}$ catalysts with a low Pd content. Moreover, the production rate of H$_2$O$_2$ based on Pd kept increasing with the decrease of Pd content in 1 wt% Au-Pd M$_{Im}$ catalysts. Both of the observations further support the concept that isolated Pd atoms are the active and selective sites for the direct formation of H$_2$O$_2$, as for homogeneous Au-Pd alloys, the increase of Au content in 1 wt% metal loading is able to induce a higher ratio of individual Pd sites. This indicates the ensemble effect of Au addition to Pd given that Au by itself has been proved to be inactive for H$_2$O$_2$ synthesis, and the assumption was made on the basis of the dismissing of the ligand effect.

For the effect of the modified impregnation method on the catalytic performance, the source of Cl$^-$ was from 0.58 M HCl which assisted the dissolution of PdCl$_2$ and also helped the formation of a homogeneous complex mixture – [AuCl$_4$]$^-$ and [PdCl$_4$]$^{2-}$,[4] therefore resulted in well dispersed homogeneous Au-Pd alloys after the reducing heat treatment. Hence, the M$_{Im}$ is the method which is able to make full use of Pd through the formation of Au-Pd strong interaction, as it can highly disperse Au with Pd atoms resulting in a high ratio of effective site-isolated Pd sites.

6.2 Future work

In this thesis, it was suggested that relative to high energy sites on relative small particles/rough surfaces of Pd (0), low energy sites on large particles/smooth surfaces

are selective towards H_2O_2 synthesis. Whereas, in the comparison of Pd only and supported Pd catalysts with a secondary metal the bimetallic catalysts demonstrated superior catalytic performance compared to the Pd monometallic catalysts. Because isolated Pd atoms are considered to be selective sites for H_2O_2 formation compared with continuous Pd sites. The secondary metal may not be active for the direct synthesis of hydrogen peroxide or probably demonstrates a lower hydrogenation activity than Pd since the target reaction is a hydrogenation reaction of O_2 molecules rather than an oxidation reaction of H_2. If all the inferences stated until now are true, the alloys of Pd with other hydrogenation base metals such as Co may also be able to demonstrate outstanding catalytic performance for H_2O_2 direct synthesis. Moreover, the modified impregnation method may be one of the options for the preparation of low loading base metal-Pd alloys. Hence, the future work will focus on supported base metal-Pd catalysts for H_2O_2 synthesis prepared by a simple and effect method that consequently reduce the cost of catalytic materials.

6.3 References

1.   *www.metalbulletin.com*.

2.   F. Gao and D. W. Goodman, *Chem. Soc. Rev.*, 2012, **41**, 8009–8020.

3.   J. K. Edwards, B. E. Solsona, P. Landon, A. F. Carley, A. A. Herzing, C. J. Kiely, and G. J. Hutchings, *J. Catal.*, 2005, **236**, 69–79.

4.   M. Sankar, Q. He, M. Morad, J. Pritchard, S. J. Freakley, J. K. Edwards, S. H. Taylor, D. J. Morgan, A. F. Carley, D. W. Knight, C. J. Kiely, and G. J. Hutchings, *ACS Nano*, 2012, **6**, 6600–6613.

Appendix

Table A-1: The effect of precursors on hydrogen peroxide synthesis over carbon supported Ni/Pd catalysts

Catalyst	Precursor		Productivity $(mol_{H2O2}\, kg_{cat.}^{-1}\, h^{-1})$
	Ni	Pd	
2.5 wt% Pd/C	-	$Pd(NO_3)_2$	18
2.5 wt% Ni/C	$Ni(NO_3)_2$	-	8
	$Ni(Cl)_2$	-	1
2.5 wt% Ni-2.5 wt% Pd/C	$Ni(NO_3)_2$	$Pd(NO_3)_2$	40
	$Ni(Cl)_2$	$Pd(NO_3)_2$	51